AD-764 512

A FORWARD FACING STEP STUDY: THE STEP HEIGHT LESS THAN THE BOUNDARY-LAYER THICKNESS

Richard T. Driftmyer

Naval Ordinance Laboratory
White Oak, Maryland

11 May 1973

NOLTR 73-98

AD764512

A FORWARD FACING STEP STUDY: THE STEP HEIGHT LESS THAN THE BOUNDARY-LAYER THICKNESS

BY
Richard T. Driftmyer

11 MAY 1973

NOL

NAVAL ORDNANCE LABORATORY, WHITE OAK, SILVER SPRING, MARYLAND

NOLTR 73-98

APPROVED FOR PUBLIC RELEASE;
DISTRIBUTION UNLIMITED

UNCLASSIFIED

Security Classification

DOCUMENT CONTROL DATA - R & D

(Security classification of title, body of abstract and indexing annotation must be entered when the overall report is classified)

1. ORIGINATING ACTIVITY (Corporate author) Naval Ordnance Laboratory White Oak, Silver Spring, Maryland 20910	2a. REPORT SECURITY CLASSIFICATION Unclassified 2b. GROUP N/A

3. REPORT TITLE

A Forward Facing Step Study: The Step Height Less Than the Boundary-Layer Thickness

4. DESCRIPTIVE NOTES (Type of report and inclusive dates)

5. AUTHOR(S) (First name, middle initial, last name)

Richard T. Driftmyer

6. REPORT DATE	7a. TOTAL NO. OF PAGES	7b. NO. OF REFS
11 May 1973	~~78~~ 82	8

8a. CONTRACT OR GRANT NO. b. PROJECT NO. A320 320C/004B/WF32-322-202 c. d.	9a. ORIGINATOR'S REPORT NUMBER(S) NOLTR 73-98 9b. OTHER REPORT NO(S) (Any other numbers that may be assigned this report)

10. DISTRIBUTION STATEMENT

This document has been approved for public release, its distribution is unlimited.

11. SUPPLEMENTARY NOTES	12. SPONSORING MILITARY ACTIVITY Naval Air Systems Command Washington, D. C. 20361

13. ABSTRACT

An experimental investigation involving a thick, adiabatic, naturally turbulent, two-dimensional boundary layer undergoing separation has been completed at the Naval Ordnance Laboratory (NOL). Forward facing steps (with attached end plates) were used to induce boundary-layer separation for the particular case where the step heights, h, were less than the boundary-layer thickness, δ. The tests were conducted at a free-stream Mach number of 4.9 with a range of unit Reynolds numbers varying from 0.8×10^6 per foot to 4.0×10^6 per foot. The pressure distributions measured in the separated region ahead of the steps were found to be functions of both Re_δ and h/δ for the turbulent boundary-layer separation case where $h < \delta$. Since the induced side forces are determined from these same pressure distributions, these forces are also functions of Re_δ and h/δ. The major result of this study is the definition of a universal pressure distribution valid for two-dimensional steps.

DD FORM 1 NOV 65 1473 (PAGE 1)

S/N 0101-807-6801

UNCLASSIFIED

Security Classification

UNCLASSIFIED
Security Classification

14 KEY WORDS	LINK A		LINK B		LINK C	
	ROLE	WT	ROLE	WT	ROLE	WT
forward facing step two dimensional supersonic flow boundary-layer separation viscous interaction						

DD FORM 1 NOV 65 1473 (BACK)
(PAGE 2)

UNCLASSIFIED
Security Classification

1a

A FORWARD FACING STEP STUDY:

THE STEP HEIGHT LESS THAN THE BOUNDARY-LAYER THICKNESS

Prepared by:
Richard T. Driftmyer

ABSTRACT: An experimental investigation involving a thick, adiabatic, naturally turbulent, two-dimensional boundary layer undergoing separation has been completed at the Naval Ordnance Laboratory (NOL). Forward facing steps (with attached end plates) were used to induce boundary-layer separation for the particular case where the step heights, h, were less than the boundary-layer thickness, δ. The tests were conducted at a free-stream Mach number of 4.9 with a range of unit Reynolds numbers varying from 0.8×10^6 per foot to 4.0×10^6 per foot. The pressure distributions measured in the separated region ahead of the steps were found to be functions of both Re_δ and h/δ for the turbulent boundary-layer separation case where $h < \delta$. Since the induced side forces are determined from these same pressure distributions, these forces are also functions of Re_δ and h/δ. The major result of this study is the definition of a universal pressure distribution valid for two-dimensional steps.

NAVAL ORDNANCE LABORATORY
WHITE OAK, MARYLAND

NOLTR 73-98 11 May 1973

A FORWARD FACING STEP STUDY: THE STEP HEIGHT LESS THAN THE BOUNDARY-LAYER THICKNESS

This report describes the results of a two-dimensional, thick, turbulent boundary-layer separation study conducted at the Naval Ordnance Laboratory. The purpose of this investigation was to obtain pressure distribution data in the separation region ahead of the forward facing step (used to separate the boundary layer) for the case where the step height was less than the boundary-layer thickness. This study was performed for the Naval Air Systems Command under Task Number A320 320C/004B/WF32-322-202.

ROBERT WILLIAMSON II
Captain, USN
Commander

L. H. Schindel

L. H. SCHINDEL
By direction

CONTENTS

ILLUSTRATIONS

INTRODUCTION

This report describes the experimental results of a thick, two-dimensional turbulent boundary-layer separation study conducted at the Naval Ordnance Laboratory (NOL). The separation was induced by a forward facing step. The purpose of this investigation was to obtain pressure distribution data in the separation region ahead of the step for the case where the step height was less than the boundary-layer thickness. This information is technically important to those studying boundary-layer separation and has a variety of possible applications which include supersonic flight controls. Numerous investigators (Refs. (1), (2), (3) and (4)) have studied separation phenomena ahead of forward facing steps for the turbulent boundary-layer case. Of these, the work of Zukoski (Ref. (1)) is particularily good since it is both a review and an analysis of numerous two-dimensional experimental works. As a result of these reported works, simple correlations have been determined for the upstream pressure distributions and for the side-force calculations of the forward facing step model limited to the case for $h/\delta > 1.5$.

In a recent jet interaction control study at NOL, (Ref. (5)), the similarity of the upstream pressure distributions for both the step and interacting jet separation regions was demonstrated. This similarity established the fact that jet and step separation phenomena are analogous. The study of Reference (5) was limited to the case where the boundary layers were thin relative to the height of the particular obstruction which inducesthe boundary-layer separation. Hence, the thick boundary-layer case ($h < \delta$) remained to be investigated and is the subject of this report.

SYMBOLS

D	see Equation (4), inch
F	side force, lbf/inch
g	any dimensional flow-field property
G	any dimensionless flow-field parameter
h	step height, inch
M	Mach number
n	exponent of the turbulent boundary-layer profile
P	pressure, psia
Pl	first plateau pressure, psia
R	gas constant, ft-lbf/lbm °R
Re_δ	Reynolds number based upon boundary-layer thickness
T	temperature, °R
X	distance, measured along the flat plate surface, inch

SYMBOLS (Continued)

XP	projected shock distance, see sketch Page 8, inch
XS	separation distance, see sketch Page 8, inch
ΔXS	initial steep pressure rise distance, see sketch Page 8, inch
α	see Figure 14d
β	see Figure 14d
γ	specific heat ratio
δ	boundary-layer thickness, inch
μ	dynamic viscosity, slug/ft sec
ρ	density, lbm/ft^3

Subscripts

∞	remote free stream
o	stagnation
oil	oil flow study

EXPERIMENTAL APPARATUS

The experimental tests were performed in the NOL Boundary Layer Channel (Ref. (6)). A schematic of the Boundary Layer Channel is presented in Figure 1. The flexible nozzle plate is directly opposed to a flat test plate along which thick boundary layers are generated for testing. The flat test plate is 106 inches long and 14 inches wide. The wind-tunnel nozzle side walls are hinged to the flat test plate and serve as access doors to the test section. In the closed position, the doors are sealed by pressing against sealing gaskets located in the edges of the flat and flexible plates. Glass viewing ports were located in the doors thereby permitting one to view the flow field.

The flexible nozzle plate is held in position by 13 screw jacks. The particular contour selected for the flexible plate determines the pressure gradient along the length of the wind-tunnel nozzle. These gradients, of course, directly influence the test boundary layer generated along the flat plate. For this experimental study, a constant pressure gradient contour equal to zero was specified for the test section. This contour was computed using the method of characteristics which included corrections for the boundary-layer displacement thickness. Figure 2a presents the experimental Mach numbers obtained in the test rhombus for the various wind-tunnel supply pressures while Figure 2b presents the boundary-layer thickness distribution along the plate. The Mach number fluctuations in Figure 2a ranged from 2.5 percent to 0.5 percent as the supply pressure varied from 1 to 5 atmospheres. The overall change of the Mach number in this pressure range was about 4.8 percent. This overall Mach number change was attributed to changes in the boundary-layer displacement thickness. The local fluctuations in Mach numbers were attributed to measurement errors with the maximum errors occurring at the lowest stagnation pressures.

Figure 3 is an oblique view of the step model and the installed glass-ported end plates. These end plates (details are given in Fig. 4) were mounted eight inches apart, symmetrically about the centerplane of the half nozzle at zero angle of attack. The forward most tips of the two end plates were located at the 76.0-inch station (measured from the sonic throat station of the wind-tunnel nozzle). This distance aligned the various glass windows properly for viewing. The metal retaining ring which held the door's glass window in place, blocked the flow-field view for the first 0.25 inch off the test plate surface as seen in Figure 4.

A simple, Z configuration, spark shadowgraph system was used to record all photographic data.

The primary experimental data were the upstream pressure distributions. Figure 5 shows the physical arrangement of the static pressure taps. The numbers shown on the right-hand side of the taps are the hole identification numbers; those on the left-hand side are the hole distances measured from the step mounting plane. The two test locations of the step face were located 0.375 and 0.6875 inches ahead of this step mounting plane. A total of seven steps were tested. The installation detail and a listing of the step heights tested are given in Figure 6. To obviate any possibility that the high-pressure gas found in the forward separation bubble could leak out, black plastic tape was used to seal all interior cracks and corners. These seals are visible in the photograph of Figure 3.

To measure the static pressure distributions, eight strain-gage pressure transducers were directly connected to eight scanner valves. These scanner valves were switched sequentially through 12 valve positions according to the pressure tap array of Table 1. Note that the valve position 1 was reserved for calibration purposes. This array identifies the various pressure tap locations (Fig. 5) with the corresponding scanner valve and sequence position. Tap numbers 65 through 78 were not used for this step study. The electrical switching equipment was designed to permit only forward sequential switching of the scanner valves. The switch position was sensed and recorded along with each sample of pressure data thus eliminating error with regard to the static pressure tap matrix. Steady tunnel conditions were maintained over the two-to-four-minute time period required to measure all static pressures. Instantaneous wind-tunnel conditions were used for all data reduction.

TABLE 1

STATIC PRESSURE TAP IDENTIFICATION ARRAY

SCANNER VALVE AND PRESSURE TRANSDUCER NUMBER \ SCANNER VALVE SEQUENCE POSITION	1	2	3	4	5	6	7	8	9	10	11	12
1	(CALIBRATION INPUT POSITION 1)	65	67	69	71	73	75	77				
2		66	68	70	72	74	76	78				
3		1	4	9	15	21	25	29	33	37	41	43
4		2	5	11	14	23	27	31	35	39	43	47
5		3	7	13	19	12	28	44	51	55	59	63
6		6	18	30	42	16	32	48	52	56	60	64
7		10	22	34	46	20	36	49	53	57	61	
8		14	26	38	8	24	40	50	54	62		

The transducer signals were recorded using NOL's updated "Portable Automatic Data Recording Equipment," (PADRE), an earlier version of which is described in Reference (7). This recording unit, shown in Figure 7, provides a visual display of the data output. These data are recorded on IBM cards which are then used in an IBM 7090 computer for the final data reduction.

The final piece of equipment used in this study was the boundary-layer probe (See Appendix B for further information and reference works). This boundary-layer survey mechanism was externally attached to the flat test plate of the wind-tunnel nozzle (shown in Fig. 7) at each of two available probing ports. These probing ports were located on the wind-tunnel nozzle's centerplane, 48.0 and 60.0 inches downstream of the wind-tunnel throat. The boundary-layer description as determined from the probe measurements is presented in Appendix B.

DIMENSIONAL ANALYSIS

The test program was organized using the technique of dimensional analysis. Figure 8 is a schematic representation of the wind-tunnel nozzle-step geometry. For this analysis it is assumed that no heat-transfer or chemical reactions take place. Consideration of the associated wind-tunnel variables and the simple two-dimensional flat plate-step geometry results in the following general dimensional relationship for any flow-field property, g.

$$g = g\ [\bar{u},\ P,\ \rho,\ R,\ \gamma,\ \mu,\ \delta,\ h] \qquad (1)$$

An analysis of the variables and primary dimensions in Equation (1) above reveals that a nondimensional parameter, G, may be determined which will be a function of at least four dimensionless numbers. This can be written as

$$G = G\ [Re_\delta, M, \gamma, h/\delta] \qquad (2)$$

Since both $\gamma = 1.4$ and $M = 4.9$ were constants for this test, Equation (2) above reduces to

$$G = G\ [Re_\delta, h/\delta] \qquad (3)$$

Equation (3) expresses the fact that ıy dimensionless flow-field property, G, (as for instance the upstream pressure signature of the separated flow region) is to be investigated as a function of the flow geometry, h/δ, and the Reynolds number based upon the boundary-layer thickness, Re_δ. As seen in Equation (3), the significant length to be associated with the fluid was the boundary-layer thickness, δ, measured at the point where the boundary-layer separates from the flat plate. Normally, one may also choose as fluid lengths either the flat plate distance measured from a leading edge or the distance measured from the end of transition (turbulent case). However, for this test, the first length did not exist (by wind-tunnel design), and the second length was unknown. Even if the precise location of the end of transition had been known, though, the significance of the distance measured from this point would be unclear as transition certainly occurred within the accelerating flow region of the wind-tunnel nozzle and not in the test rhombus.

EXPERIMENTAL PROGRAM AND PROCEDURE

The experimental test program outline is given in Table 2. This outline follows the functional expression given by Equation (3).

TABLE 2

PRESSURE TEST PROGRAM*

Tunnel Supply Pressure (Atm)	Re/L x 10^{-6} (1/ft)	STEP HEIGHT (INCHES)					
		1.502	1.400	1.205	0.903	0.603	0.247
5	4.0	x	x	x	x	x	x
4	3.2	-	x	-	-	-	-
3	2.4	-	x	-	-	-	-
2	1.6	-	x	-	-	-	-
1	0.8	x	x	x	x	x	-

*An oil flow separation study was conducted at Re/L = 4.0×10^6 per foot. Included in this study was a 0.130-inch high step not listed above.

The Boundary Layer Channel contour was checked prior to testing by experimentally measuring the pressure gradient throughout the test rhombus. Several preliminary pressure surveys and contour adjustments were necessary to produce satisfactory results. Subsequently, the glass-ported end plates were installed and the final pressure gradients were measured using the surface static pressure taps located between the glass end plates. The results of this survey are presented in Figure 9.

The procedure followed to record the pressure gradient data was identical with that followed later to record the pressure distributions ahead of the step. Quite simply, this procedure required a sequential shifting of the scanner valves, a pause to observe steadiness of the pressure transducer outputs, and a recording operation. One can identify the time sequence followed for taking data and also identify the particular pressure tap-transducer combination used by comparison of Table 1 with Figure 5.

Two pressure distributions were recorded for each step, one distribution for each of the two available step mounting positions (see Fig. 6). This provided offset pressure distributions for comparison purposes and assured repeatibility since separate wind-tunnel startups were involved. Figure 10 shows a typical example of offset pressure distributions. Excellent repeatibility was obtained for all cases. Hence, only one distribution is presented in this report.

EXPERIMENTAL RESULTS

The significant experimental test parameters determined by dimensional analysis were Re_δ and h/δ. However, the more practical dimensional parameters, Re/L and h, were used experimentally as the independent test variables. No problem was created with this simplification since δ varied only fractionally over the range of Reynolds numbers covered in this experiment, (Fig. 2b). Hence, variations in Re_δ follow almost directly the experimental variations in Re/L and similarly so for h/δ and h.

UPSTREAM PRESSURE DISTRIBUTION

Figure 11 presents three sets of pressure distributions. The data shown in Figures 11a and 11b were taken at Reynolds numbers of 4.0×10^6 per foot and 0.8×10^6 per foot, respectively, over the test range of step heights. In contrast, Figure 11c presents data taken at the constant step height of 1.400 inches over the experimental range of Reynolds numbers (Table 1). As indicated by the data, the step height influences both the extent of separation and the value of the maximum pressure at the first pressure plateau, whereas the Reynolds number per foot is observed to influence the pressure profile in the upstream region near the beginning of the pressure rise.

The small amount of scatter observed in the data in Figure 11b may be attributed to the very low values of static pressures which existed in the flow field for those test conditions. Pressures as low as 0.03 psia were measured using 0-5.0 psia full-scale pressure transducers calibrated over a reduced pressure range of 0-1.0 psia. Thus, the pressures of 0.03 psia were measured near the practical lower limit of the pressure transducer and some fluctuations were inevitable.

OIL FLOW RESULTS

Figure 12 presents all of the oil flow photographic data obtained. Silicon oil (300 centistokes), with white Titanium oxide powder in suspension, was painted in vertical strips on the flat test plate of the Boundary Layer Channel (the wind-tunnel nozzle is oriented vertically). After operating the wind tunnel for a few minutes the oil flow pattern was developed. When the wind tunnel was shut down, the accumulation of oil located at the separation line flowed (under the influence of gravity) downward on the flat test plate. This explains the rather wide separation lines seen in Figure 12. Separation distance was measured from the step face to the topmost edge of this line. One rather interesting finding of this oil flow study was the result of Figure 13. By making all measured oil flow points coincident, it appears that a single pressure signature exists with local, individual deviations occurring only near the region where the reattachment pressure rise exists. Note, however, that the plateau pressures are also different for each step. In all cases, oil flow separation was located at the point in the pressure distribution where $P/P_\infty = 1.2$. This compares favorably with the recently reported results of $P/P_\infty = 1.2$ to 1.25 (Ref. (8)).

SELECTION AND CORRELATIONS OF THE SCALING LENGTHS

In Reference (5) pressure distributions ahead of steps and jets for $h/\delta > 1.5$ were obtained by plotting $(P-P_\infty)/(P1-P_\infty)$ versus X/XS. In these correlations the plateau pressure rise, $(P1-P_\infty)$, and the known separation distance, XS, were used as the normalizing parameters. Because of this previous success identical parameters were selected for correlating the pressure data of the thick boundary-layer case. The plateau pressure rise data were taken from the pressure distributions of Figure 11 and the separation distances were available from the previously mentioned oil flow study. However, the use of these normalizing parameters did not produce a universal pressure profile. Rather, the diverging nature of the plotted results indicated that the fault was related to the measured oil flow separation distance. Since this distance did not scale the pressure distributions, a separation criterion established by Zukoski (Ref. (1)) was selected for use hopefully to obtain a scaling length which would correlate the data. According to this criterion, the separation pressure rise is 73 percent of the plateau pressure rise. Application of this rule to the upstream pressure distributions of Figure 11 determined a complete set of separation distances (in reality a set of scaling distances since the exact location of separation by any means other than the oil is unknown).

Subsequent plots using these data established a universal curve over the range $o \leq X/XS \leq 1.0$; however, when extended to values of $X > XS$, the pressure profile again diverged into a family of curves. Hence, a change in relevant scale length is implied as $|X|$ exceeds $|XS|$. The pressure distributions of Figure 11 were available from which an appropriate distance, significant to the initial steep pressure rise region, could be defined and measured. This distance was designated as the "initial steep pressure rise distance" ΔXS.

The following sketch presents the simple graphical method used to obtain ΔXS.

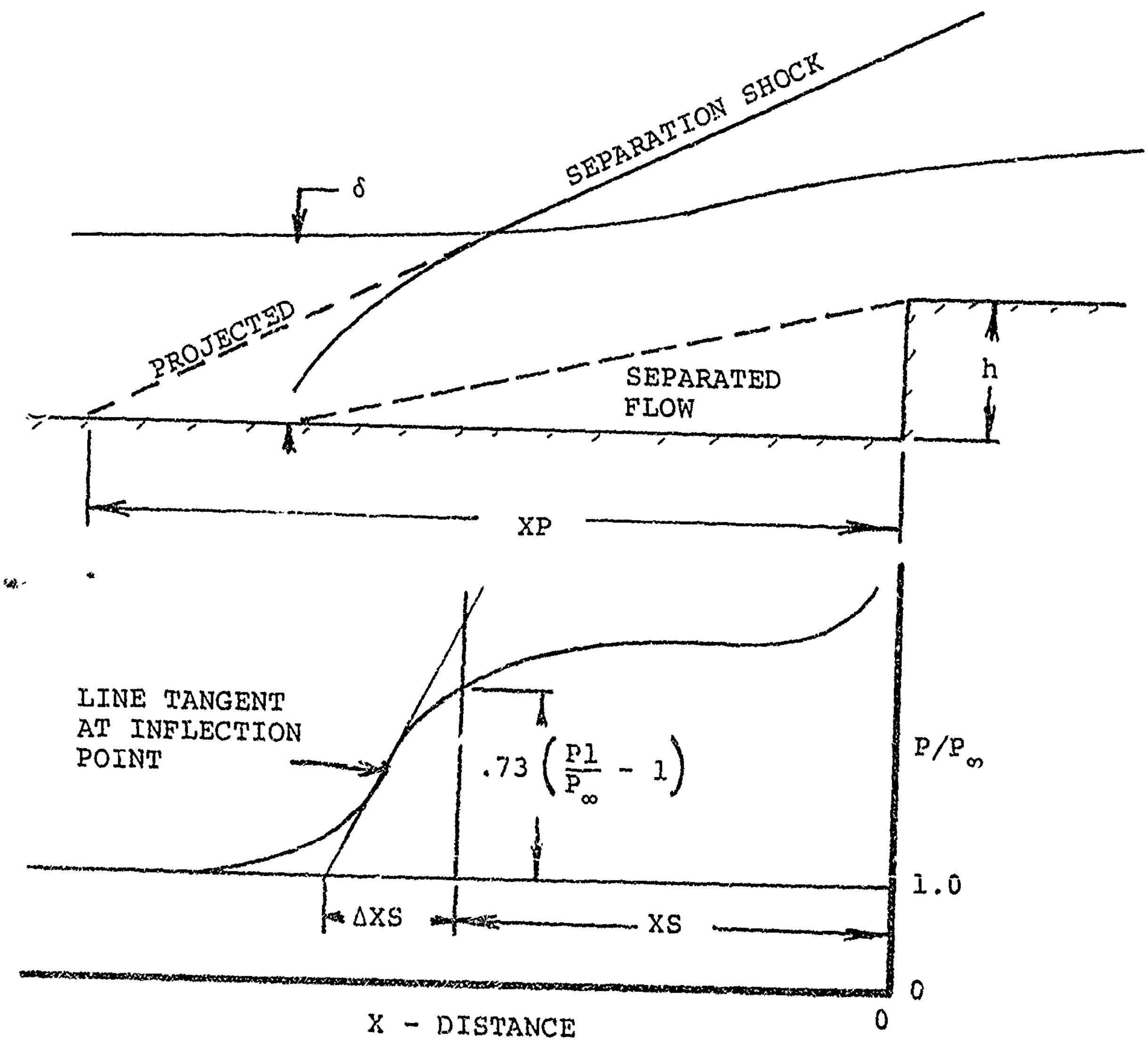

The use of ΔXS as a scaling length completed the universal pressure distribution. For convenience, in the presentation of the universal pressure distribution curve of Figure 14, the separation point determined by Zukoski's criterion (Ref. (1)) as established as the point X = 0, permitting both sets of normalized distances to vary from 0 to 1.0. The experimental results of this correlation are presented in Figures 14a, 14b, and 14c. These three distributions appear to be of the same parent population and are adequately represented by the curve in Figure 14d, the Composite Universal Pressure Distribution.

The existence of a universal pressure profile implies that the functional dependence of the pressure distributions with Re/L and h/δ (see Fig. 11) is incorporated in the scale parameters ΔXS and XS.

To investigate this functional dependence, the projected shock distance, XP (see previous sketch), was introduced.

As seen, XP is determined by the straight line extension of the separation shock from the inviscid flow region to the flat test plate.

This distance, XP, was first compared with the sum (ΔXS + XS), for it was believed that the difference between these two-dimensional quantities, defined as

$$D = XP - (\Delta XS + XS) \tag{4}$$

would be such that

$$D = D\ (Re/L, h, \delta, n) \tag{5}$$

where n is the exponent of the turbulent boundary-layer profile. The plotted results, shown in Figure 15 imply that this difference, D, is in fact independent of Re/L and h within the range of values covered in this study. Further, since δ changed only fractionally throughout this experimental study and n was nearly constant (see Appendix B), it is logical to assume that

$$D = D\ (\delta, n) = \text{constant} = 1.0'' \tag{6}$$

is realistic.

Using XP as a normalixing distance, the ratios $\Delta XS/XP$ and XS/XP may be broadly interpreted as the fraction of the shock projection distance assigned to the initial steep pressure rise process and the fraction of the shock projection distance assigned to the separated region, respectively. For the case of the step, Figure 16 shows the functional dependence of these fractional distances on h/δ for different values of Re/L. It is not unreasonable to expect when one also considers the results of Werle, et al (Ref. (5)) that as h/δ increases without limit, that is, either h becoming large or δ becoming small, or both, $\Delta XS/XP$ approaches zero. For the same conditions, XS/XP approaches unity. On the other hand, as h/δ decreases XS/XP approaches zero. An example of this behavior is seen in the pressure distribution of Figure 11a for $h = 0.247$ inch. The limiting behavior of $\Delta XS/XP$ as h/δ approaches zero is not known. It is seen experimentally that $\Delta XS/XP$ increases as h/δ decreases.

The variation in the bluntness of the pressure distributions in the free interaction region was observed previously in Figure 11. Since the magnitude of ΔXS is related to this bluntness and the bluntness appears to vary with Re/L, one would expect, based upon this variation, that $\Delta XS/XP$ decreases with increasing Re/L (for constant h/δ). In the same fashion XS/XP increases with increasing Re/L (for constant h/δ). These two facts are readily verified in Figure 16.

Figure 17 presents the geometric parameters $\Delta XS/h$, XS/h and XP/h as functions of Reynolds number per foot. A simple interpretation of the last parameter, XP/h may be made. This parameter establishes the shock standoff distance relative to the step and may be interpreted as the cotangent of the turning angle necessary to produce the oblique shock found in the inviscid flow field. The proof of this last statement is presented in Figure 18 where a comparison is made between the experimentally measured plateau pressures and those computed using the turning angle consistent with the experimental cotangent, XP/h. The data comparison seems to support the interpretation given XP/h.

Returning to Figure 17, the opposite slopes exhibited by $\Delta XS/h$ and XS/h are such that XP/h is observed to be nearly constant for a given value of h--a result consistent with Equations (4) and (6).

Zukoski (Ref. (1)) reports that the wedge appears to be a reasonable model for the separation region when $h > 1.5\delta$. For this case, the cotangent of the wedge angle is 4.2 (and constant) for fully developed turbulent boundary-layer flow. Note in Figure 17, XP/h is approximately 6.8 for a step of height $h = 0.603$ inch ($h/\delta \sim 0.2^+$) and 6.3 for a step of height $h = 1.502$ inches ($h/\delta \sim 0.5^+$). Hence, the experimental trend of XP/h with increasing h/δ does not appear inconsistent with Zukoski's model for $h > 1.5\delta$.

SIDE FORCE CALCULATION

The induced control force due to the flow separation may be evaluated from the upstream pressure distributions as follows:

$$F = \int_X (P-P_\infty)\, dx \qquad (7)$$

After normalizing, Equation (7) may be expanded into the following form:

$$\frac{F}{P_\infty h} = \frac{P1-P_\infty}{P_\infty h}\left[\Delta XS \int_{1.0} \frac{P-P_\infty}{P1-P_\infty}\, d\left(\frac{X}{\Delta XS}\right) + XS \int_{1.0} \frac{P-P_\infty}{P1-P_\infty}\, d\left(\frac{X}{XS}\right)\right] \tag{8}$$

which includes the two pressure integrals, α and β, of Figure 14d. Introducing the shock standoff distance, XP, and substituting for the pressure integrals, Equation (8) becomes:

$$\frac{F}{P_\infty h} = \frac{P1-P_\infty}{(P_\infty)}\left(\frac{XP}{h}\right)\left(\frac{\Delta XS}{XP}\ \alpha + \frac{XS}{XP}\ \beta\right) \tag{9}$$

where the two integral expressions, α and β, have constant values of 0.400 and 0.969, respectively.

By a similar analysis based upon an inviscid, turning flow wedge model (the separation region is replaced with a wedge), the control force may be calculated as:

$$\frac{F}{P_\infty h} = \left(\frac{P1-P_\infty}{P_\infty}\right)\left(\frac{XS}{h}\right) \tag{10}$$

Using the following approximations of Zukoski (Ref. (1))

$$\frac{P1-P_\infty}{P_\infty} = \frac{M_\infty}{2} \tag{11}$$

and

$$\frac{XS}{h} = 4.2 \tag{12}$$

Equation (10) reduces to:

$$\frac{F}{P_\infty h} = 2.1\ M_\infty \tag{13}$$

and is shown plotted in Figure 19 for $h/\delta > 1.5$.

The control force results, obtained by integrating the experimental pressure distributions, are also presented in Figure 19 as a function of h/δ. Note that these experimental results, $F/P_\infty h$, increase with increasing Re/L and h/δ and indicate that for $h/\delta > 1.5$, the dimensionless force approaches the results of (13) above. For this approach to be true, however, Equation (9) must reduce to Equation (10). Quite obviously, two conditions must be satisfied: First, XP must approach XS as h/δ exceeds 1.5, and secondly, the ratio $\Delta XS/XP$ must approach zero as h/δ exceeds 1.5. These two trends have already been demonstrated by the data in Figure 16. As a result, the pressure coefficient term, $(\Delta XS/XP\ \alpha + XS/XP\ \beta)$, in Equation (9) also approaches 1.0 as $h/\delta > 1.5$. Figure 20 simply verifies this fact. Hence, Equation (9) reduces to Equation (10) as $h/\delta > 1.5$.

CONCLUSION

The pressure distributions measured in the separated region ahead of steps were found to be functions of both Re_δ and h/δ for the turbulent boundary-layer separation case where $h < \delta$. Since the induced side forces are determined from these same pressure distributions, these forces are also functions of Re_δ and h/δ. The major result of this study is the definition of a universal pressure distribution valid for two-dimensional steps.

Three geometric lengths, ΔXS, XS, and XP were defined. The ratio, XP/h, was interpreted as the cotangent of the wedge angle necessary to produce the plateau pressure, P1. By definition, XP locates the inviscid shock relative to the step face. Since the wedge angle is known, the shock angle, itself, is satisfactorily computed using the two-dimensional oblique shock relations.

The ratios ΔXS/XP and XS/XP are indicative of the fractional distances necessary for the occurrence of the initial steep pressure rise and for the extent of the separated region, respectively. This last point should perhaps be further qualified. Zukoski's separation criterion (Ref. (1) as used for this study locates a point on the pressure signature which must be interpreted as a scale change point, not necessarily a separation point as the title of this criterion would suggest. The separation point per se is not known.

The difference between XP and the sum, (ΔXS + XS), while a constant for this study, is believed to be functionally dependent upon the actual boundary-layer thickness, δ, and the turbulent boundary-layer profile exponent, n.

REFERENCES

(1) Zukoski, Edward E., "Turbulent Boundary-Layer Separation in Front of a Forward-Facing Step," AIAA Journal, Vol. 5, No. 10, pp. 1746-1753, Oct 1967.

(2) Hahn, J. S., "Experimental Investigation of Turbulent Step-Induced Boundary-Layer Separation at Mach Numbers 2.5, 3 and 4," AEDC-TR-69-1, Mar 1969.

(3) Bogdonoff, S. M., "Some Experimental Studies of the Separation of Supersonic Turbulent Boundary Layers," Princeton University, Report 336, Jun 1955.

(4) Chapman, D. R., Kuehn, D. M., and Larson, H. K., "Investigation of Separated Flows in Supersonic and Subsonic Streams with Emphasis on the Effect of Transition," NACA TN 3869, Mar 1957.

(5) Werle, M. J., Driftmyer, R. T., and Shaffer, D. G., "Two-Dimensional Jet Interaction with a Mach 4 Mainstream," NOLTR 70-50, May 1970.

(6) Lee, R. E., Yanta, W. J., Leonas, A. C., and Carner, J. W., "The NOL Boundary Layer Channel," NOLTR 66-185, Nov 1966.

(7) Kendall, J. M., "Portable Automatic Data Recording Equipment (PADRE)," NAVORD Report 4207, Aug 1959.

(8) Spaid, Frank W. and Frishett, J. C., "Incipient Separation of a Supersonic, Turbulent Boundary Layer, Including Effects of Heat Transfer," AIAA Journal, Vol. 10, No. 7, pp. 915-922, Jul 1972.

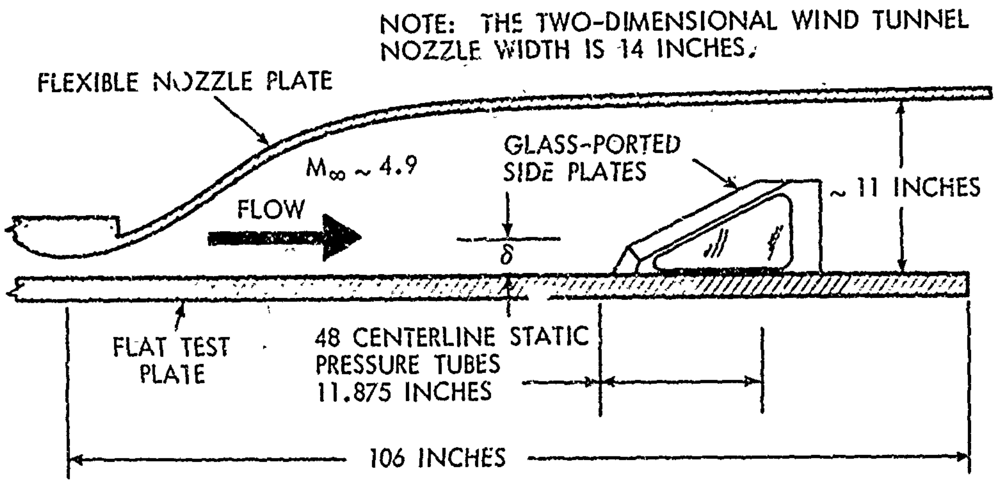

FIG. 1 THE TWO-DIMENSIONAL BOUNDARY LAYER CHANNEL'S ADJUSTABLE NOZZLE SHOWING THE GLASS-PORTED SIDE PLATES INSTALLED

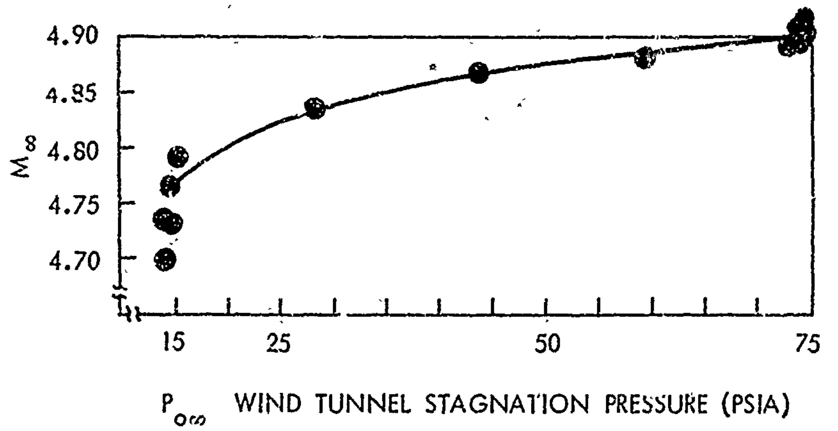

(a) THE TEST SECTION MACH NUMBER VARIATION AS A FUNCTION OF THE WIND TUNNEL SUPPLY PRESSURE

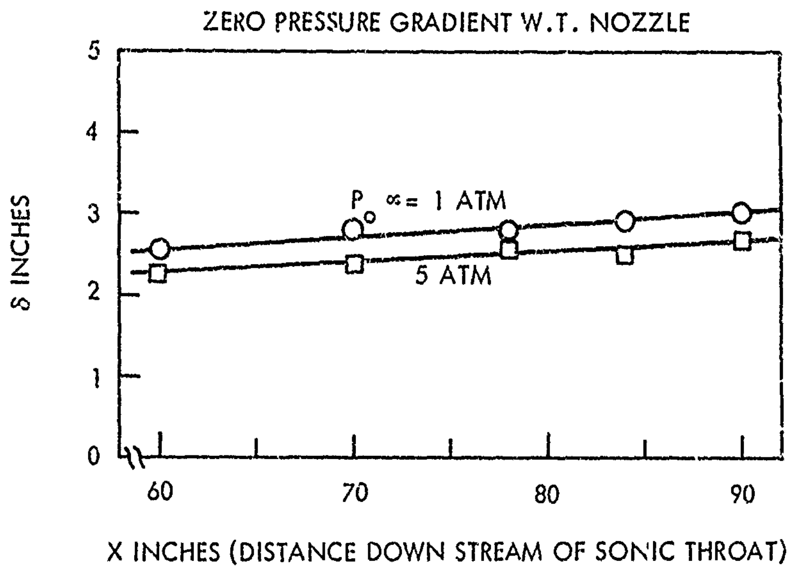

(b) THE BOUNDARY LAYER THICKNESS DISTRIBUTION ALONG THE FLAT TEST PLATE

FIG. 2 MACH NUMBER AND BOUNDARY LAYER THICKNESS VARIATIONS WITH WIND TUNNEL SUPPLY PRESSURE

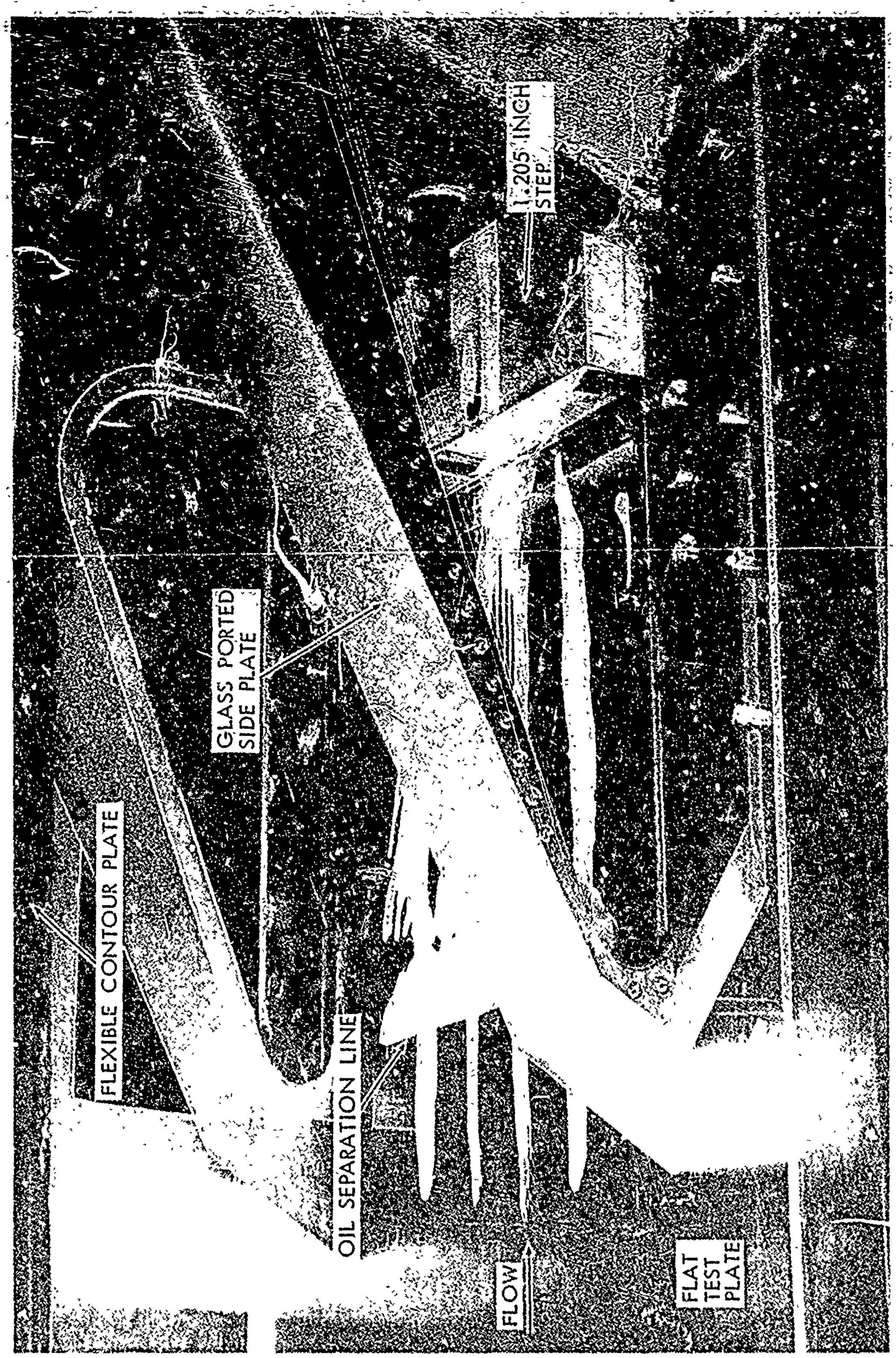

FIG. 3 STEP MODEL (WITH END PLATES) INSTALLED IN THE TEST SECTION

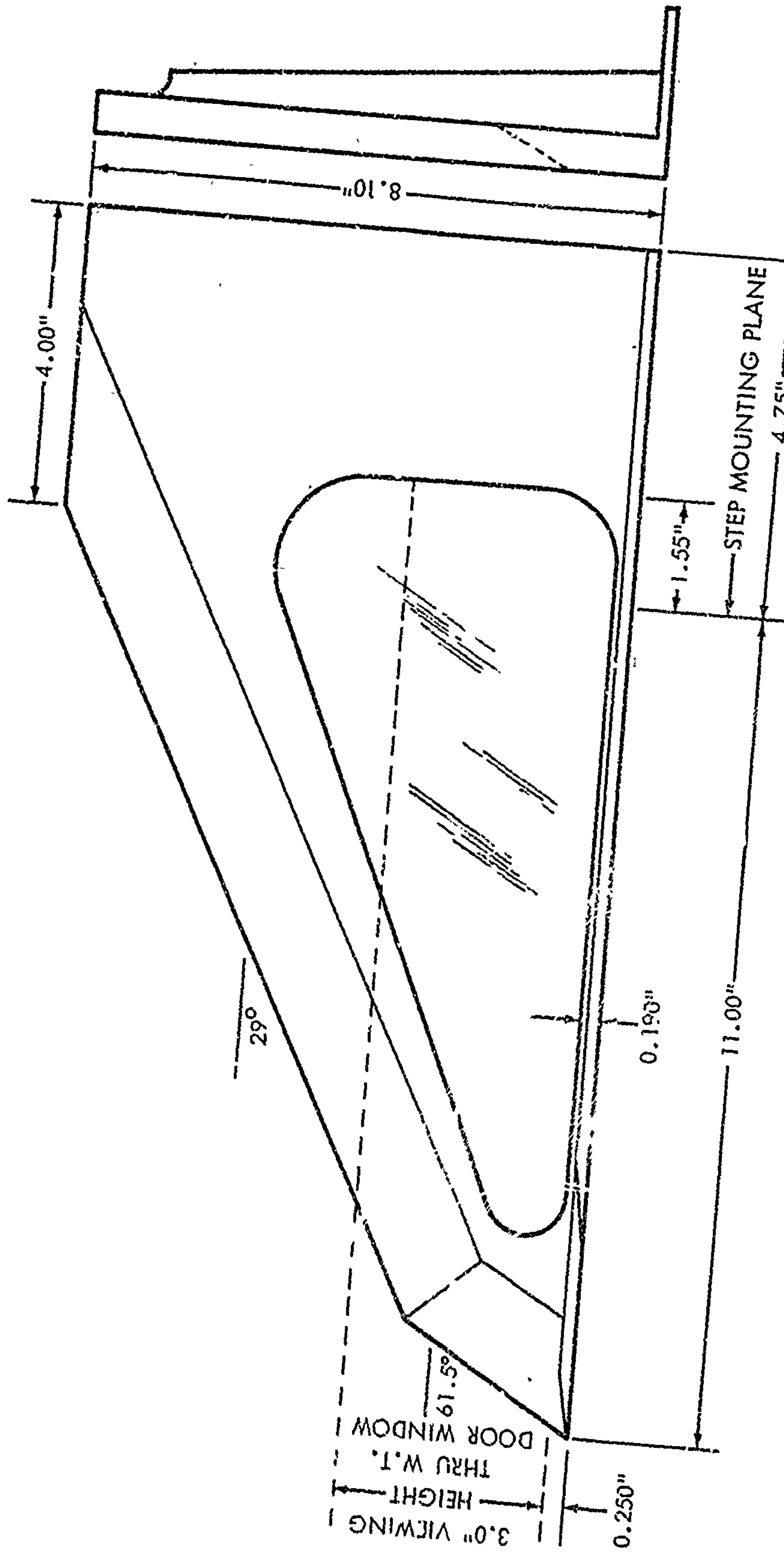

FIG. 4 END PLATE DETAIL

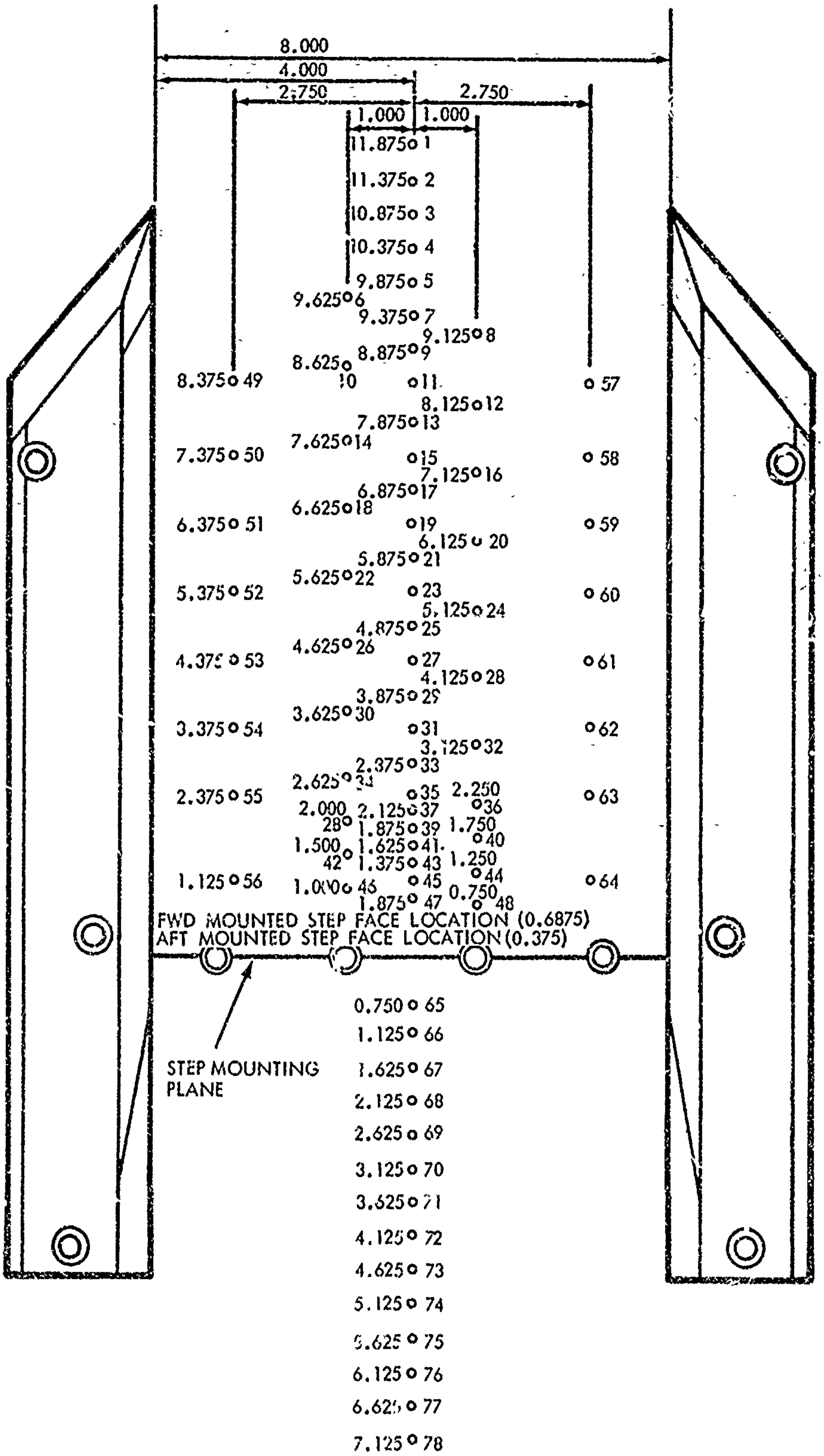

FIG. 5 FLAT PLATE SURFACE PRESSURE TAP IDENTIFICATION NUMBERS AND HOLE LOCATIONS RELATIVE TO THE END PLATES AND STEP MOUNTING PLANE

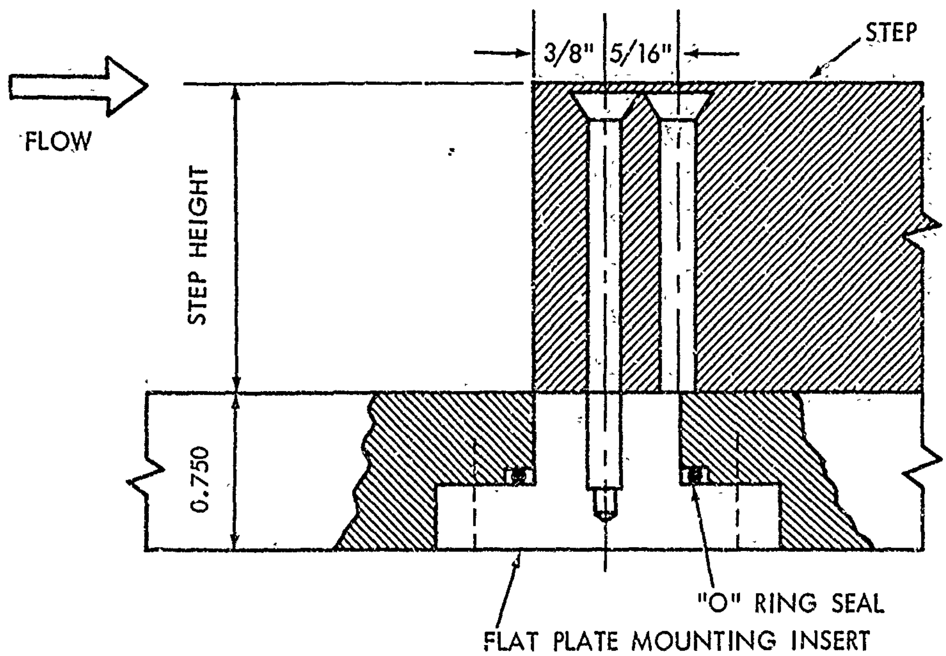

A SECTIONAL SIDE VIEW SHOWING THE DETAILS OF THE STEP ATTACHED TO THE FLAT TEST PLATE

TEST STEP HEIGHTS h = 1.502, 1.400, 1.205, 0.903, 0.603, 0.247, AND 0.130 INCHES

FIG. 6 FORWARD FACING STEP MOUNTING DETAIL

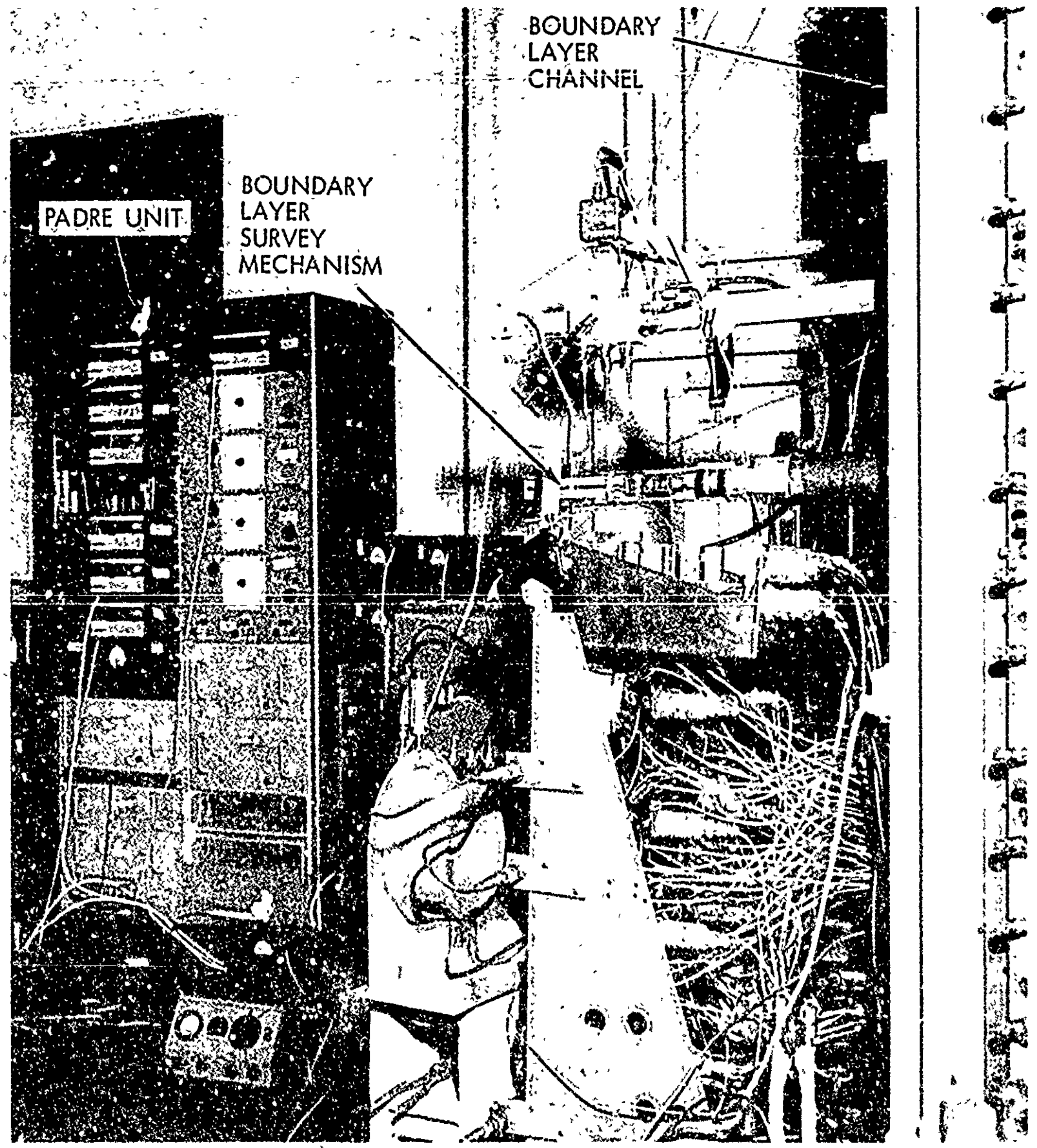

FIG. 7 SCANNER VALVE ARRANGEMENT AND RECORDING UNIT

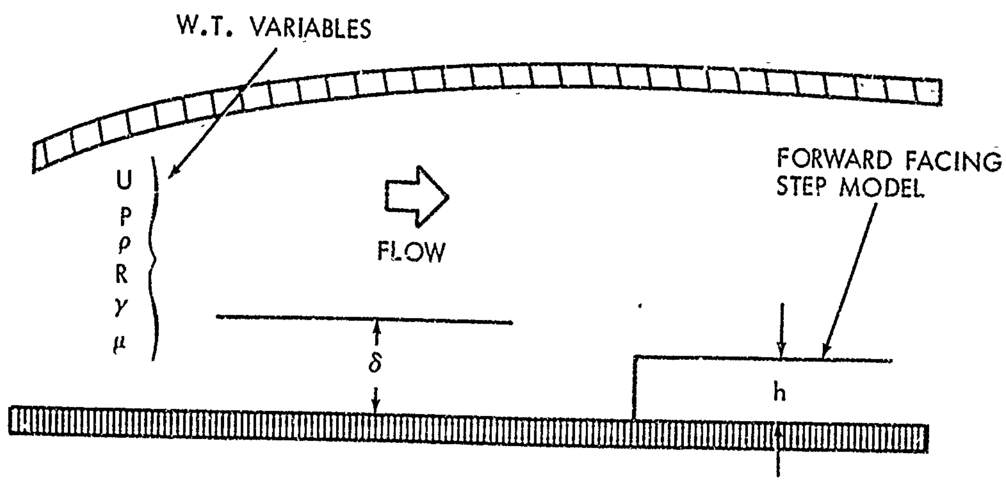

FIG. 8 BOUNDARY LAYER CHANNEL AND STEP MODEL CONFIGURATION

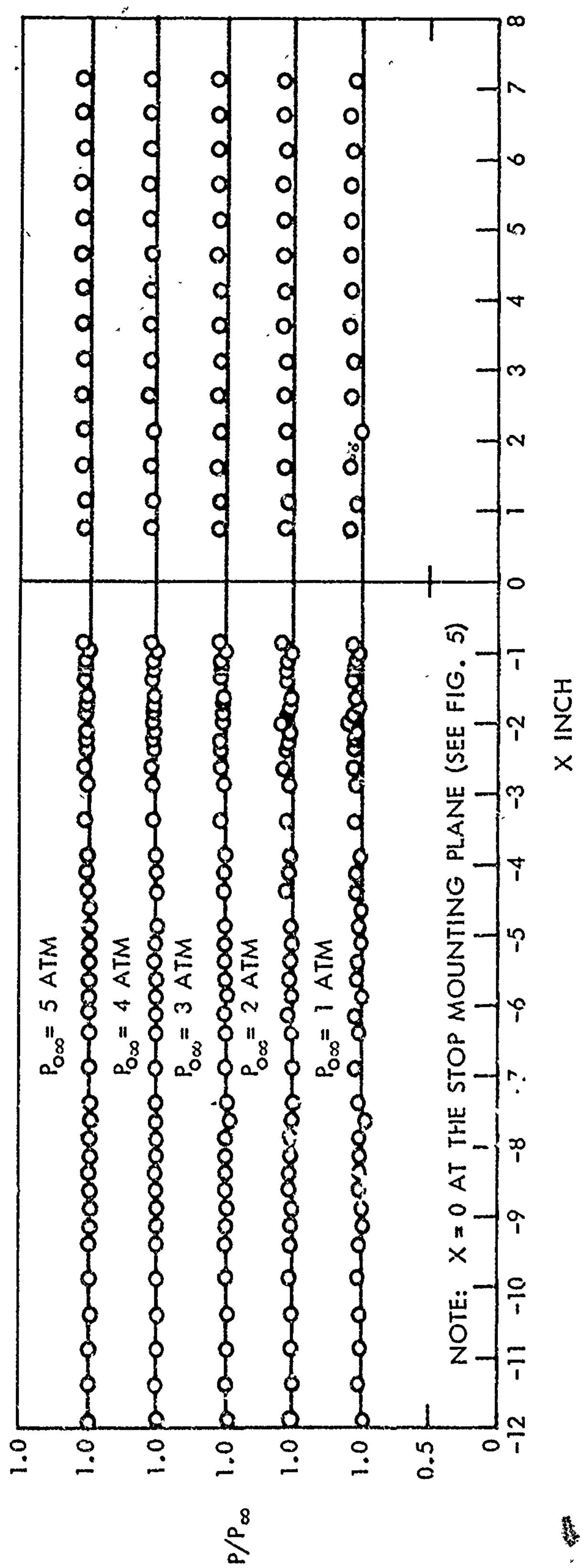

FIG. 9 TEST SECTION STATIC PRESSURE MEASUREMENTS WITH SIDE PLATES AND WITHOUT STEPS

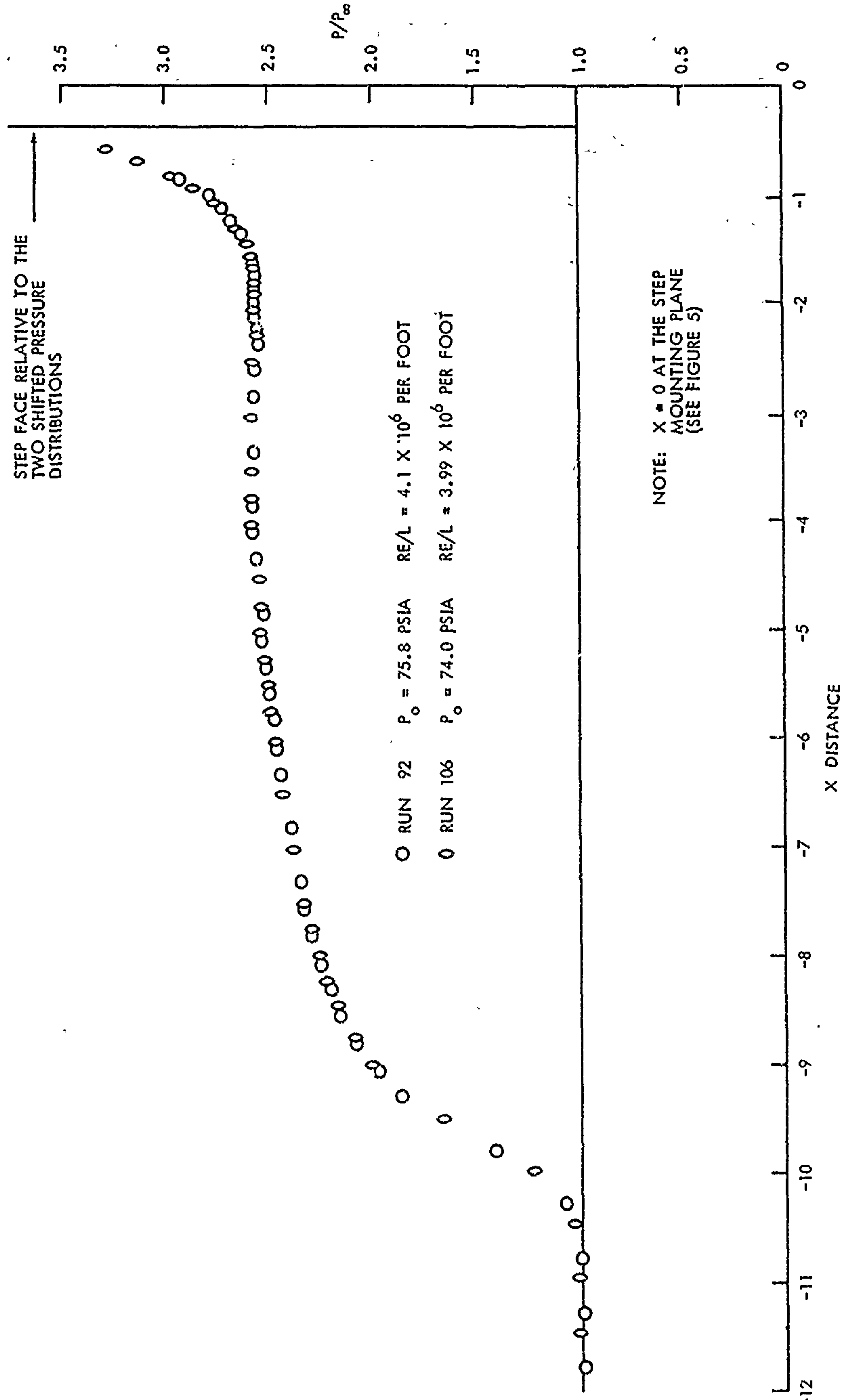

FIG. 10 TYPICAL REPEATED PRESSURE DISTRIBUTIONS WITH STEP FACE SHIFTED USING ALTERNATE MOUNTING HOLES

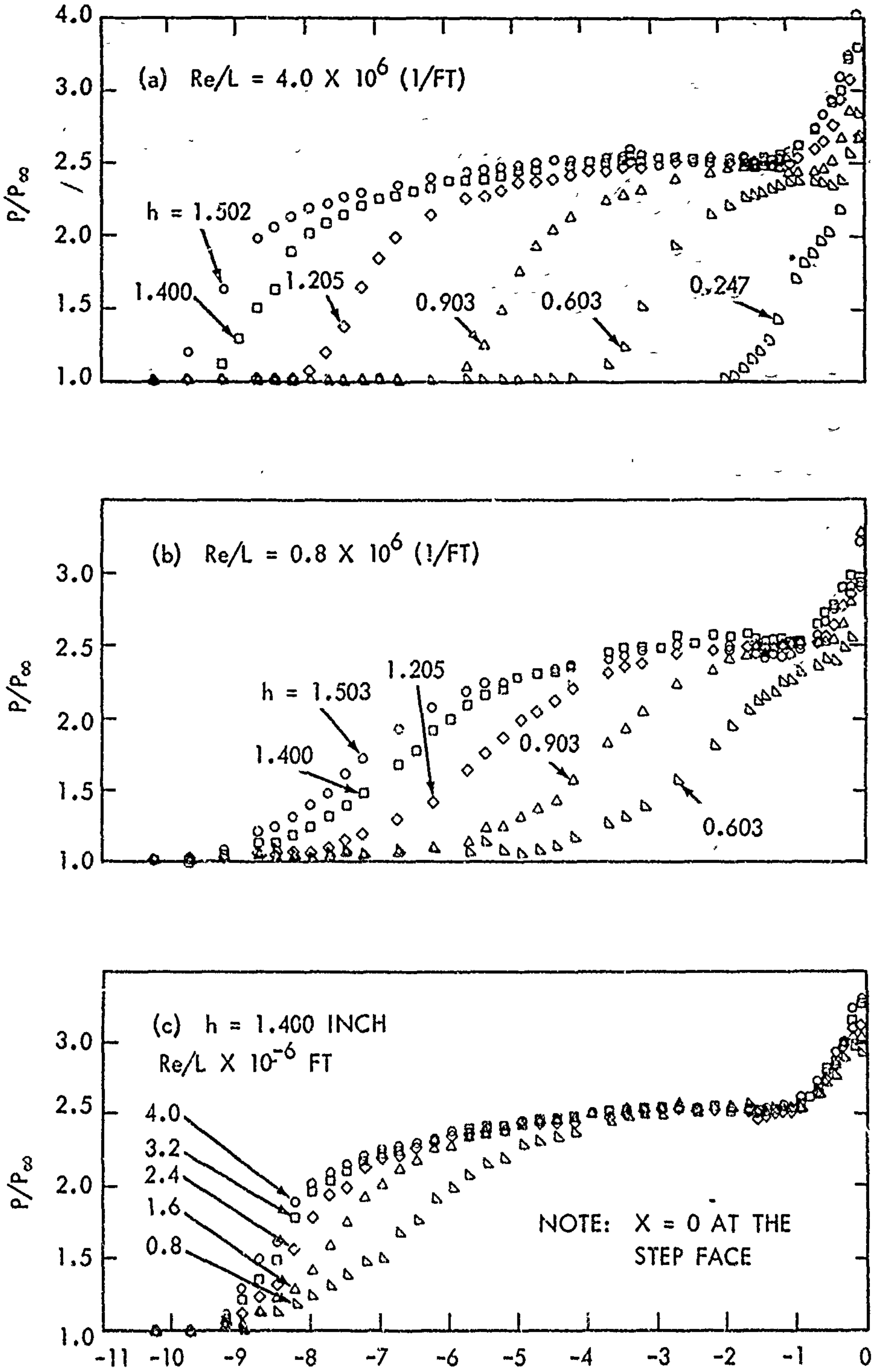

FIG. 11 STEP HEIGHT AND REYNOLDS NUMBER INFLUENCE UPON THE PRESSURE DISTRIBUTION

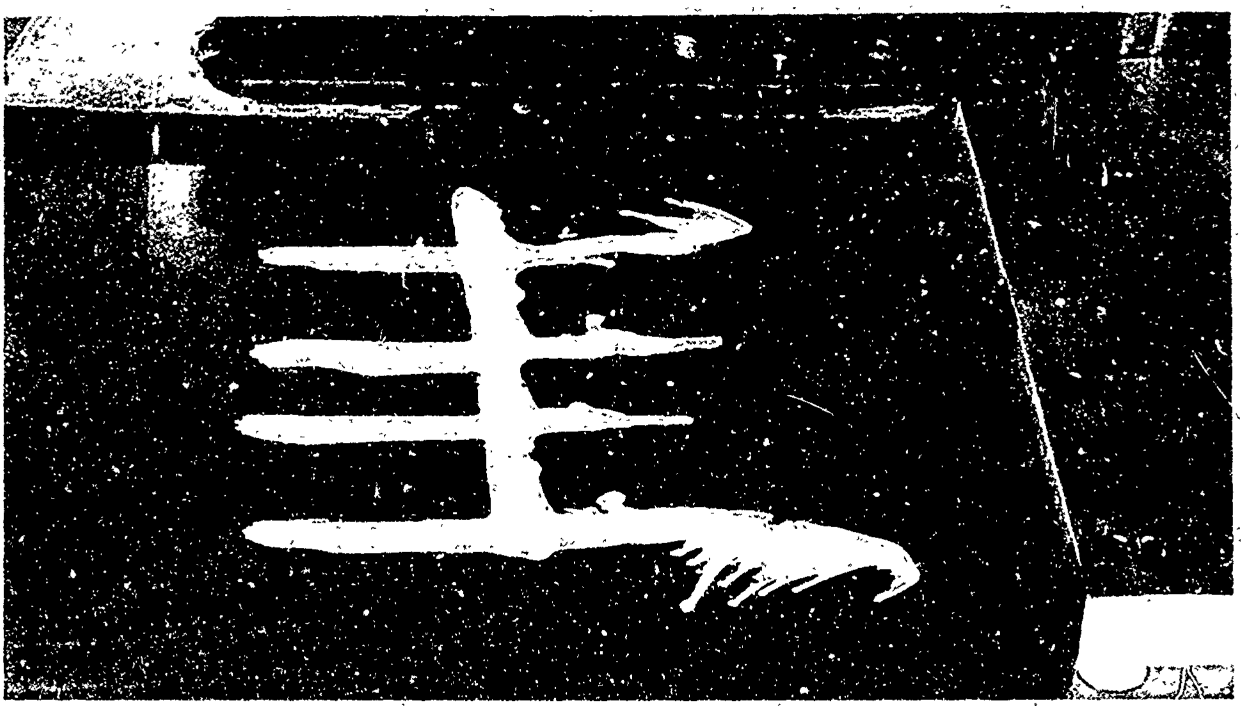

h = 0.903 INCH T_o = 592°R
P_o = 5 ATM X_{OIL} = 5.50 INCHES

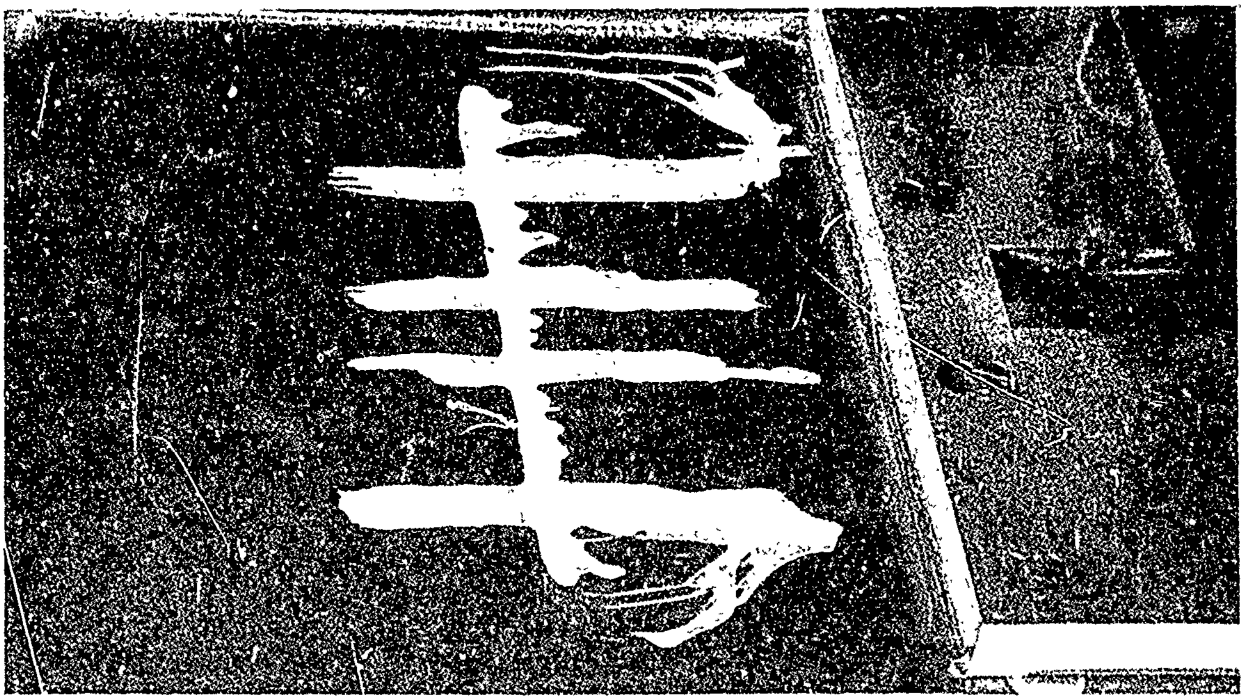

h = 0.603 INCH T_o = 592°R
P_o = 5 ATM X_{OIL} = 3.50 INCHES

FIG. 12 OIL FLOW SEPARATION STUDY (CONTINUED)

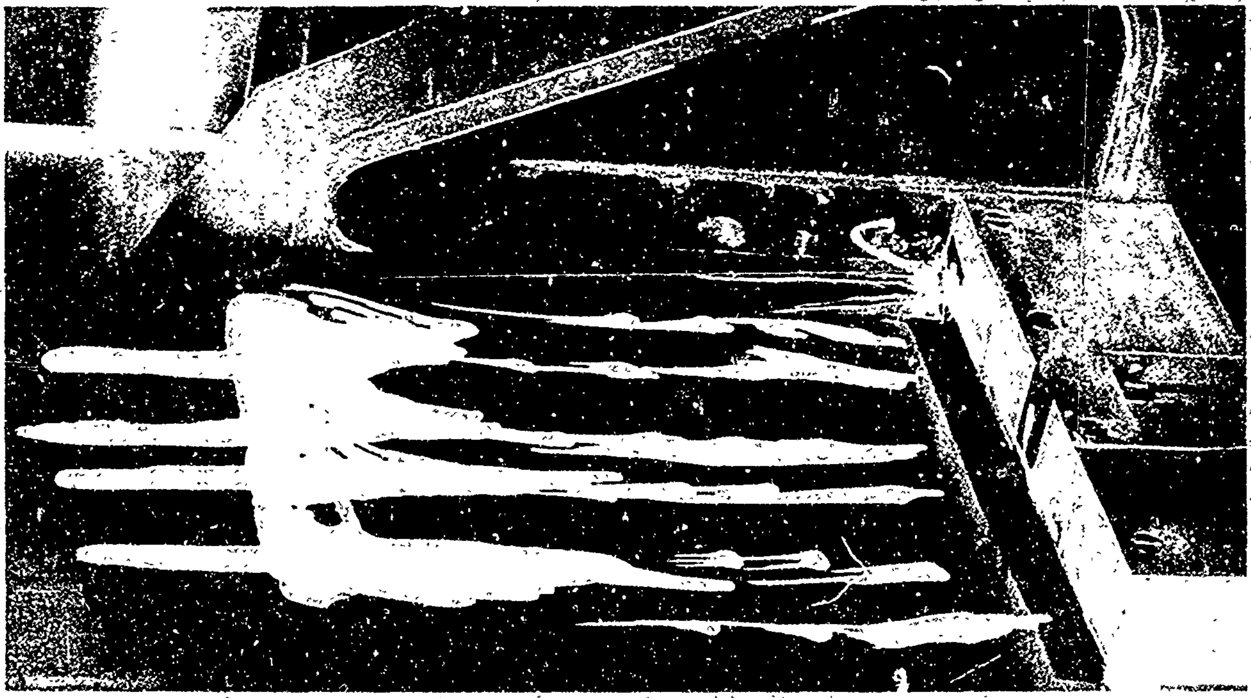

h = 1.502 INCHES T_o = 592°K
P_o = 5 ATM X_{OIL} = 9.750 INCHES

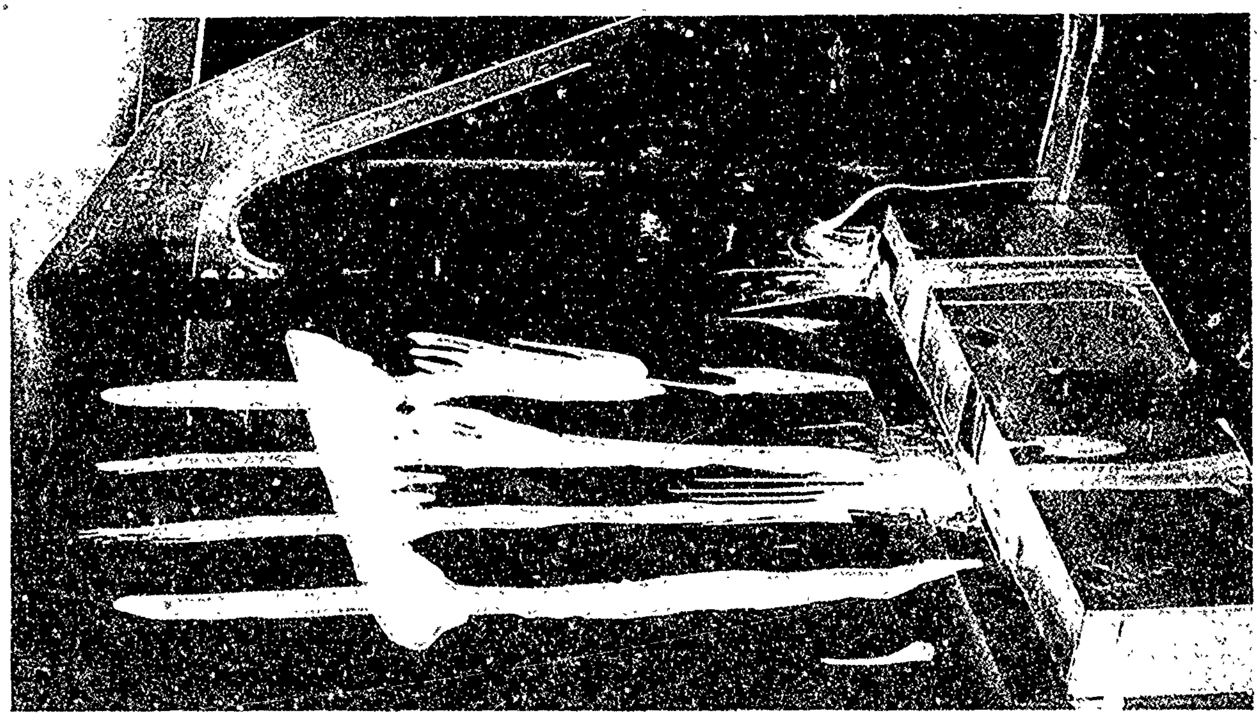

h = 1.205 INCHES T_o = 592°R
P_o = 5 ATM X_{OIL} = 7.70 INCHES

FIG. 12 OIL FLOW SEPARATION STUDY

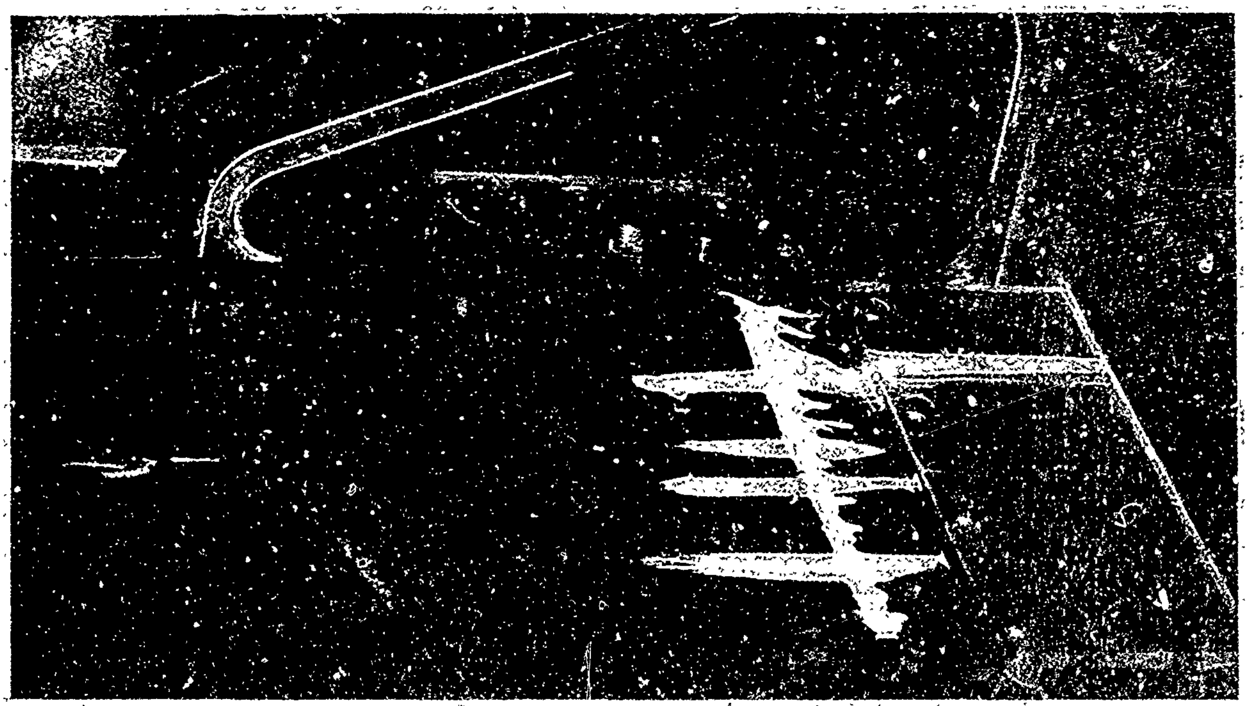

h = 0.247 INCH T_o = 592°R

P_o = 5 ATM X_{OIL} = 1.5 INCHES

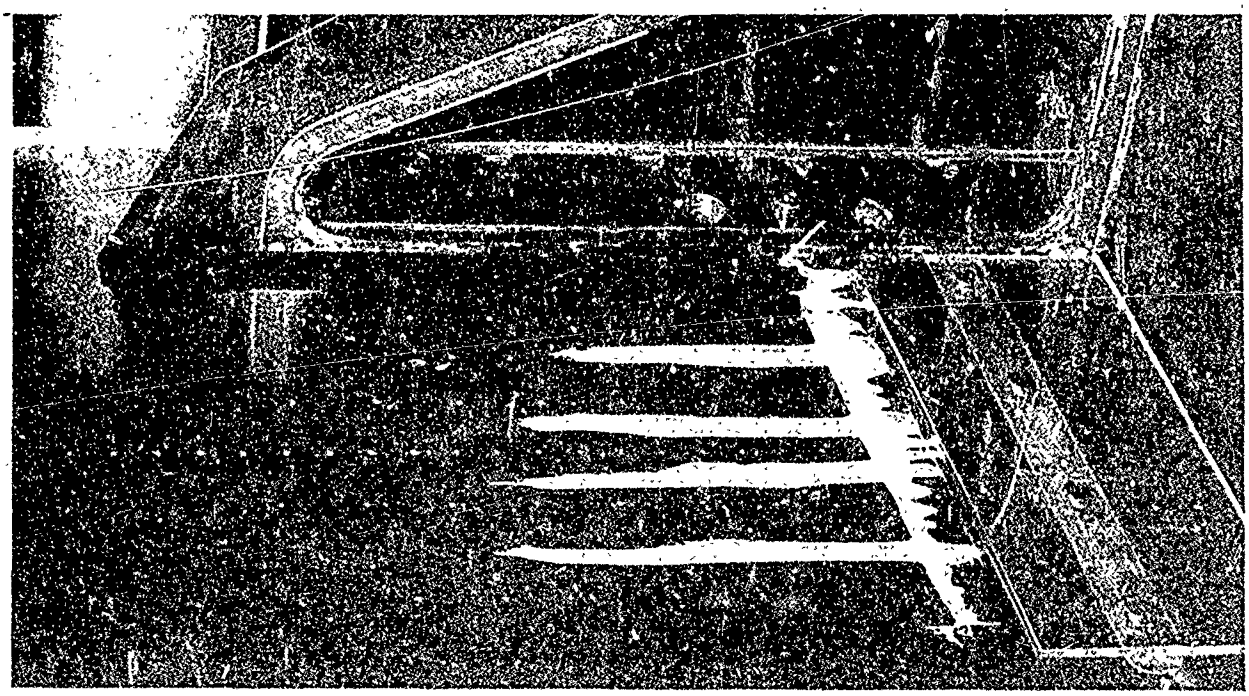

h = 0.130 INCH T_o = 592°R

P_o = 5 ATM X_{OIL} = 0.90 INCH

FIG. 12 OIL FLOW SEPARATION STUDY (CONCLUDED)

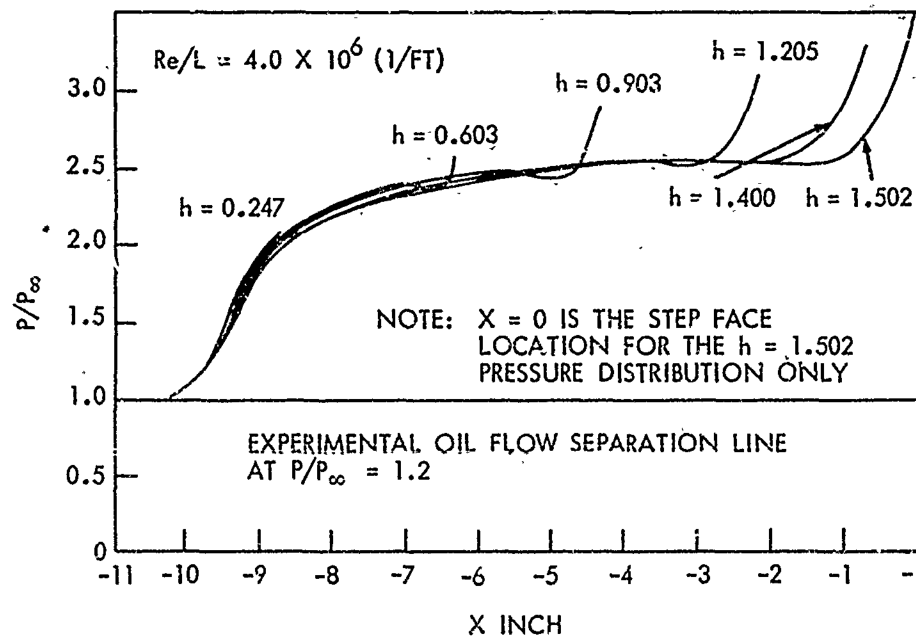

FIG. 13 SIMILAR PRESSURE DISTRIBUTIONS

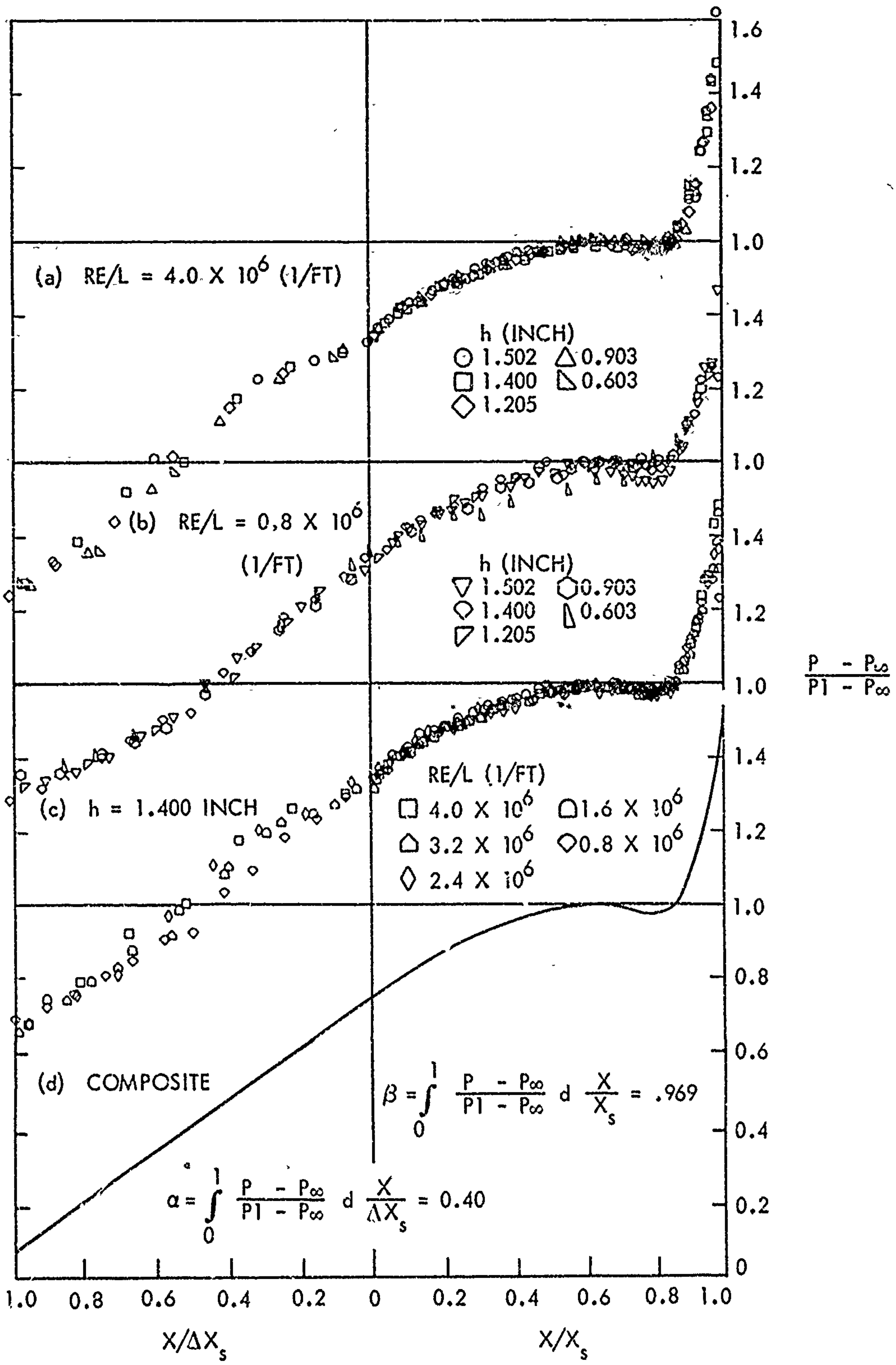

FIG. 14 THE UNIVERSAL PRESSURE DISTRIBUTION

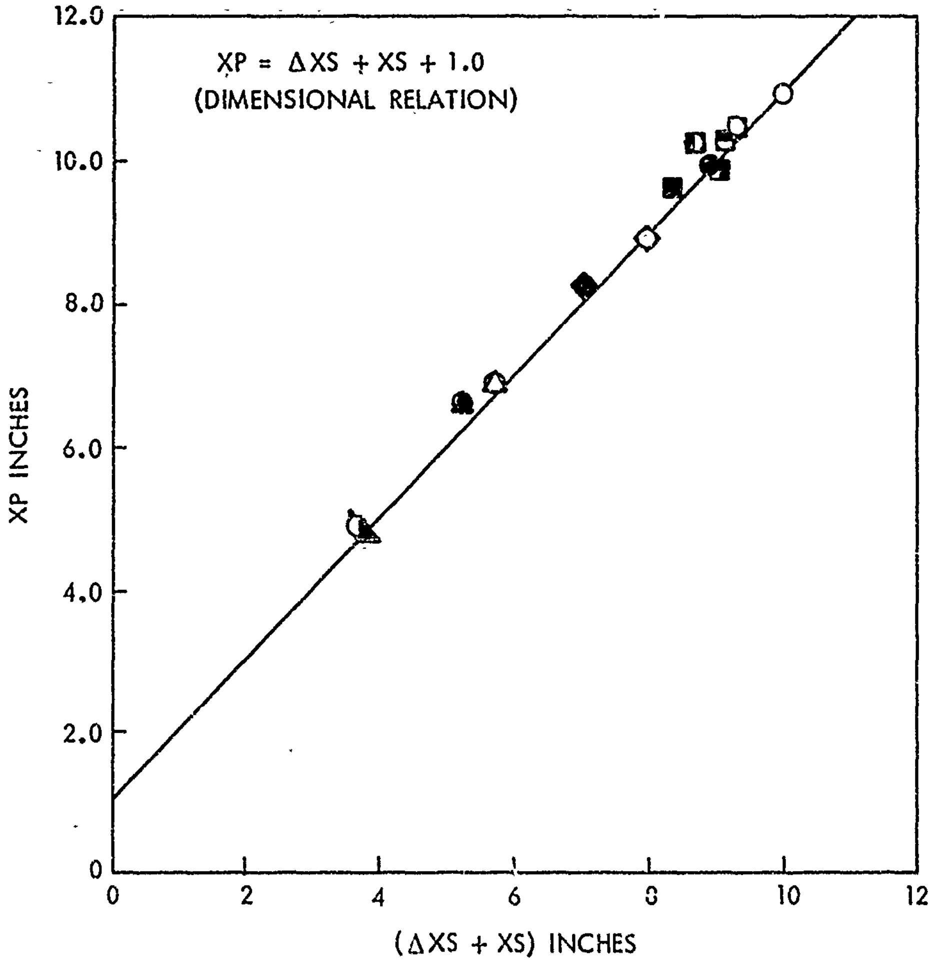

FIG. 15 THE DIFFERENCE CORRELATION

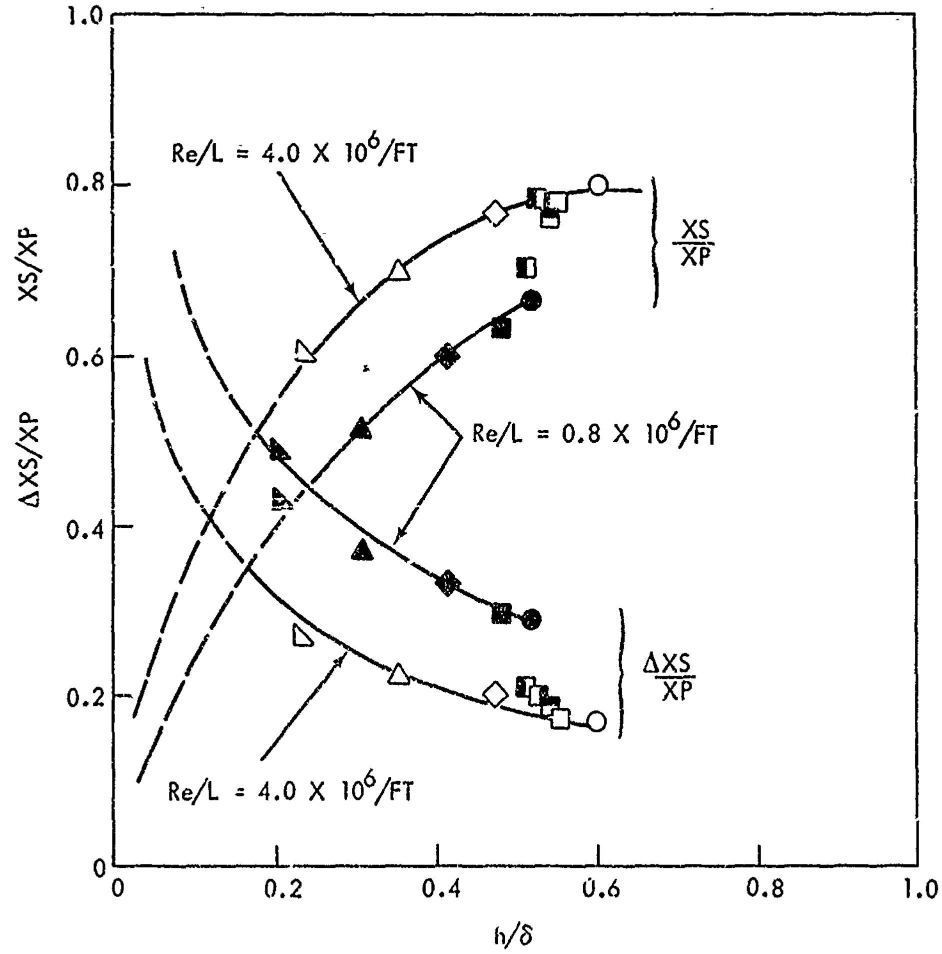

FIG. 16 THE DEPENDENCE OF THE GEOMETRIC VARIABLES WITH THE DIMENSIONLESS STEP HEIGHT

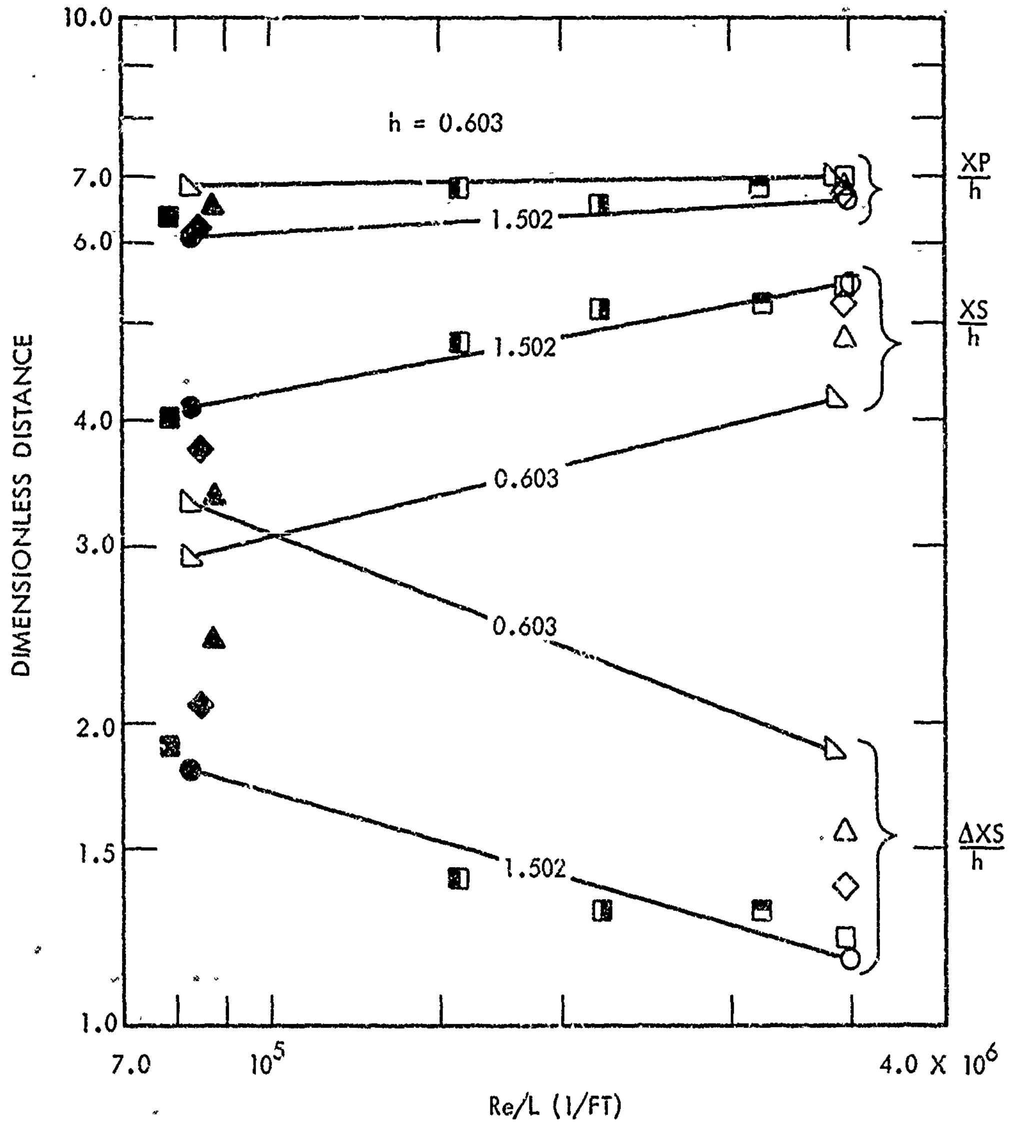

FIG. 17 DIMENSIONLESS DISTANCES CORRELATED WITH UNIT REYNOLDS NUMBER

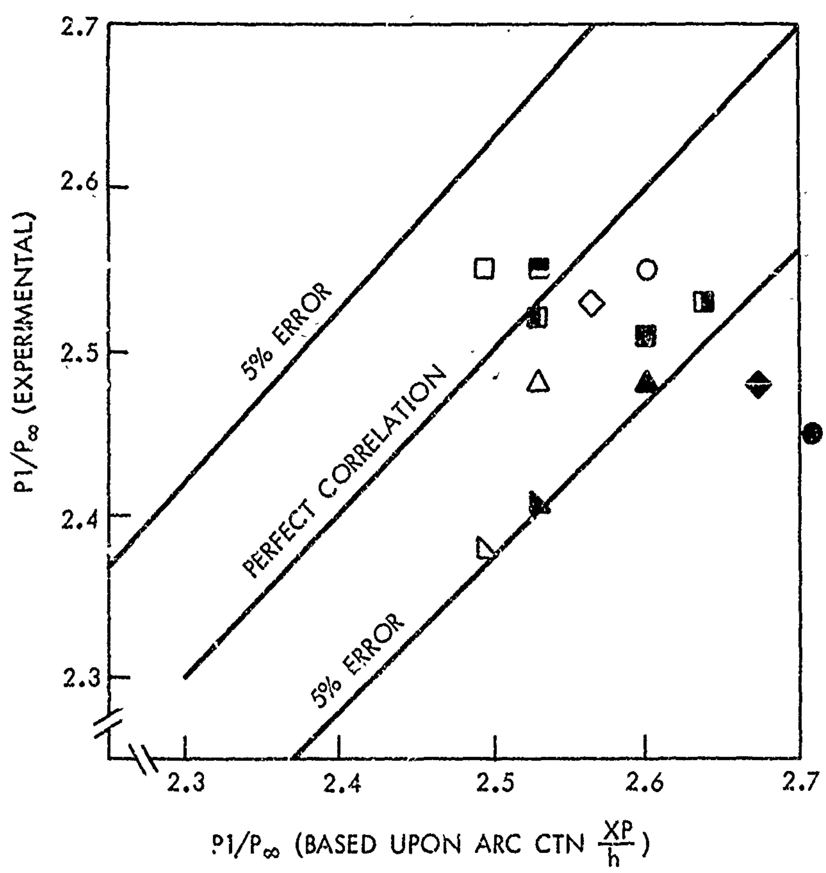

FIG. 18 EXPERIMENTAL PLATEAU PRESSURES COMPARED WITH CALCULATED VALUES BASED UPON ARC CTN (XP/h)

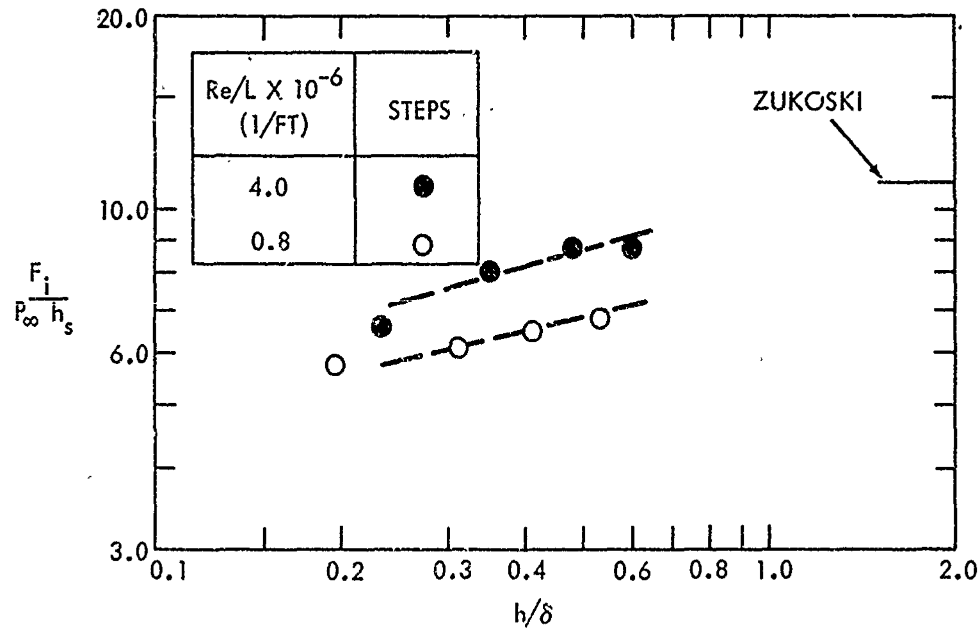

FIG. 19 THE DIMENSIONLESS FORCE, EVALUATED BY INTEGRATING THE PRESSURE DISTRIBUTIONS, COMPARED WITH ZUKOSKI'S APPROXIMATION FOR $h/\delta \geq 1.5$

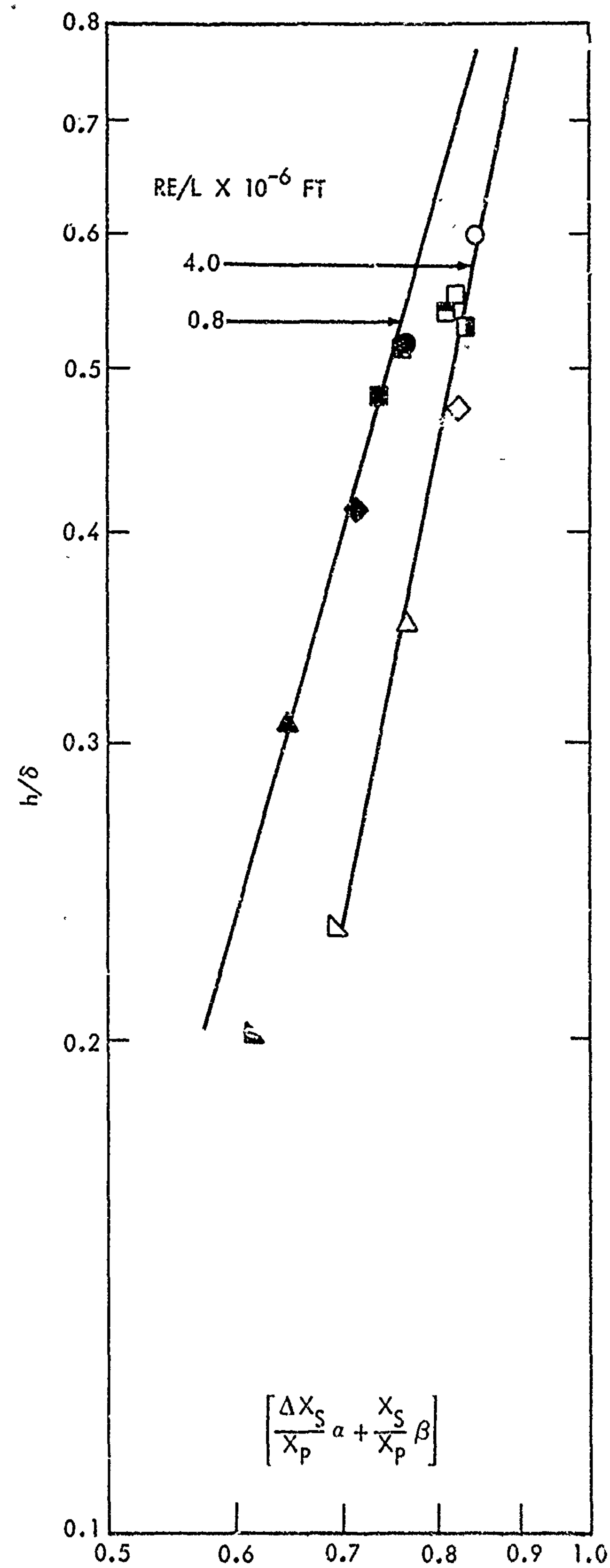

FIG. 20 THE VARIATION OF $\left[\frac{\Delta X_S}{X_P}\alpha + \frac{X_S}{X_P}\beta\right]$ WITH h/δ AND Re/L

APPENDIX A

FORWARD FACING STEP, TEST DATA

This appendix lists the experimental test data for the forward facing step test program. Photographs, taken during the tests, may be identified with the corresponding data by means of the run number.

The reader should be cautioned that visible oil streaks (in addition to the obvious crack in the glass) appear in some of the pictures cf., Runs 135 and 193. The source of this oil was the glass retaining ring located on the inside surface of the ported end plates. No effect was observed on the flow field as a result of this oil flow.

Starting with Run 193 and continuing through 196, a black elliptical shaped spot can be observed on the photographs. This spot was caused by the condensation of high humidity wind-tunnel room air on the outside of the wind-tunnel window. The picture of Run 197, without the black spot, was taken after the condensation was evaporated by surface blowing on the outside of the wind-tunnel door window.

TABLE A-1 EXPERIMENTAL DATA

RUN NUMBER

PARAMETER	106	107	134	135
h (inch)	1.502	1.502	1.205	1.205
M	4.902	4.675	4.903	4.732
P_o (psia)	73.97	14.04	73.49	14.71
T_o (°R)	592.	597.	594.	597.
$Re/L \times 10^{-6}$ (1/ft)	4.00	0.826	3.96	0.846

RUN NUMBER

PARAMETER	150	151	166	167
h (inch)	0.903	0.903	0.603	0.603
M	4.911	4.792	4.888	4.764
P_o (psia)	74.04	15.19	72.66	14.47
T_o (°R)	596.	589.	604.	598.
$Re/L \times 10^{-6}$ (1/ft)	3.96	0.871	3.83	0.819

RUN NUMBER

PARAMETER	180	193	194	195
h (inch)	0.247	1.400	1.400	1.400
M	4.886	4.893	4.881	4.866
P_o (psia)	72.57	73.48	59.26	43.85
T_o (°R)	591.	596.	594.	597.
$Re/L \times 10^{-6}$ (1/ft)	3.97	3.96	3.22	2.38

PARAMETER	RUN NUMBER 196	RUN NUMBER 197
h (inch)	1.400	1.400
M	4.834	4.735
P_o (psia)	28.40	13.85
T_o (°R)	596.	602.
Re/L x 10^{-6} (1/ft)	1.57	0.784

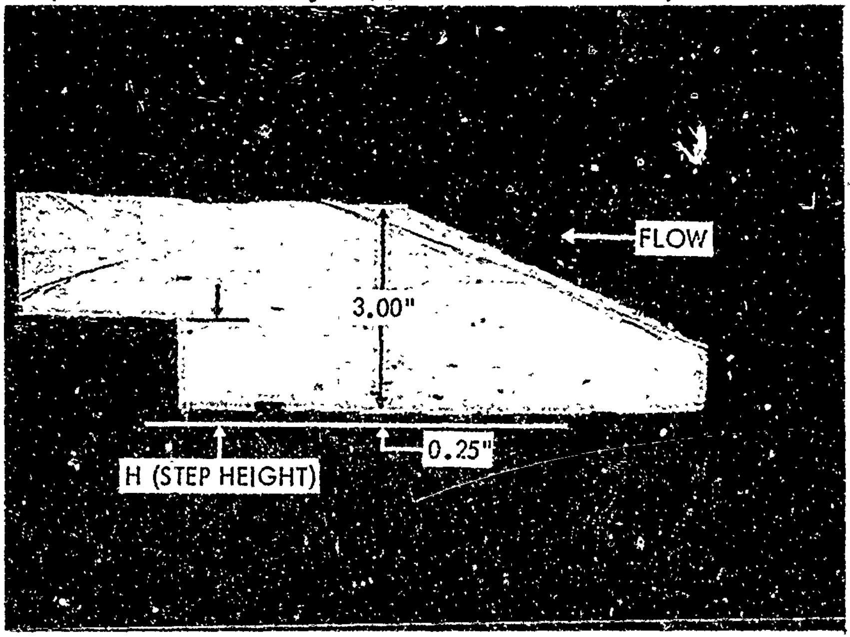

RUN 106

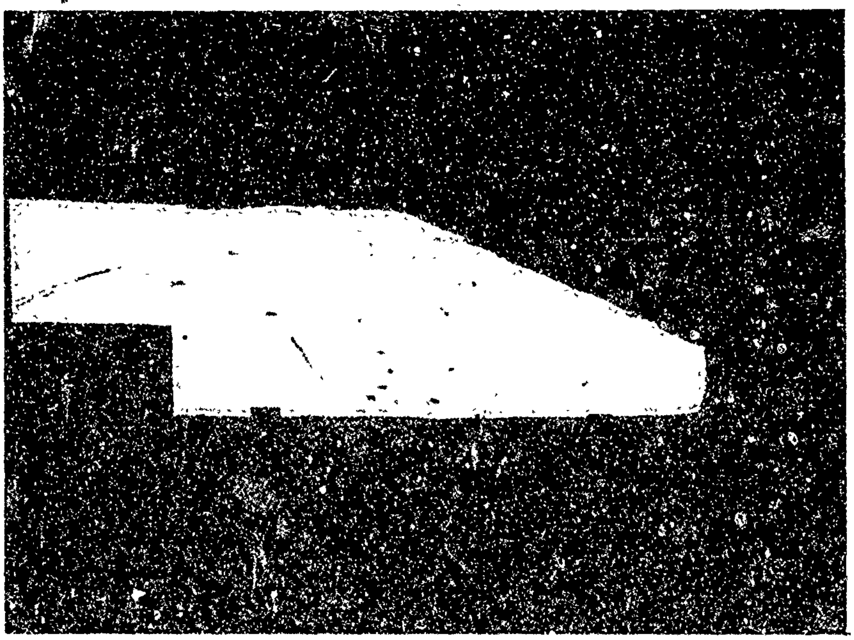

RUN 107

FIG. A-1, H 1.500 INCHES

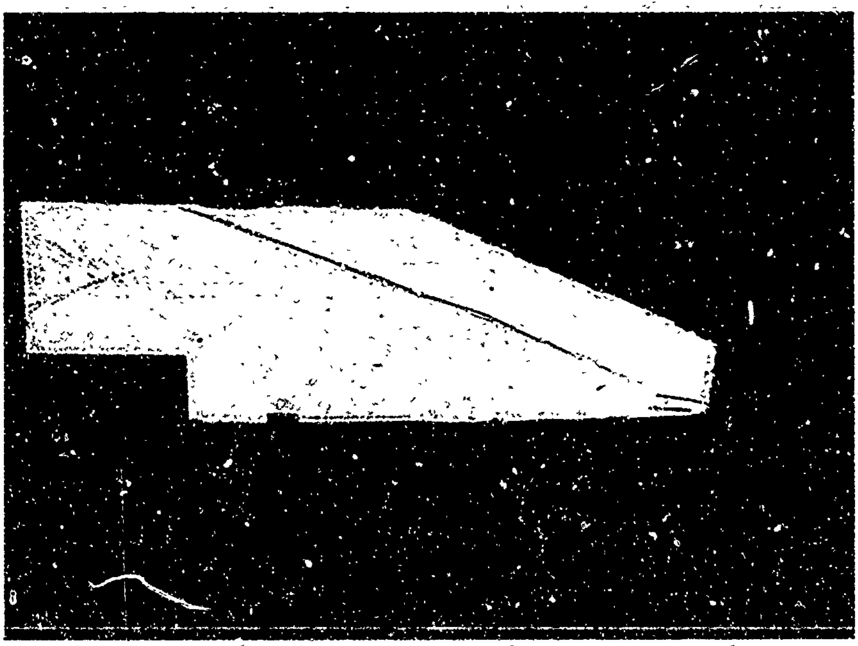

RUN 134

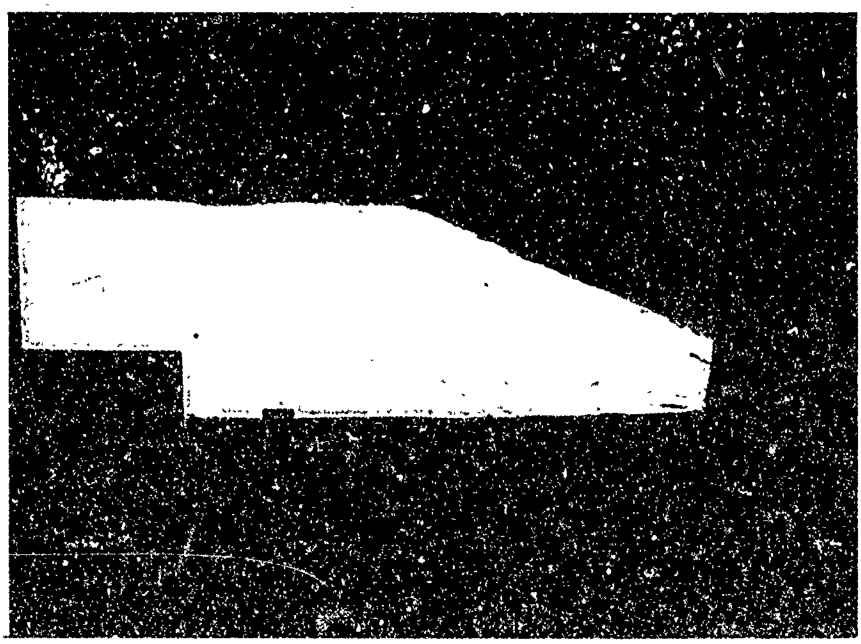

RUN 135

FIG. A-2, H 1.205 INCHES

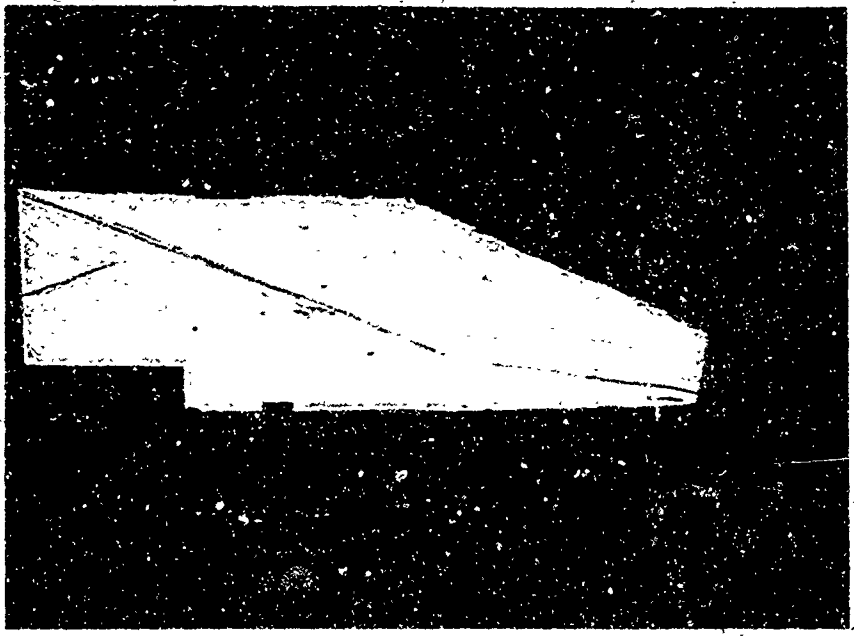

RUN 150

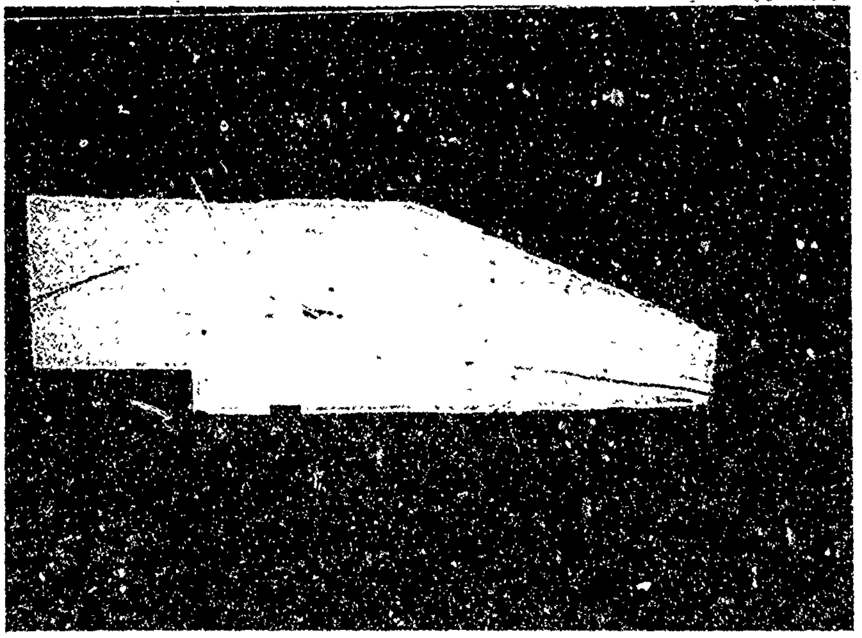

RUN 151

FIG. A-3 H 0.903 INCHES

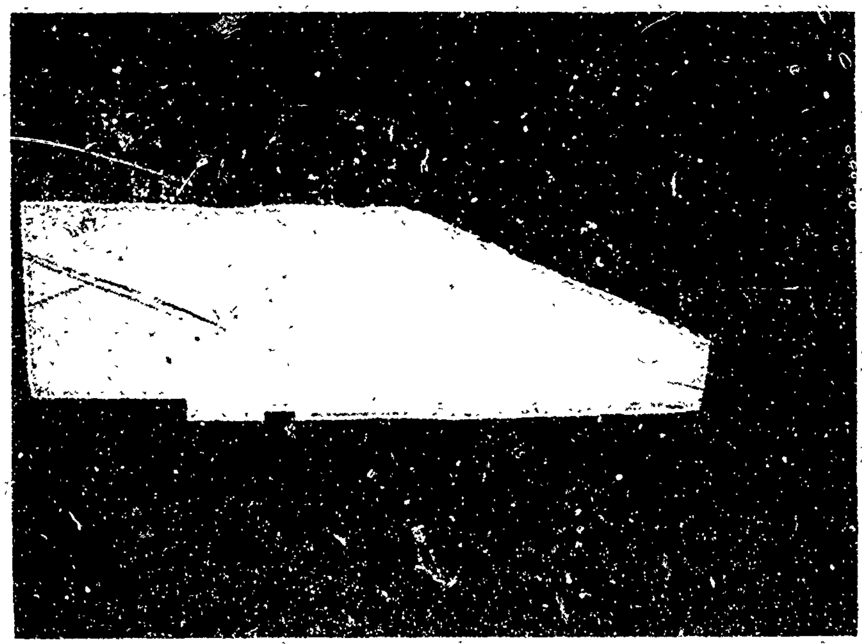

RUN 166

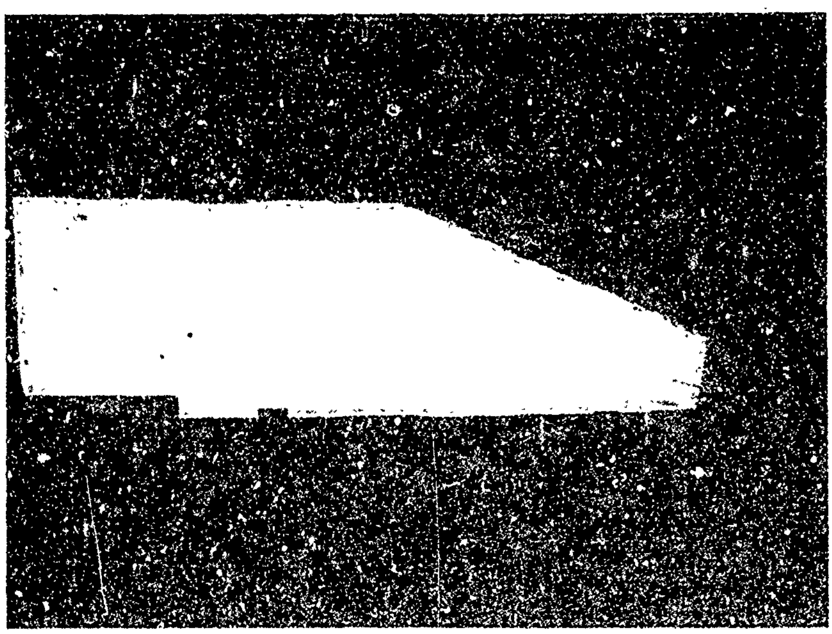

RUN 167

FIG. [illegible]

RUN 180

FIG. A-5, H = 0.247 INCHES

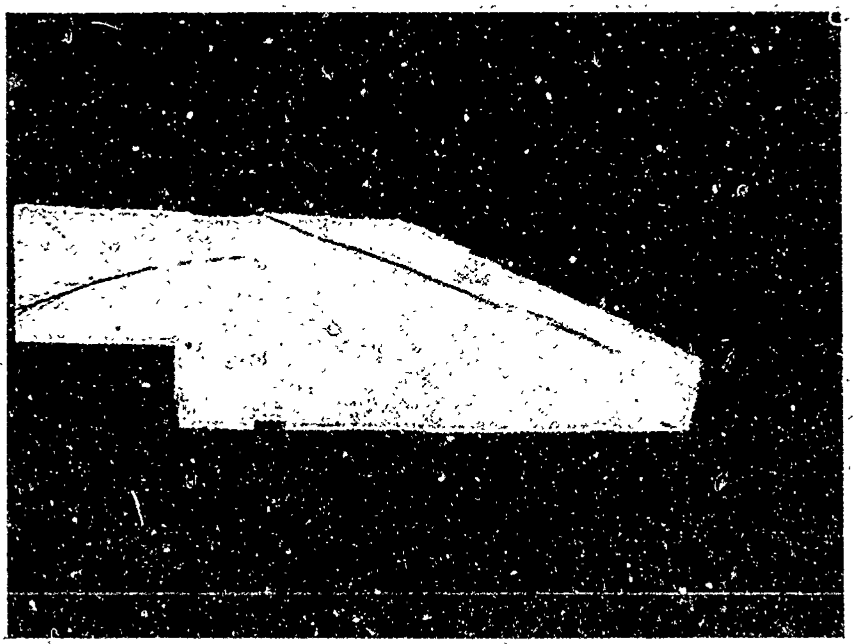

RUN 193

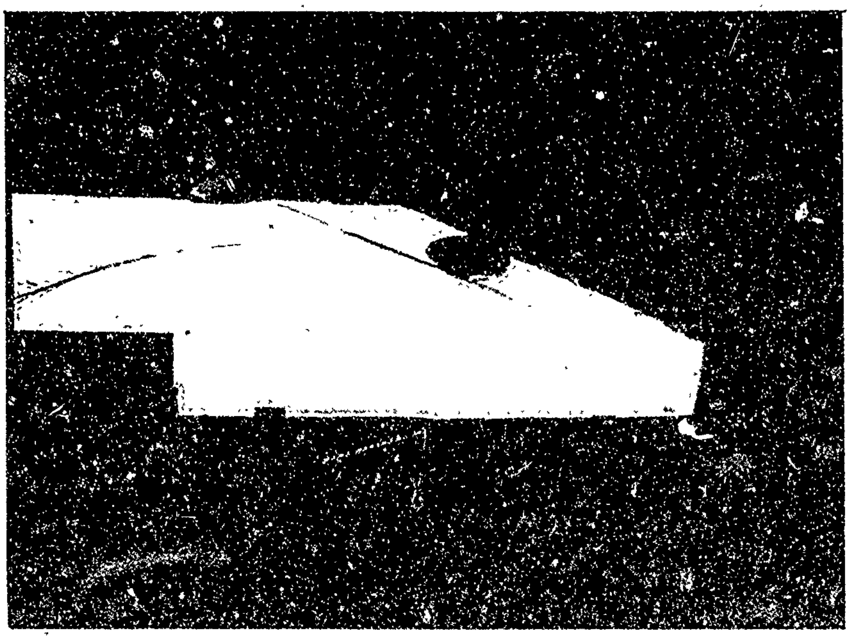

RUN 194

FIG. A-6, H = 1.400 INCHES

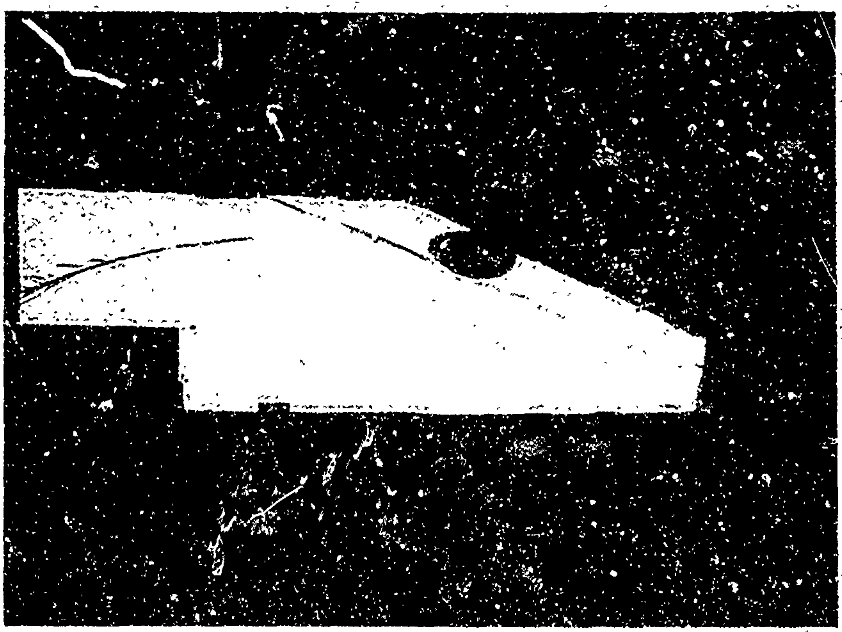

RUN 195

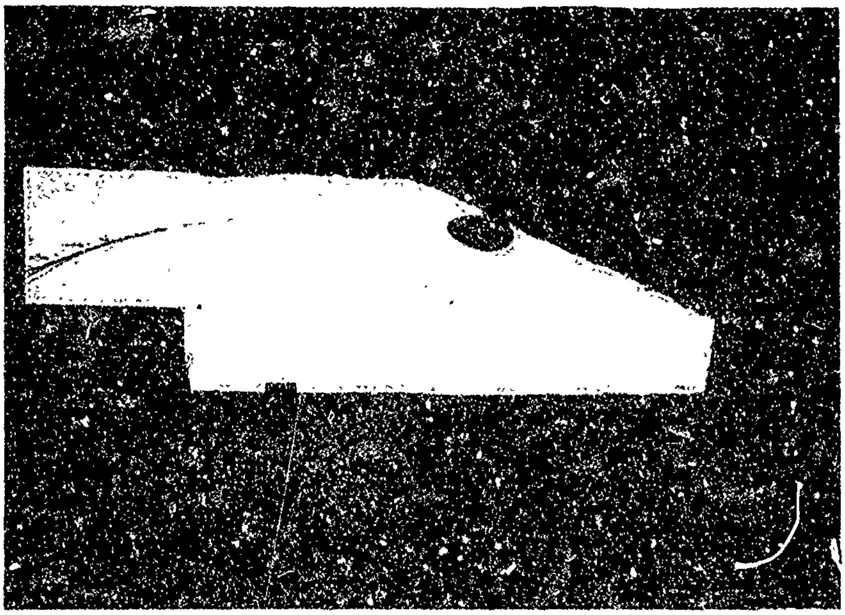

RUN 196

FIG. A-7, H 1.400 INCHES

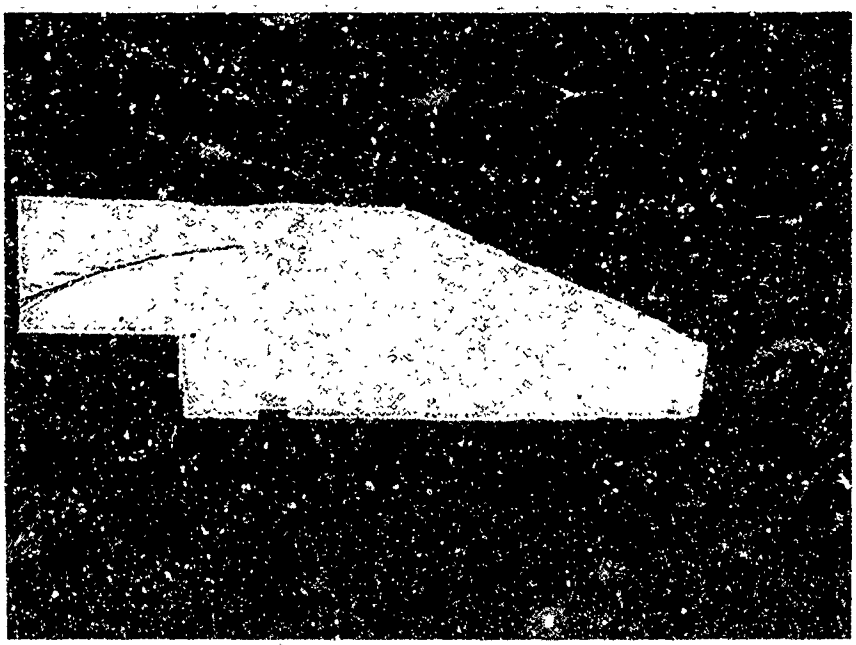

RUN 197

FIG. A-8, H 1.400 INCHES

APPENDIX B

THE BOUNDARY-LAYER DESCRIPTION

The description of the boundary layer ahead of the step is given in this Appendix. The character of the boundary layer is adequately described by graphs and tables for the two test Reynolds numbers of 4.0 x 10^6 and 0.8 x 10^6 per foot. The boundary-layer data is the result of probe surveys taken at two probing ports, located 48 and 60 inches downstream of the sonic throat of the NOL Boundary Layer Channel (Ref. (B-1)). The probe tips were located three inches ahead of the port location. Therefore, three inches must be subtracted from the 48- and 60-inch station values to determine the true physical location where the probe data apply. The leading static pressure tap (Number 1 in Fig. 5 of the text) in the test section was located at the 76.875-inch station. Measurements made at the two survey locations therefore represent the boundary-layer conditions located 19.875, i.e., 76.875 less 60.0 plus 3.0, and 31.875 inches upstream of this leading static pressure top position.

The reasons for presenting these data are two-fold. First, the character of the boundary layer is identified, and, second, numerical data are provided for those who might wish to study this step separation problem by numerical methods.

The variables recorded at each probing port included Pitot pressure, equilibrium temperature (Ref. (B-2)) and distance. The Boundary Layer Channel's stagnation pressure and temperature were also recorded. Data reduction followed procedures similar to those described in References (B-3), (B-4) and (B-5). Since the step separation test was conducted in a zero-pressure gradient boundary layer, Reference (B-3) also serves as a valuable source of additional background material.

SYMBOLS

DELTA	boundary-layer thickness, inch
DELSTAR	boundary-layer displacement thickness, inch
H	shape factor, DELSTAR/THETA
M	Mach number
P	pressure, psia
RE/L	unit Reynolds number per foot
RETHETA	Reynolds number based on momentum
RHO	density, LBM/FT^3
T	temperature, °R
THETA	boundary-layer momentum thickness, inch
THETAE	boundary-layer energy thickness, inch
THETAH	boundary-layer total enthalpy thickness, inch
U	velocity, ft/sec
Y	distance normal to plate surface, inch

Suffix

FS	free stream
L	local
O	stagnation
S	static
W	wall

REFERENCES

(B-1) Lee, R. E., Yanta, W. J., Leonas, A. C., and Carner, J. W., "The NOL Boundary Layer Channel," NOLTR 66-185, Nov 1966.

(B-2) Danberg, James E., "The Equilibrium Temperature Probe, A Device for Measuring Temperatures in Hypersonic Boundary Layers," NOLTR 61-2, Feb 1962.

(B-3) Lee, R. E., Yanta, W. J., and Leonas, A. C., "Velocity Profile, Skin-Friction Balance and Heat-Transfer Measurements of the Turbulent Boundary Layer at Mach 5 and Zero-Pressure Gradient," NOLTR 69-106, Jun 1969.

(B-4) Brott, David L., Yanta, William J., Voisinet, R. L., and Lee, R. E., "An Experimental Investigation of the Compressible Turbulent Boundary Layer with a Favorable Pressure Gradient," NOLTR 69-143, Aug 1969.

(B-5) Voisinet, R. L., Lee, R. E., and Yanta, W. J., "An Experimental Study of the Compressible Turbulent Boundary Layer with an Adverse Pressure Gradient," Paper No. 9, AGARD Conference 93 on Turbulent Shear Flows, London, U. K., Sep 1971.

STATION	48		
MFS	4.728	RE/L	4.21×10^6
POFS	73.2	RETHETA	1.86×10^4
TOLFS	592	DELTA	1.476
UFS	2410	DELSTAR	0.508
RHOFS	.00468	THETA	0.053
TSFS	108.1	THETAE	0.098
PW	0.185	THETAH	-0.013
TW	520.5	H	9.560

POINT	Y INCH	ML	PSL/PW	TOL/TOLFS	RHOL/RHOLFS	TSL/TSLFS	UL/ULFS
1	0.0000	0.0000	1.0000	.8800	.2065	4.8138	0.0000
2	.0025	.2058	1.0000	.8822	.2077	4.7953	[illegible]
3	.0035	.2741	1.0000	[illegible]	.2073	[illegible]	.1268
4	.0045	.3427	1.0000	.8941	.2060	4.7791	.1584
5	.0045	.3720	1.0000	.8921	[illegible]	4.7486	.1715
6	.0065	.4833	1.0000	.8902	.2137	4.6523	.2205
7	.0065	.4863	1.0000	.8928	.2132	4.6634	.2221
8	.0106	.7035	1.0000	.9058	.2205	4.5086	.3159
9	.0116	.7920	1.0000	.9117	.2243	4.4317	.3526
10	.0136	.8888	1.0000	.9103	.2312	4.3002	.3899
11	.0156	1.0169	1.0000	.9093	.2412	4.1215	.4367
12	.0187	1.1663	1.0000	.9192	.2515	3.9531	.4905
13	.0207	1.2728	1.0000	.9283	.2592	3.8355	.5273
14	.0267	1.4198	1.0000	.9404	.2711	3.6662	.5750
15	.0298	1.4975	1.0000	.9377	.2807	3.5411	.5961
16	.0338	1.5710	1.0000	.9298	.2919	3.4053	.6132
17	.0389	1.6436	1.0000	.9314	.3005	3.3078	.6323
18	.0500	1.7228	1.0000	.9291	.3117	3.1893	.6508
19	.0570	1.7799	1.0000	.9342	.3178	3.1284	.6659
20	.0581	1.7797	1.0000	.9362	.3171	3.1351	.6665
21	.0732	1.8498	1.0000	.9377	.3264	3.0456	.6828
22	.0873	1.9123	1.0000	.9329	.3372	2.9477	.6945
23	.1005	1.9709	1.0000	.9294	.3474	2.8612	.7052
24	.1207	2.0631	1.0000	.9328	.3607	2.7562	.7245
25	.1449	2.1570	1.0000	.9377	.3741	2.6571	.7437
26	.1692	2.2494	1.0000	.9452	.3868	2.5699	.7627
27	.2005	2.3678	1.0000	.9500	.4058	2.4497	.7839
28	.2328	2.4940	1.0000	.9497	.4294	2.3151	.8026
29	.2550	2.5760	1.0000	.9502	.4451	2.2336	.8143
30	.2742	2.6441	1.0000	.9529	.4574	2.1735	.8245
31	.3267	2.8271	1.0000	.9608	.4915	2.0227	.8504
32	.3591	2.9395	1.0000	.9665	.5129	1.9380	.8655
33	.4005	3.0745	1.0000	.9721	.5403	1.8398	[illegible]
34	.4399	3.1896	1.0000	.9760	.5650	1.7593	[illegible]
35	.4914	3.3428	1.0000	.9792	.6003	1.6560	.9099
36	.5508	3.5019	1.0000	.9772	.6421	1.5463	.9217
37	.6212	3.6727	1.0000	.9833	.6834	1.4546	[illegible]
38	.6806	3.8027	1.0000	.9873	.7164	1.3877	[illegible]
39	.7369	3.9123	1.0000	.9896	.7453	1.3329	[illegible]
40	.8285	4.0682	1.0000	.9920	.7595	1.2591	[illegible]
41	.9331	4.2088	1.0000	.9928	.8315	1.1955	[illegible]
42	1.0387	4.3197	1.0000	.9932	.8658	1.1432	[illegible]
43	1.1605	4.4241	1.0000	.9949	.8977	1.1074	[illegible]
44	1.2872	4.5244	1.0009	.9966	.9297	1.0702	[illegible]
45	1.3818	4.5885	1.0018	.9981	.9504	1.0478	[illegible]
46	1.4763	4.6424	1.0028	.9996	.9680	1.0297	[illegible]
47	1.5619	4.6720	1.0036	.9997	.9788	1.0192	[illegible]
48	1.6735	4.6960	1.0049	.9997	.9882	1.0108	[illegible]

Best Available Copy

POINT	Y INCH	ML	PSL/PW	TOL/TOLFS	RHOL/RHOLFS	TSL/TSLFS	UL/ULFS
49	1.7681	4.7278	1.0060	1.0000	1.0000	1.0000	1.0000
50	1.8778	4.7424	1.0073	.9986	1.0077	.9936	.9999
51	1.9844	4.7472	1.0085	.9996	1.0097	.9929	1.0005
52	2.0810	4.7466	1.0092	.9998	1.0100	.9933	1.0006
53	2.1755	4.7421	1.0148	1.0006	1.0131	.9957	1.0009
54	2.2349	4.7415	1.0155	1.0013	1.0129	.9966	1.0012
55	2.3476	4.7373	1.0205	1.0006	1.0172	.9973	1.0007
56	2.4371	4.7373	1.0205	1.0002	1.0176	.9969	1.0005
57	2.5226	4.7351	1.0233	1.0016	1.0182	.9990	1.0011
58	2.6222	4.7307	1.0289	1.0020	1.0218	1.0010	1.0011
59	2.7067	4.7261	1.0346	1.0023	1.0255	1.0029	1.0011
60	2.7842	4.7193	1.0431	1.0022	1.0316	1.0051	1.0008
61	2.8778	4.7125	1.0517	1.0024	1.0375	1.0077	1.0006
62	2.9824	4.6948	1.0746	1.0035	1.0524	1.0150	1.0005
63	3.0770	4.6791	1.0954	1.0033	1.0672	1.0204	.9997
64	3.1645	4.6726	1.1041	1.0032	1.0733	1.0226	.9994
65	3.2701	4.6685	1.1094	1.0027	1.0775	1.0235	.9990
66	3.3456	4.6664	1.1123	1.0036	1.0785	1.0252	.9994
67	3.4381	4.6601	1.1210	1.0040	1.0841	1.0279	.9993
68	3.5317	4.6519	1.1322	1.0035	1.0923	1.0303	.9988
69	3.6564	4.6434	1.1440	1.0041	1.0998	1.0340	.9987
70	3.7570	4.6306	1.1622	1.0049	1.1114	1.0395	.9986
71	3.8908	4.6223	1.1741	1.0044	1.1202	1.0419	.9980
72	4.0055	4.6137	1.1865	1.0052	1.1277	1.0459	.9980

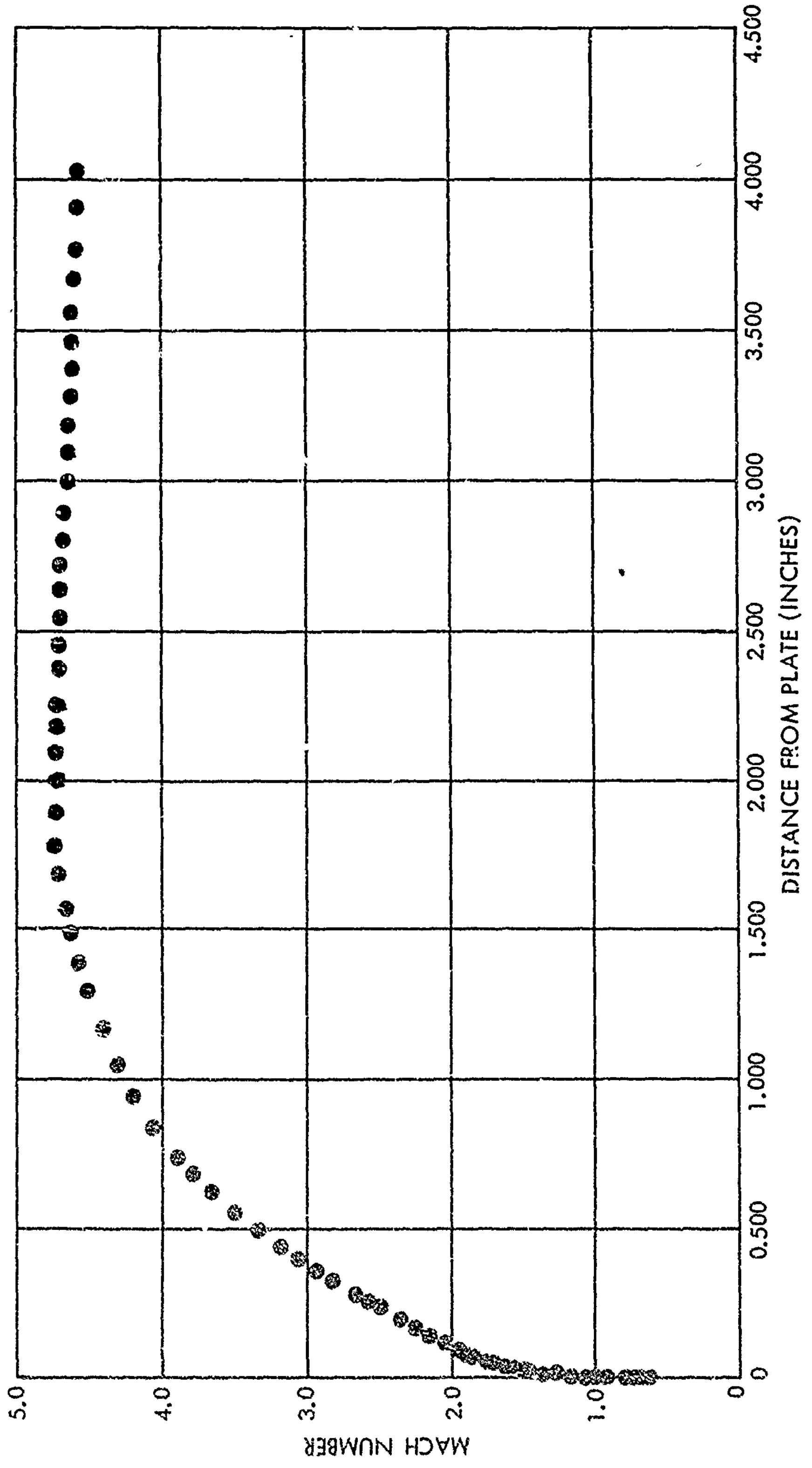

FIG. B-1 (U) MACH DISTRIBUTION: PO = 73.2 PSIA; TO = 592 °R; STATION = 48 INCHES (U)

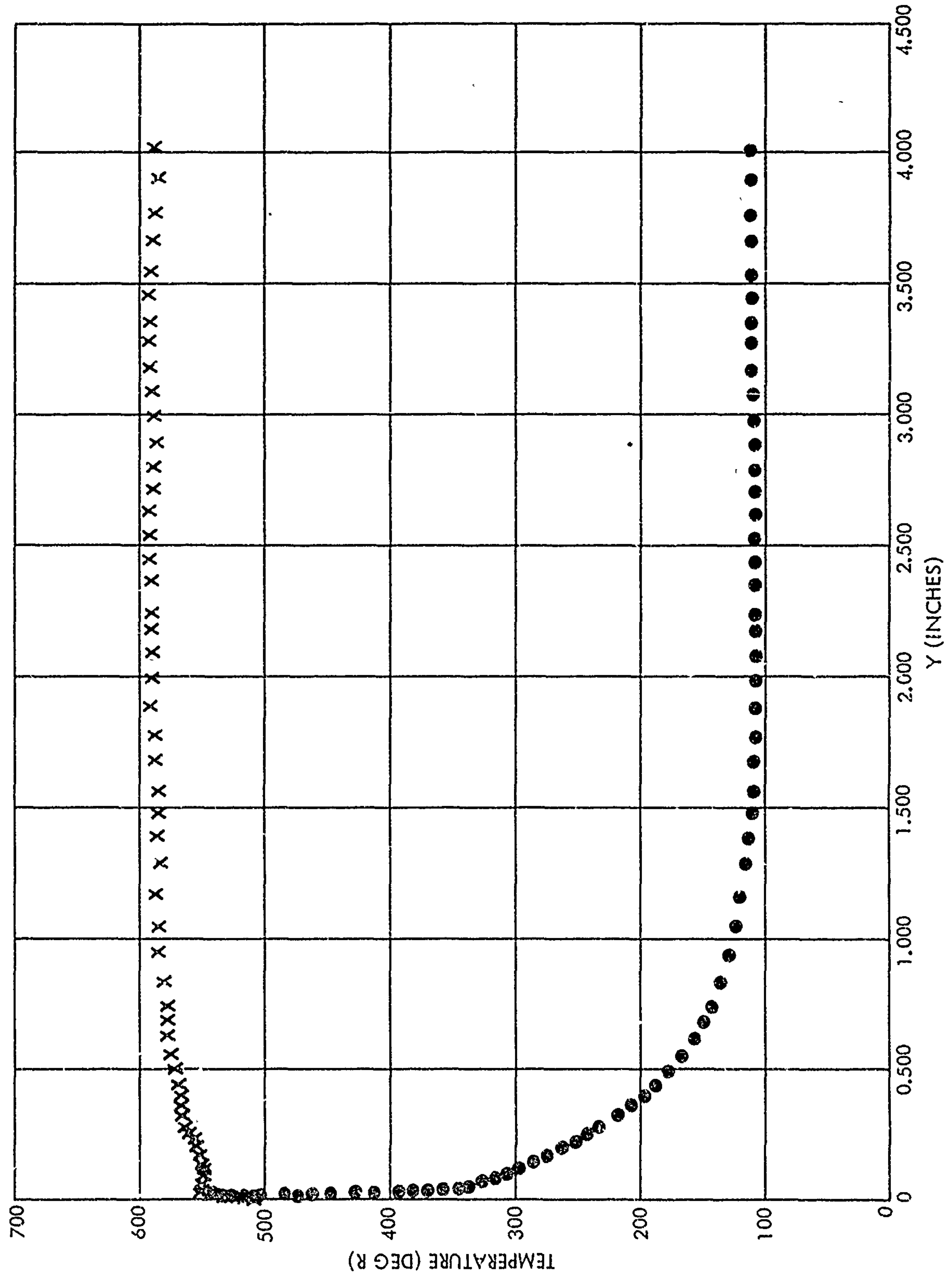

FIG. B-2 (U) TEMPERATURE DISTRIBUTION: PO = 73.2 PSIA; TO = 592 °R; STATION = 48 INCHES (U)

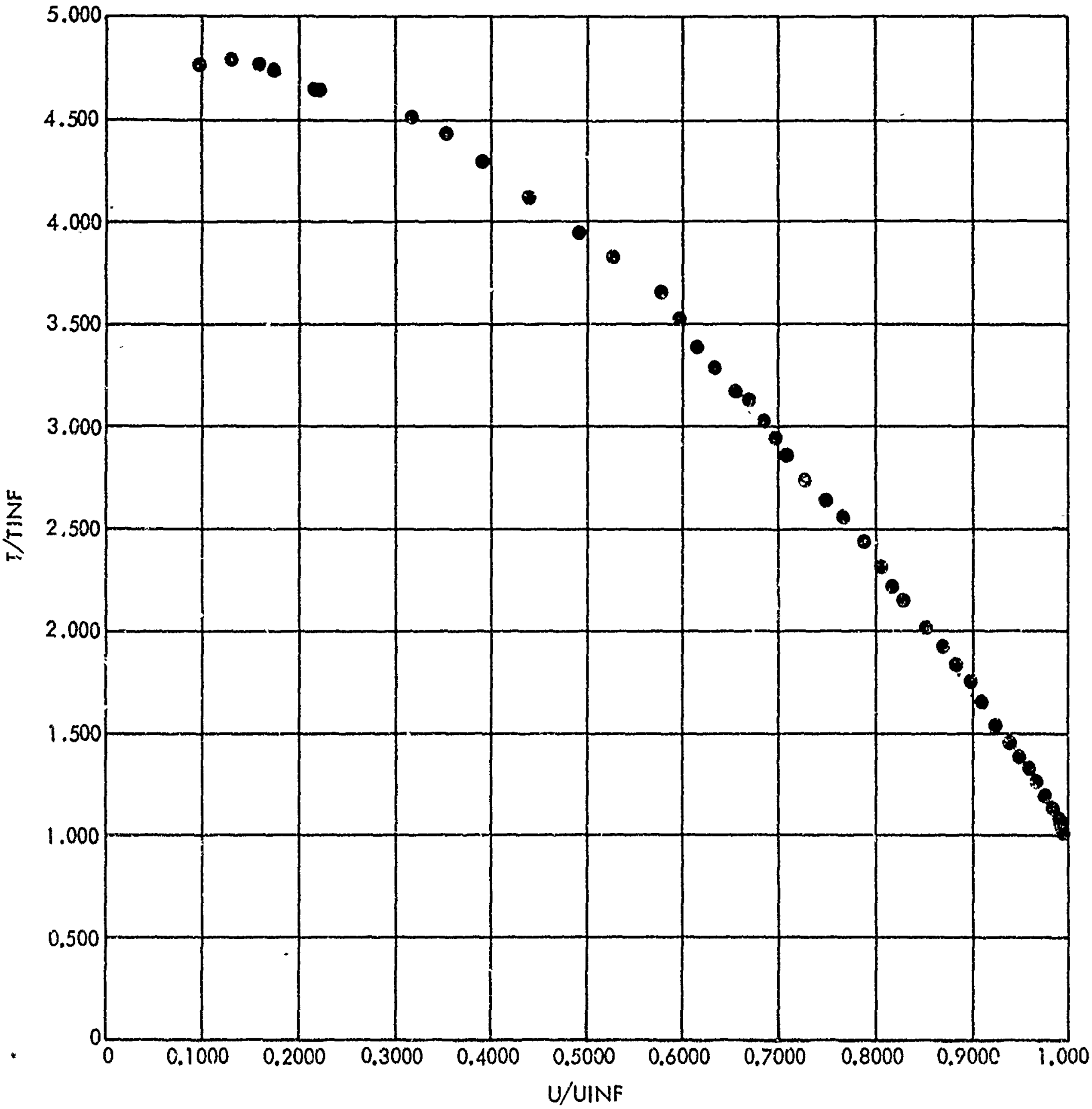

FIG. B-3 (U) DIMENSIONLESS TEMPERATURE-DIMENSIONLESS VELOCITY DISTRIBUTION:
PO = 73.2 PSIA; TO = 592 °R; STATION = 48 INCHES (U)

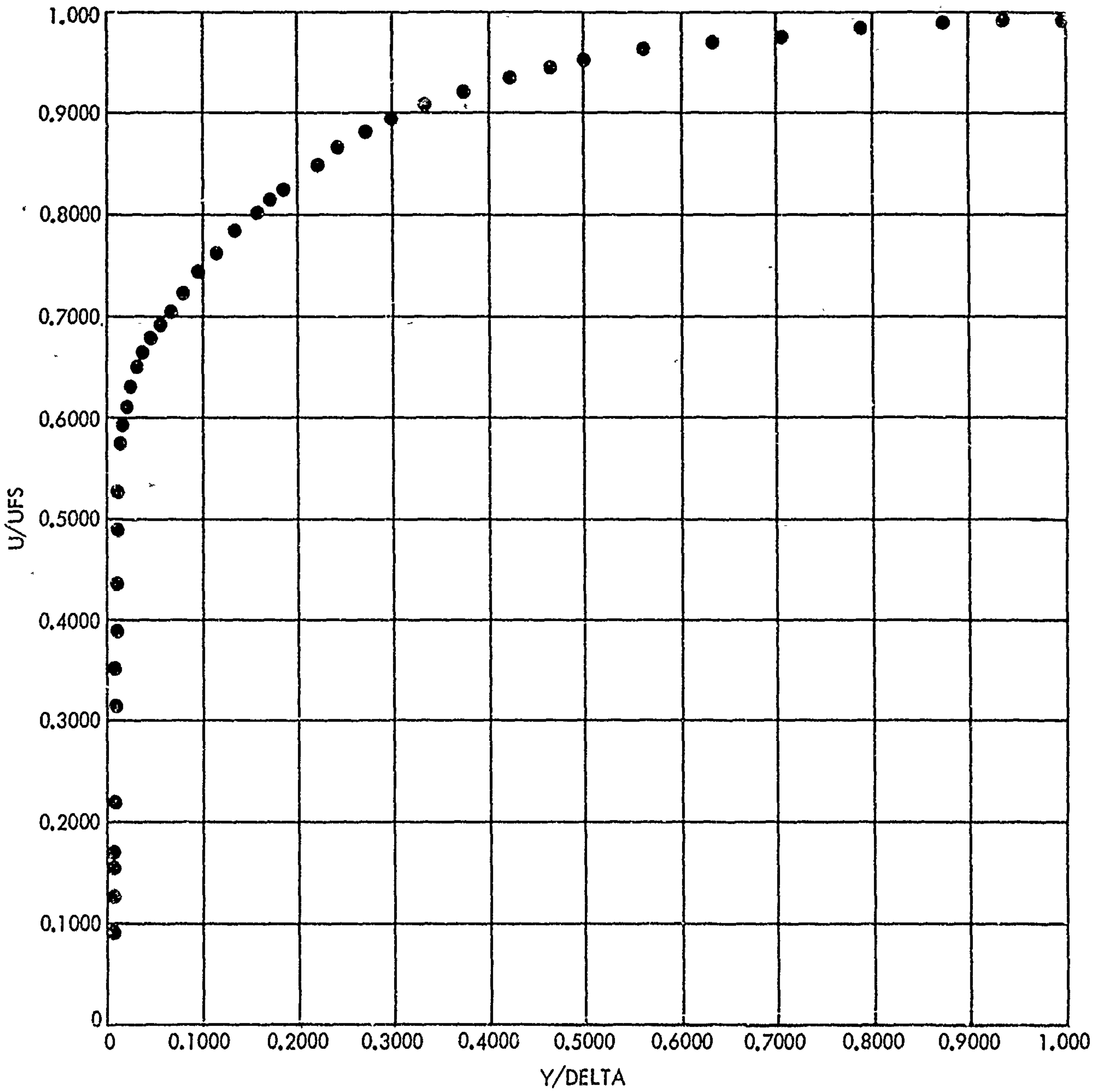

FIG. B-4 (U) DIMENSIONLESS VELOCITY-DISTANCE DISTRIBUTION:
PO = 73.2 PSIA; TO = 592 °R; STATION = 48 INCHES (U)

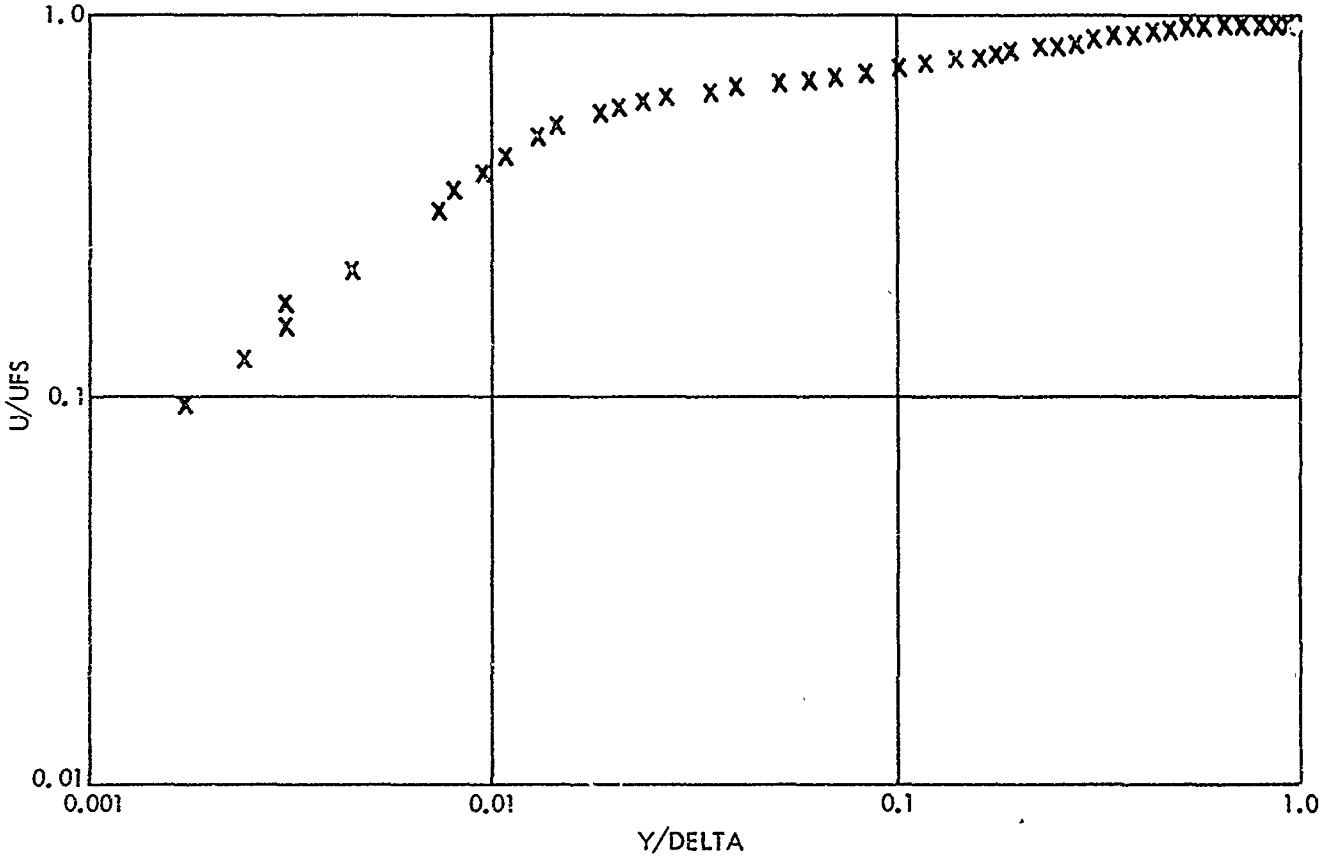

FIG. B-5 (U) LOGARITHMIC VELOCITY DISTRIBUTION: PO = 73.2 PSIA; TO = 592 °R; STATION = 48 INCHES (U)

STATION	48		
MFS	4.662	RE/L	0.88×10^{6}
POFS	14.97	RETHETA	0.54×10^{4}
TOLFS	588	DELTA	1.913
UFS	2396	DELSTAR	0.708
RHOFS	.00100	THETA	0.074
TSFS	109.9	THETAE	0.136
PW	0.040	THETAH	-0.018
TW	524.1	H	9.600

POINT	Y INCH	ML	PSL/PW	TOL/TOLFS	RHOL / RHOLFS	TSL / TSLFS	UL/ULFS
1	0.0000	0.0000	1.0000	.8918	.2067	4.7672	0.0000
2	.0025	.0813	1.0000	.8937	.2065	4.7715	.0381
3	.0025	.0827	1.0000	.8937	.2065	4.7713	.0388
4	.0035	.1101	1.0000	.8946	.2065	4.7709	.0516
5	.0045	.1440	1.0000	.8951	.2068	4.7651	.0674
6	.0055	.1637	1.0000	.8959	.2068	4.7641	.0766
7	.0076	.2022	1.0000	.8967	.2072	4.7549	.0946
8	.0106	.2578	1.0000	.8991	.2078	4.7432	.1205
9	.0136	.3295	1.0000	.9018	.2088	4.7185	.1535
10	.0166	.3929	1.0000	.9046	.2101	4.6912	.1826
11	.0227	.5123	1.0000	.9096	.2133	4.6201	.2362
12	.0257	.6158	1.0000	.9155	.2146	4.5491	.2818
13	.0308	.7347	1.0000	.9180	.2225	4.4293	.3317
14	.0348	.8338	1.0000	.9233	.2274	4.3332	.3723
15	.0399	.9471	1.0000	.9266	.2346	4.2002	.4164
16	.0439	1.0271	1.0000	.9310	.2398	4.1098	.4467
17	.0490	1.1082	1.0000	.9372	.2450	4.0223	.4768
18	.0621	1.3274	1.0000	.9522	.2618	3.7638	.5525
19	.0783	1.4995	1.0000	.9562	.2795	3.5262	.6040
20	.0924	1.6182	1.0000	.9565	.2937	3.3557	.6359
21	.1126	1.7473	1.0000	.9582	.3098	3.1804	.6685
22	.1399	1.8808	1.0000	.9556	.3294	2.9917	.6979
23	.1641	1.9676	1.0000	.9544	.3427	2.8757	.7158
24	.1985	2.0873	1.0000	.9533	.3618	2.7234	.7389
25	.2449	2.2229	1.0000	.9511	.3854	2.5572	.7626
26	.2783	2.3275	1.0000	.9517	.4035	2.442[illegible]	.7803
27	.3116	2.4226	1.0000	.9507	.4215	2.3381	.7947
28	.3641	2.5637	1.0000	.9531	.4476	2.2015	.8160
29	.4035	2.6636	1.0000	.9557	.4666	2.1120	.8304
30	.4459	2.7717	1.0000	.9585	.4878	2.0202	.8451
31	.4944	2.8879	1.0000	.9618	.5113	1.9272	.8601
32	.5759	3.0328	1.0000	.9659	.5419	1.8185	.8773
33	.6896	3.2270	1.0000	.9720	.5846	1.6856	.8988
34	.7619	3.3400	1.0000	.9757	.6104	1.6143	.9104
35	.8356	3.4534	1.0000	.9802	.6366	1.5479	.9217
36	.9040	3.5630	1.0000	.9820	.6643	1.4834	.9309
37	1.0009	3.6954	1.0000	.9845	.6986	1.4105	.9415
38	1.0696	3.8191	1.0000	.9859	.7324	1.3455	.9503
39	1.1484	3.9410	1.0000	.9892	.7652	1.2878	.9594
40	1.2218	4.0459	1.0002	.9907	.7954	1.2391	.9662
41	1.2218	4.0539	1.0002	.9908	.7977	1.2355	.9667
42	1.3115	4.1686	1.0008	.9919	.8324	1.1848	.9734
43	1.4021	4.2695	1.0015	.9940	.8628	1.1438	.9796
44	1.4945	4.3517	1.0022	.9949	.8890	1.1109	.9840
45	1.6077	4.4369	1.0031	.9968	.9159	1.0793	.9888
46	1.7182	4.5028	1.0046	.9973	.9386	1.0547	.9920
47	1.8133	4.5447	1.0058	.9973	.9539	1.0390	.9938
48	1.9129	4.5825	1.0072	.9984	.9669	1.0265	.9960

POINT	Y INCH	ML	PSL/PW	TOL/TOLFS	RHOL / RHOLFS	TSL / TSLFS	UL/ULFS
49	2.0156	4.6116	1.0085	.9983	.9783	1.0159	.9971
50	2.1081	4.6325	1.0098	.9987	.9863	1.0089	.9982
51	2.1636	4.6454	1.0108	.9990	.9914	1.0047	.9989
52	2.3456	4.6615	1.0148	1.0000	1.0000	1.0000	1.0000
53	2.4281	4.6685	1.0169	.9989	1.0058	.9964	.9997
54	2.5297	4.6857	1.0196	1.0002	1.0130	.9918	1.0011
55	2.6333	4.6805	1.0261	1.0005	1.0173	.9939	1.0010
56	2.7188	4.6803	1.0265	1.0001	1.0181	.9935	1.0008
57	2.8063	4.6754	1.0325	1.0012	1.0211	.9964	1.0012
58	2.9160	4.6712	1.0379	1.0015	1.0247	.9981	1.0011
59	3.0116	4.6662	1.0442	1.0017	1.0289	1.0001	1.0011
60	3.1071	4.6587	1.0537	1.0022	1.0351	1.0031	1.0010
61	3.1977	4.6509	1.0639	1.0022	1.0422	1.0059	1.0007
62	3.2872	4.6413	1.0765	1.0027	1.0505	1.0098	1.0005
63	3.3878	4.6336	1.0867	1.0026	1.0577	1.0124	1.0002
64	3.4784	4.6282	1.0938	1.0025	1.0627	1.0142	.9999
65	3.5840	4.6194	1.1057	1.0031	1.0703	1.0180	.9999
66	3.6564	4.6133	1.1140	1.0032	1.0760	1.0203	.9996
67	3.7429	4.6034	1.1276	1.0036	1.0849	1.0242	.9994
68	3.8385	4.5928	1.1425	1.0036	1.0951	1.0281	.9990
69	3.9301	4.5844	1.1545	1.0042	1.1027	1.0317	.9989
70	4.0166	4.5794	1.1616	1.0043	1.1074	1.0336	.9988

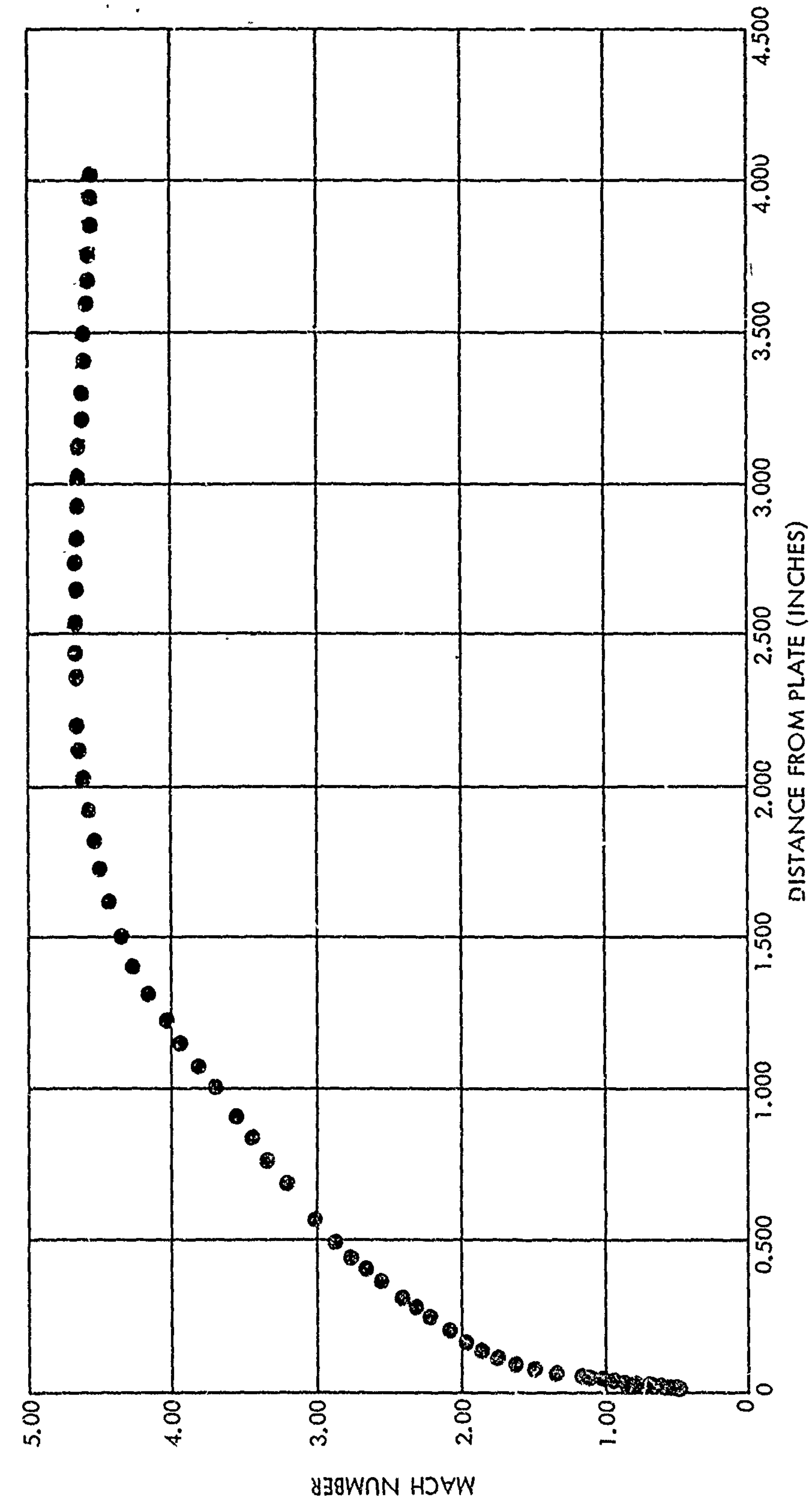

FIG. B-6 (U) MACH DISTRIBUTION: PO = 15.0 PSIA; TO = 588 °R; STATION = 48 INCHES (U)

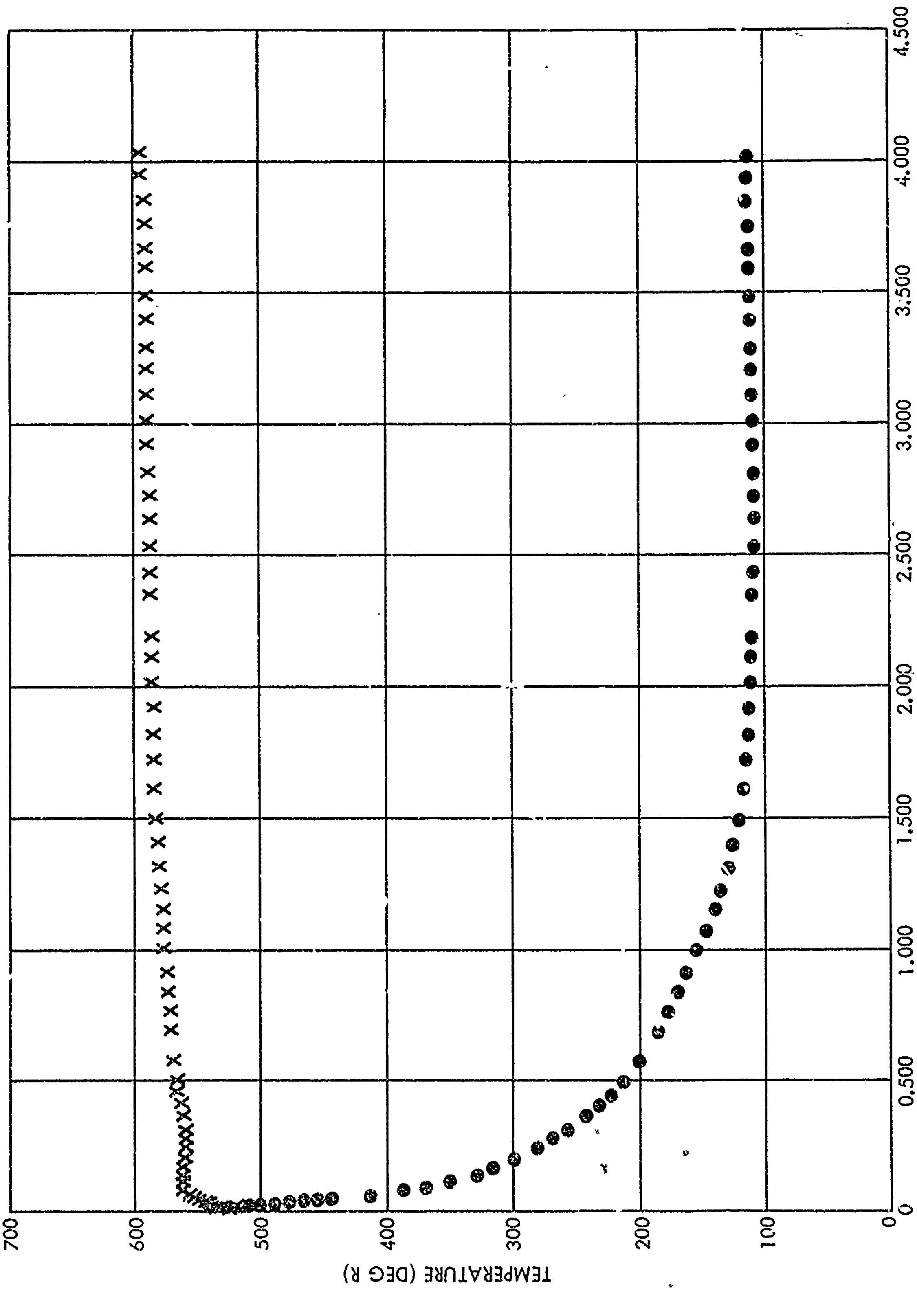

FIG. B-7 (U) TEMPERATURE DISTRIBUTION: PO = 15.0 PSIA; TO = 588 °R; STATION = 48 INCHES (U)

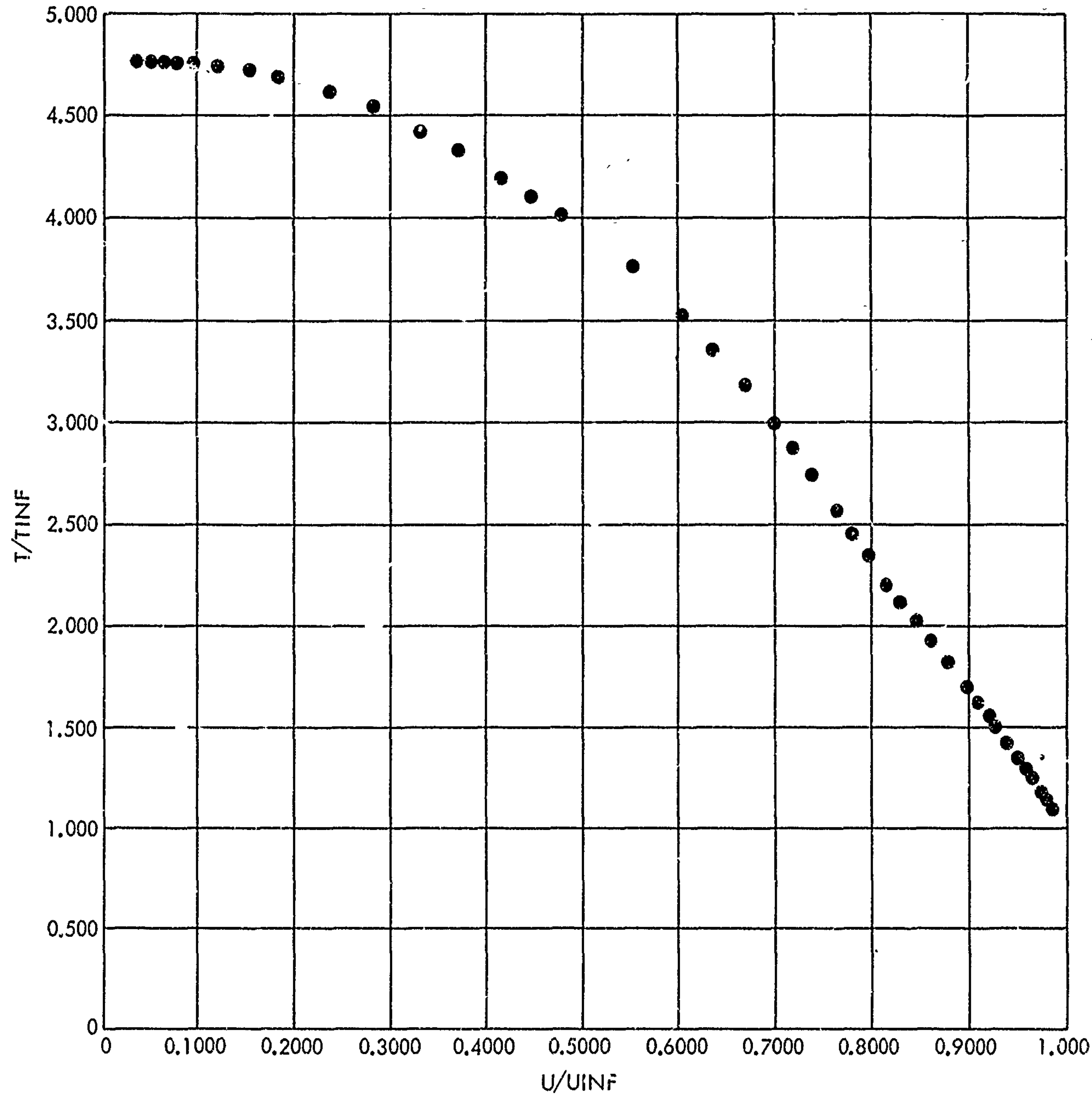

FIG. B-8 (U) DIMENSIONLESS TEMPERATURE-VELOCITY DISTRIBUTION: PO = 15.0 PSIA; TO = 588 °R; STATION = 48 INCHES (U)

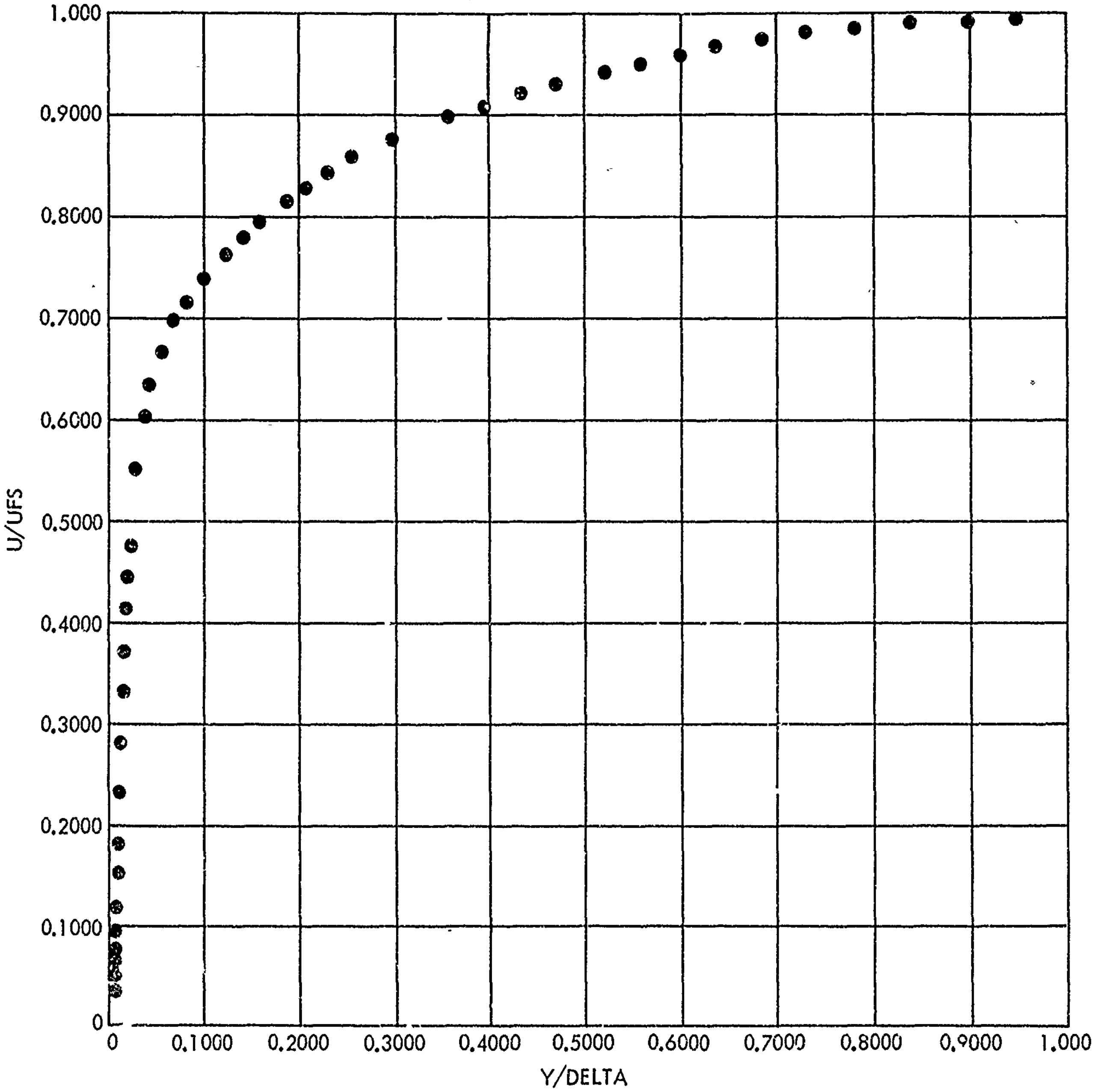

FIG. B-9 (U) DIMENSIONLESS VELOCITY-DISTANCE DISTRIBUTION:
PO = 15.0 PSIA; TO = 588 °R; STATION = 48 INCHES (U)

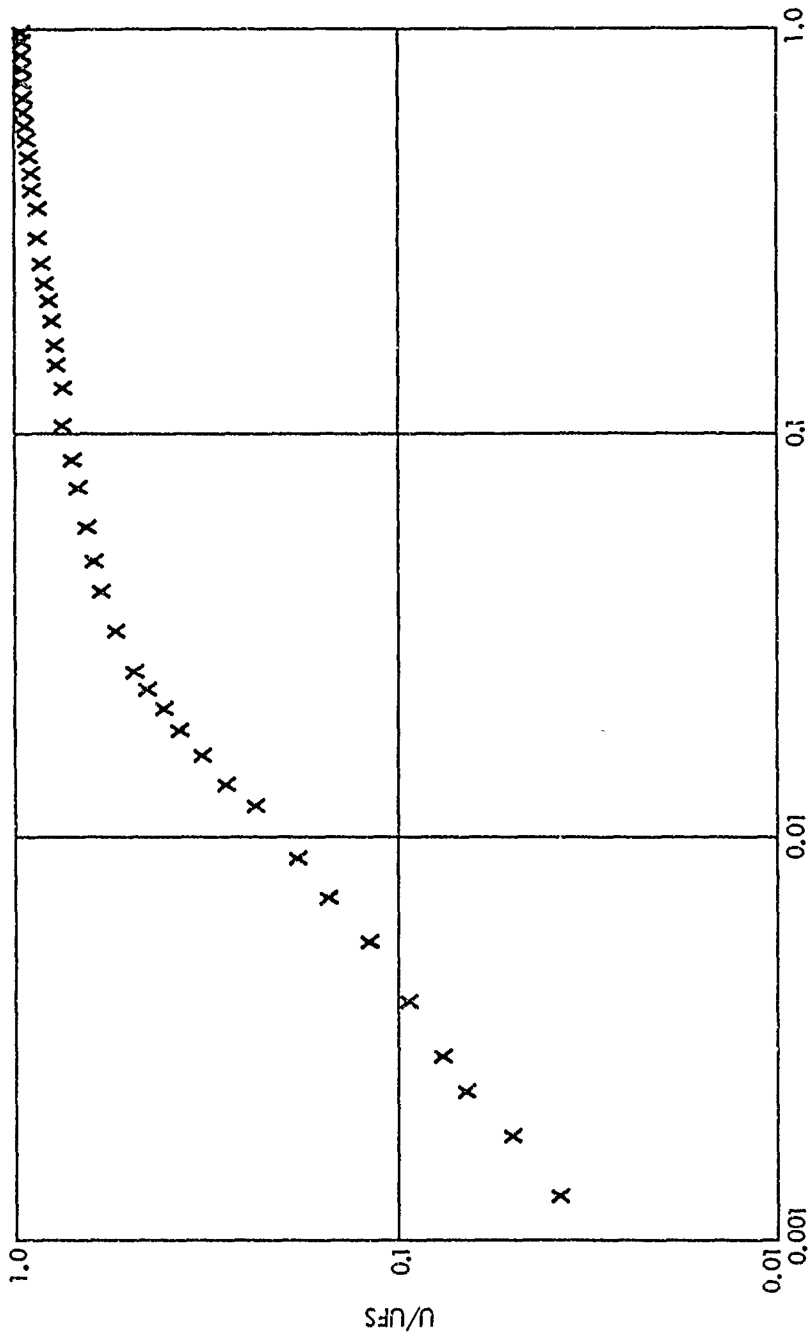

FIG. B-10 (U) LOGARITHMIC VELOCITY DISTRIBUTION: PO = 15.0 PSIA; TO = 588°R; STATION = 48 INCHES (U)

STATION	60		
MFS	4.867	RE/L	3.99×10^6
POFS	72.6	RETHETA	2.26×10^4
TOLFS	592	DELTA	1.892
UFS	2423	DELSTAR	0.714
RHOFS	.00418	THETA	0.068
TSFS	103.1	THETAE	0.125
PW	0.155	THETAH	-0.014
TW	524.7	H	10.52

POINT	Y INCH	ML	PSL/PW	TOL/TOLFS	RHOL / RHOLFS	TSL / TSLFS	UL/ULFS
1	0.0000	0.0000	1.0000	.8868	.1937	5.0879	0.0000
2	.0025	.0879	1.0000	.8885	.1936	5.0902	.0407
3	.0025	.0933	1.0000	.8896	.1934	5.0952	.0433
4	.0035	.1476	1.0000	.8875	.1944	5.0700	.0683
5	.0055	.2211	1.0000	.8920	.1945	5.0684	.1023
6	.0065	.2694	1.0000	.8948	.1948	5.0604	.1245
7	.0086	.3496	1.0000	.8921	.1972	4.9967	.1605
8	.0116	.4708	1.0000	.8996	.1994	4.9423	.2150
9	.0146	.6500	1.0000	.9088	.2050	4.8080	.2929
10	.0167	.8204	1.0000	.9106	.2140	4.6050	.3617
11	.0197	.8336	1.0000	.9128	.2143	4.5981	.3673
12	.0227	1.0110	1.0000	.9247	.2237	4.4048	.4360
13	.0278	1.1532	1.0000	.9330	.2331	4.2284	.4872
14	.0359	1.3403	1.0000	.9301	.2510	3.9260	.5457
15	.0450	1.4431	1.0000	.9322	.2610	3.7760	.5762
16	.0520	1.5054	1.0000	.9345	.2671	3.6898	.5941
17	.0682	1.5942	1.0000	.9267	.2796	3.5253	.6150
18	.0844	1.6610	1.0000	.9260	.2879	3.4237	.6315
19	.1016	1.7229	1.0000	.9277	.2951	3.3398	.6469
20	.1350	1.8337	1.0000	.9305	.3087	3.1923	.6732
21	.1784	1.9654	1.0000	.9366	.3251	3.0315	.7031
22	.2219	2.0992	1.0000	.9376	.3447	2.8596	.7293
23	.2634	2.2267	1.0000	.9415	.3634	2.7123	.7535
24	.3261	2.3951	1.0000	.9489	.3887	2.5356	.7836
25	.3796	2.5498	1.0000	.9556	.4135	2.3837	.8088
26	.4282	2.6829	1.0000	.9614	.4359	2.2611	.8289
27	.4939	2.8596	1.0000	.9676	.4673	2.1066	.8528
28	.5354	2.9629	1.0000	.9725	.4867	2.0249	.8663
29	.5758	3.0654	1.0000	.9757	.5069	1.9442	.8782
30	.6132	3.1537	1.0000	.9788	.5246	1.8768	.8882
31	.6709	3.2967	1.0000	.9796	.5565	1.7710	.9014
32	.7184	3.4064	1.0000	.9786	.5829	1.6909	.9101
33	.7669	3.5184	1.0000	.9811	.6085	1.6196	.9200
34	.8144	3.6304	1.0000	.9838	.6349	1.5524	.9294
35	.9166	3.8373	1.0000	.9873	.6864	1.4359	.9440
36	1.0337	4.0342	1.0000	.9903	.7380	1.3354	.9578
37	1.1663	4.2224	1.0000	.9934	.7895	1.2484	.9693
38	1.2909	4.3675	1.0020	.9952	.8327	1.1859	.9772
39	1.4166	4.4864	1.0047	.9971	.8699	1.1383	.9835
40	1.5291	4.5630	1.0071	.9985	.8948	1.1094	.9875
41	1.6457	4.6401	1.0097	.9997	.9205	1.0811	.9913
42	1.7653	4.7022	1.0122	1.0011	.9418	1.0593	.9944
43	1.8919	4.7488	1.0130	.9998	.9590	1.0411	.9955
44	2.0197	4.7996	1.0130	.9987	.9769	1.0220	.9969
45	2.1428	4.8355	1.0130	.9998	.9879	1.0106	.9988
46	2.2598	4.8671	1.0146	1.0000	1.0000	1.0000	1.0000
47	2.3688	4.8810	1.0176	1.0000	1.0077	.9953	1.0005
48	2.4626	4.8776	1.0217	1.0003	1.0102	.9968	1.0005

POINT	Y INCH	ML	PSL/PW	TOL/TOLFS	RHOL/RHOLFS	TSL/TSLFS	UL/ULFS
49	2.5575	4.8733	1.0270	1.0001	1.0142	.9980	1.0003
50	2.6291	4.8668	1.0349	1.0006	1.0193	1.0007	1.0003
51	2.6957	4.8595	1.0440	1.0004	1.0259	1.0030	.9999
52	2.7997	4.8491	1.0570	1.0012	1.0342	1.0073	1.0000
53	2.8834	4.8407	1.0676	1.0016	1.0412	1.0106	.9998
54	2.9500	4.8324	1.0781	1.0014	1.0486	1.0133	.9995
55	3.1020	4.8115	1.1054	1.0035	1.0653	1.0226	.9997
56	3.2156	4.8082	1.1099	1.0022	1.0698	1.0225	.9990
57	3.3382	4.8107	1.1065	1.0023	1.0673	1.0218	.9991
58	3.5040	4.8064	1.1122	1.0024	1.0712	1.0233	.9990
59	3.6548	4.8013	1.1190	1.0025	1.0758	1.0252	.9988
60	3.7975	4.7942	1.1287	1.0030	1.0819	1.0282	.9988
61	3.9120	4.7862	1.1395	1.0035	1.0887	1.0315	.9988
62	4.0327	4.7733	1.1572	1.0039	1.1003	1.0365	.9985

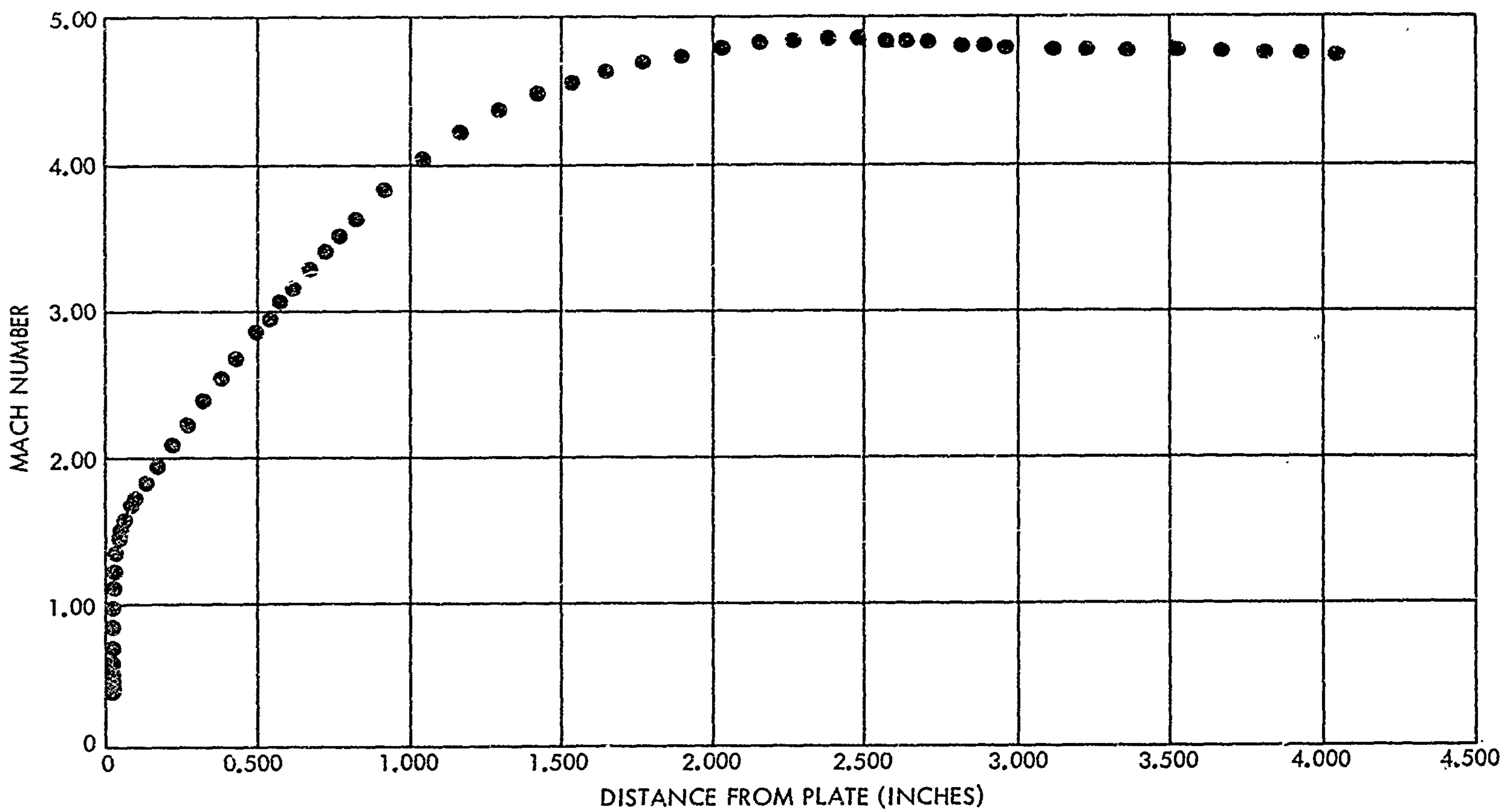

FIG. B-11 (U) MACH DISTRIBUTION: PO = 72.6 PSIA; TO = 572 °R; STATION = 60 INCHES (U)

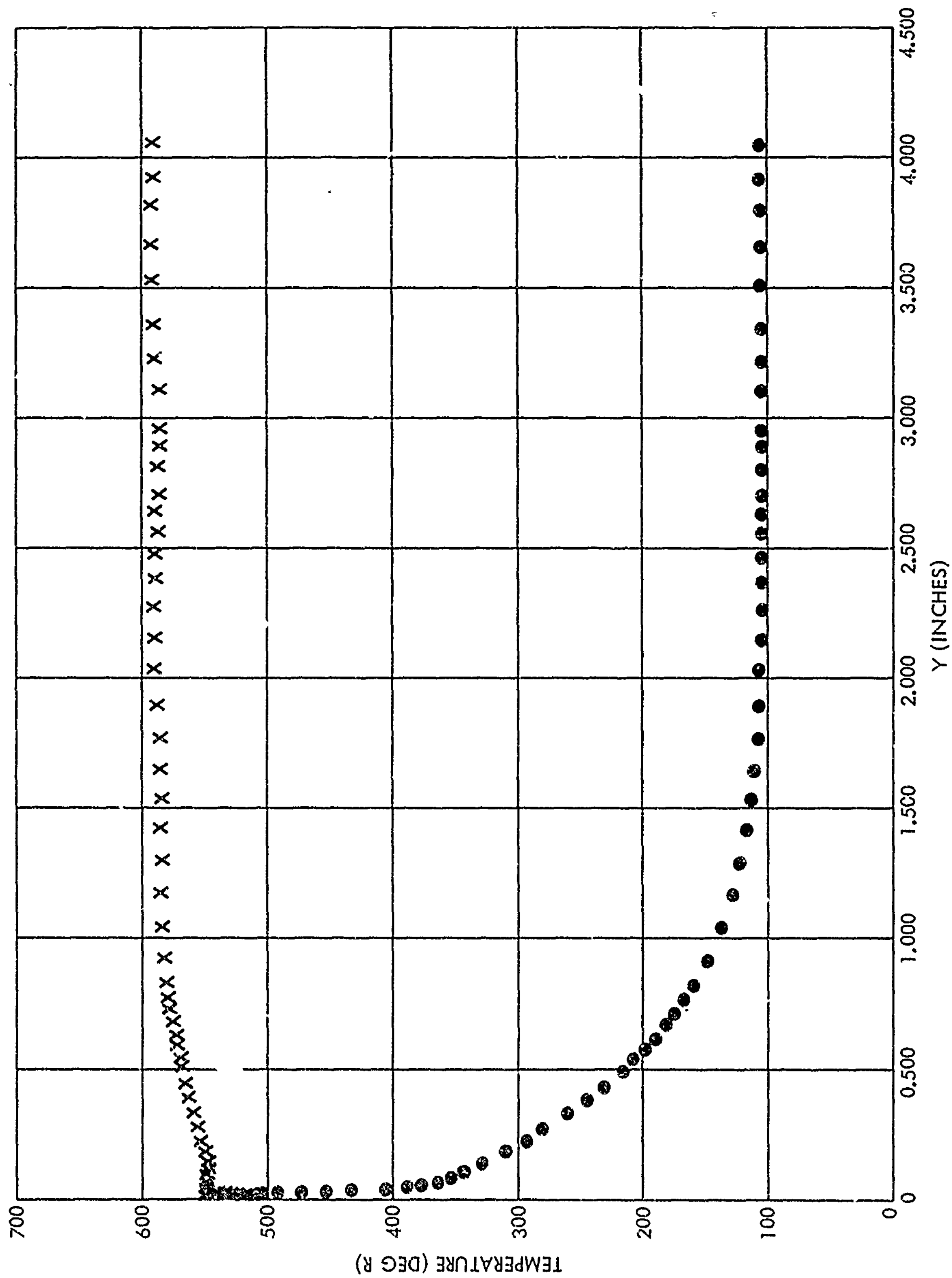

FIG. B-12 (U) TEMPERATURE DISTRIBUTION: PO = 72.6 PSIA; TO = 592 °R; STATION = 60 INCHES (U)

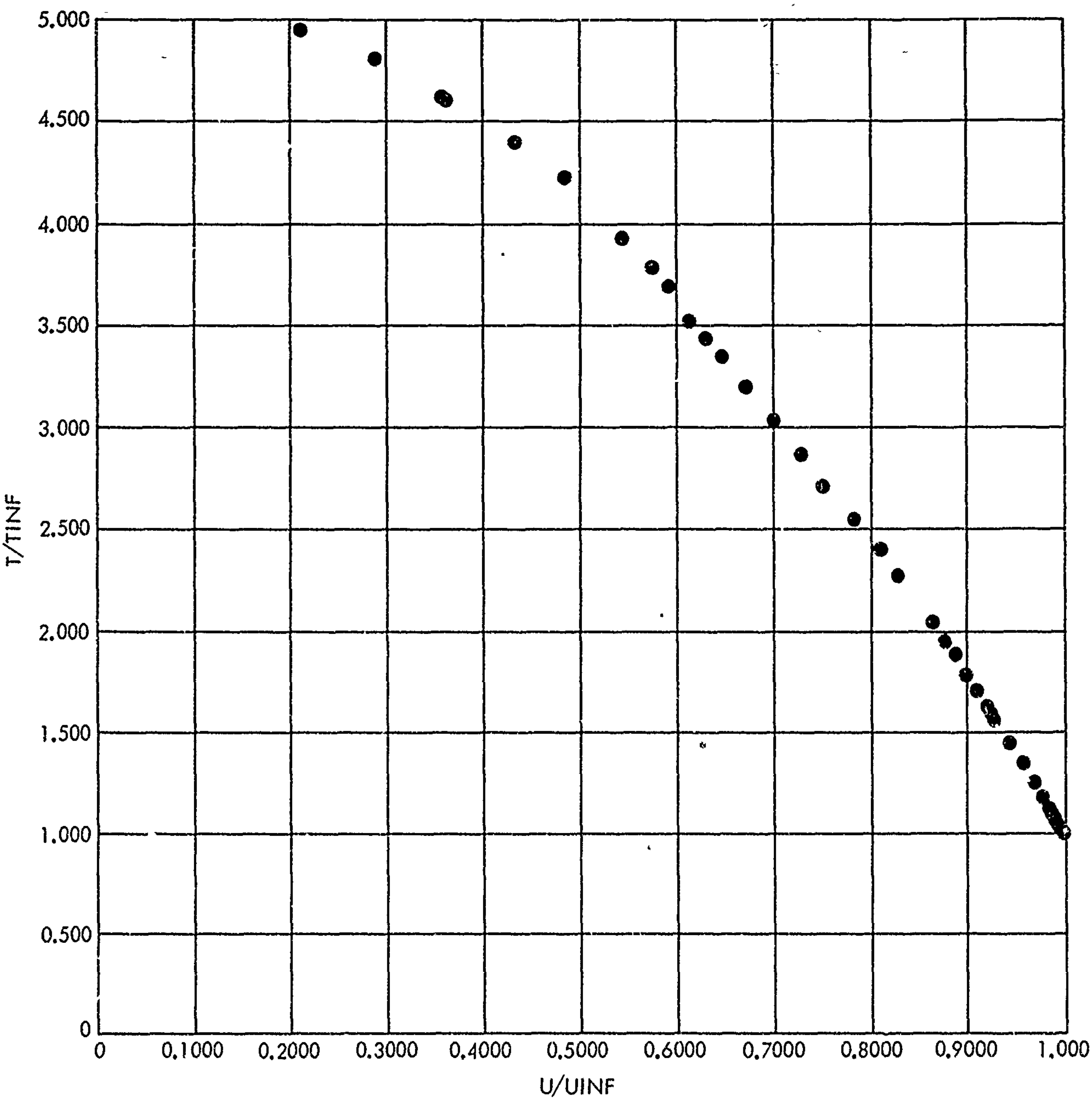

FIG. B-13 (U) DIMENSIONLESS TEMPERATURE-VELOCITY DISTRIBUTION:
PO = 72.6 PSIA; TO = 592 °R; STATION = 60 INCHES (U)

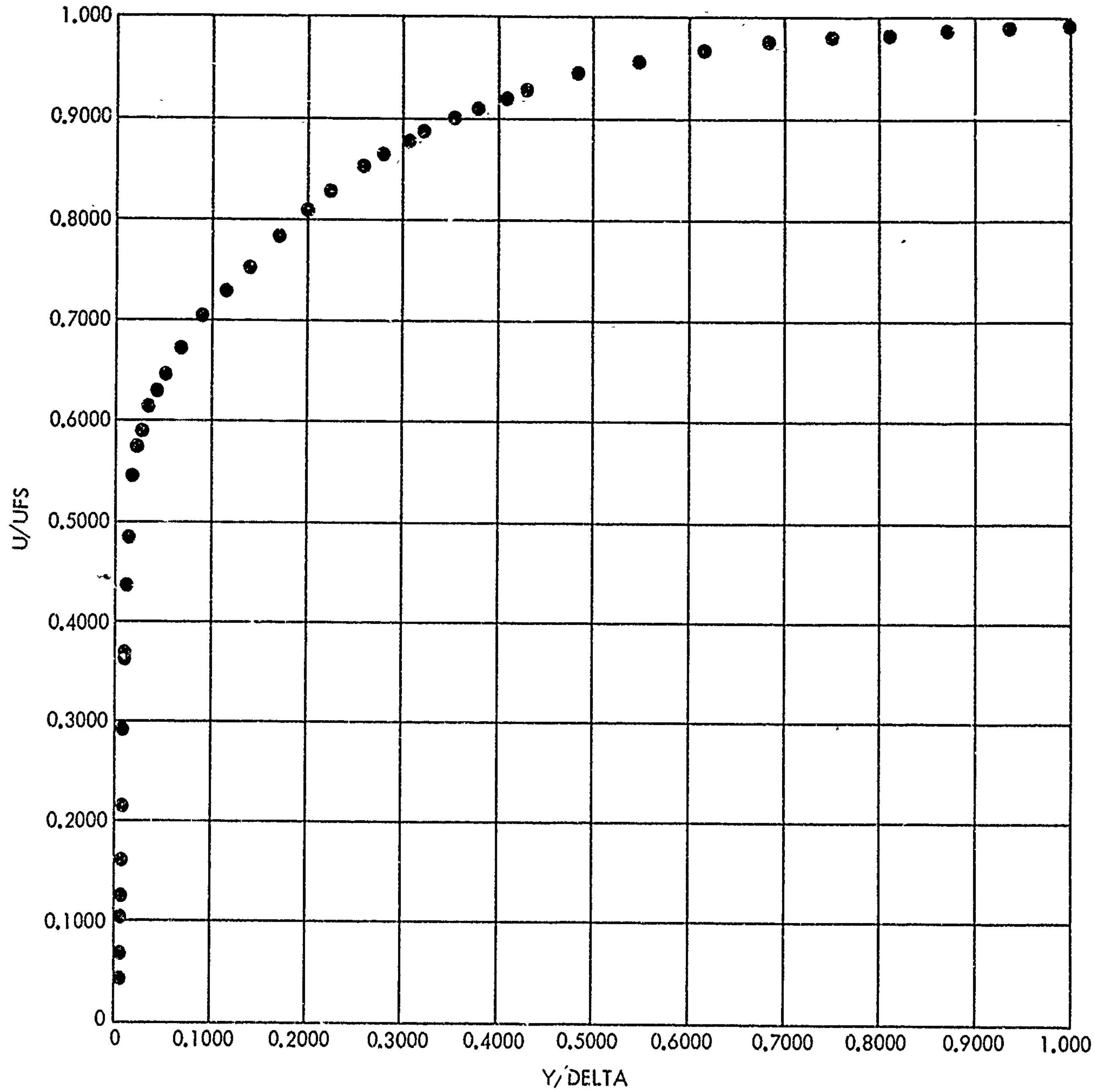

FIG. B-14 (U) DIMENSIONLESS VELOCITY-DISTANCE DISTRIBUTION:
PO = 72.6 PSIA; TO = 592 °R; STATION = 60 INCHES (U)

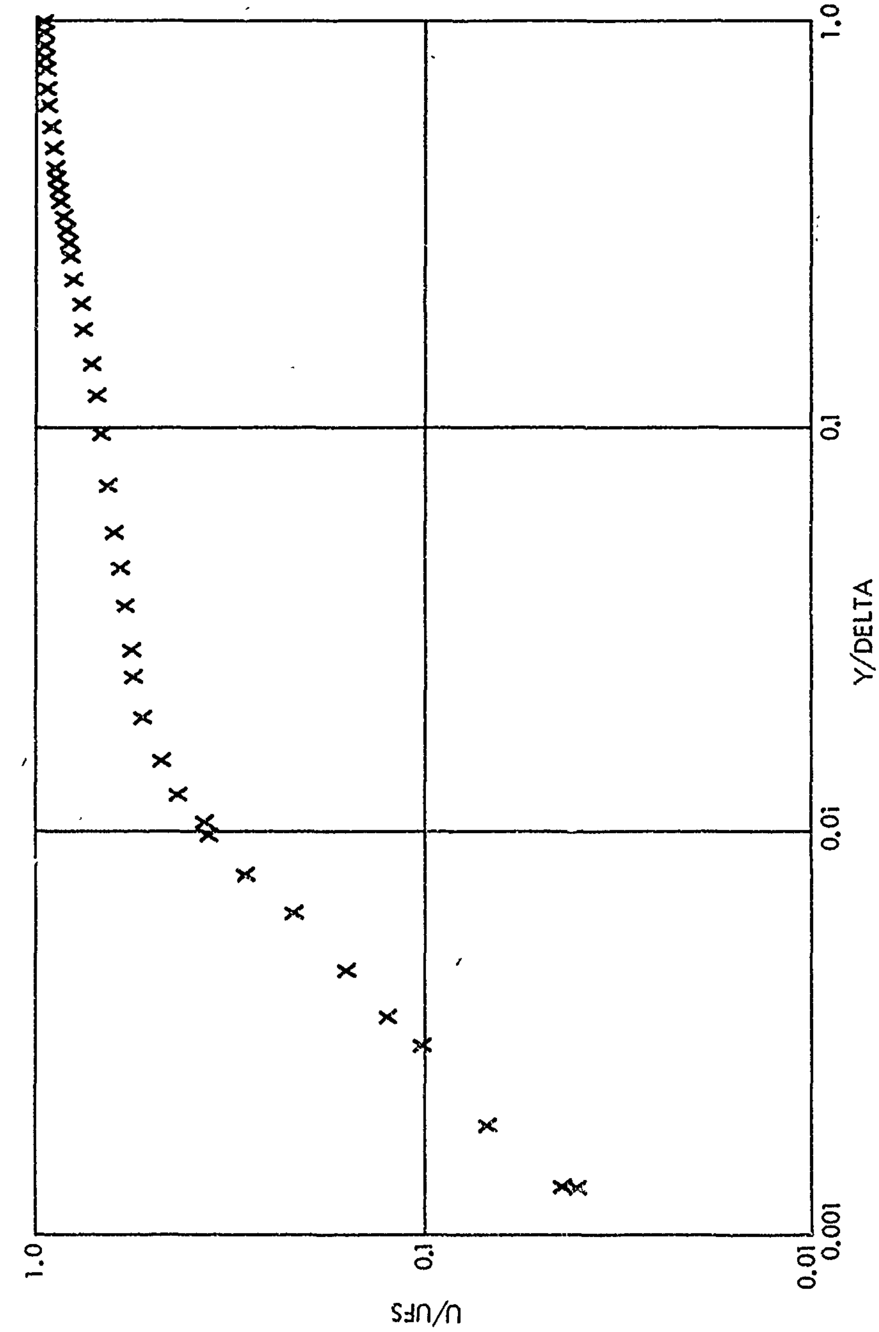

FIG. B-15 (U) LOGARITHMIC VELOCITY DISTRIBUTION: PO = 72.6 PSIA; TO = 592 °R; STATION = 60 INCHES (U)

STATION	60		
MFS	4.762	RE/L	0.84×10^6
POFS	14.89	RETHETA	0.60×10^4
TOLFS	586	DELTA	2.235
UFS	2402	DELSTAR	0.900
RHOFS	.00091	THETA	0.086
TSFS	105.9	THETAE	0.157
PW	0.034	THETAH	-0.018
TW	519	H	10.46

POINT	Y INCH	ML	PSL/PW	TOL/TOLFS	RHOL/RHOLFS	TSL/TSLFS	UL/ULFS
1	0.0000	0.0000	1.0000	.8857	.1968	4.9031	0.0000
2	.0025	.0093	1.0000	.8878	.1963	4.9147	.0043
3	.0035	.0175	1.0000	.8876	.1964	4.9135	.0082
4	.0065	.0473	1.0000	.8912	.1957	4.9317	.0221
5	.0096	.0739	1.0000	.8929	.1954	4.9374	.0345
6	.0156	.1546	1.0000	.9000	.1946	4.9586	.0723
7	.0197	.2309	1.0000	.9042	.1948	4.9525	.1079
8	.0278	.4136	1.0000	.9098	.1981	4.8701	.1917
9	.0359	.6019	1.0000	.9174	.2038	4.7356	.2751
10	.0460	.7857	1.0000	.9278	.2111	4.5719	.3527
11	.0561	.9596	1.0000	.9376	.2202	4.3831	.4219
12	.0672	1.1189	1.0000	.9435	.2310	4.1773	.4802
13	.0844	1.2932	1.0000	.9488	.2452	3.9361	.5387
14	.1168	1.5211	1.0000	.9532	.2675	3.6074	.6067
15	.1552	1.6669	1.0000	.9534	.2844	3.3925	.6447
16	.2098	1.8318	1.0000	.9540	.3053	3.1604	.6838
17	.2543	1.9413	1.0000	.9527	.3209	3.0075	.7069
18	.3028	2.0546	1.0000	.9512	.3380	2.8553	.7290
19	.3847	2.2338	1.0000	.9535	.3653	2.6418	.7624
20	.4524	2.3709	1.0005	.9556	.3877	2.4904	.7857
21	.4524	2.3784	1.0005	.9553	.3891	2.4813	.7867
22	.5677	2.6049	1.0015	.9599	.4287	2.2545	.8213
23	.6729	2.8115	1.0025	.9653	.4672	2.0705	.8495
24	.8296	3.1170	1.0039	.9729	.5294	1.8299	.8854
25	.9985	3.4301	1.0055	.9800	.5997	1.6180	.9162
26	1.1060	3.6129	1.0065	.9831	.6443	1.5074	.9314
27	1.2166	3.7905	1.0075	.9864	.6896	1.4098	.9450
28	1.3281	3.9518	1.0085	.9886	.7332	1.3273	.9560
29	1.4909	4.1477	1.0100	.9918	.7882	1.2365	.9685
30	1.6166	4.2674	1.0114	.9931	.8241	1.1842	.9751
31	1.7191	4.3597	1.0137	.9958	.8519	1.1482	.9809
32	1.8166	4.4410	1.0159	.9966	.8785	1.1159	.9851
33	1.9291	4.5127	1.0184	.9981	.9022	1.0892	.9890
34	2.1004	4.6017	1.0223	.9987	.9341	1.0560	.9930
35	2.2346	4.6582	1.0253	.9993	.9550	1.0360	.9956
36	2.3839	4.7088	1.0286	.9997	.9747	1.0184	.9978
37	2.5444	4.7478	1.0331	1.0005	.9914	1.0055	.9997
38	2.6594	4.7623	1.0363	1.0000	1.0000	1.0000	1.0000
39	2.8239	4.7869	1.0409	1.0009	1.0121	.9925	1.0014
40	2.9520	4.7996	1.0445	1.0011	1.0197	.9884	1.0020
41	3.0919	4.7959	1.0493	1.0012	1.0230	.9898	1.0019
42	3.2015	4.7918	1.0544	1.0013	1.0265	.9912	1.0018
43	3.3291	4.7867	1.0607	1.0020	1.0302	.9936	1.0019
44	3.4658	4.7764	1.0739	1.0020	1.0393	.9971	1.0015
45	3.6146	4.7669	1.0865	1.0025	1.0475	1.0009	1.0014
46	3.7653	4.7555	1.1013	1.0020	1.0581	1.0043	1.0007
47	3.9221	4.7525	1.1054	1.0026	1.0604	1.0060	1.0009
48	4.0246	4.7499	1.1089	1.0024	1.0630	1.0067	1.0007

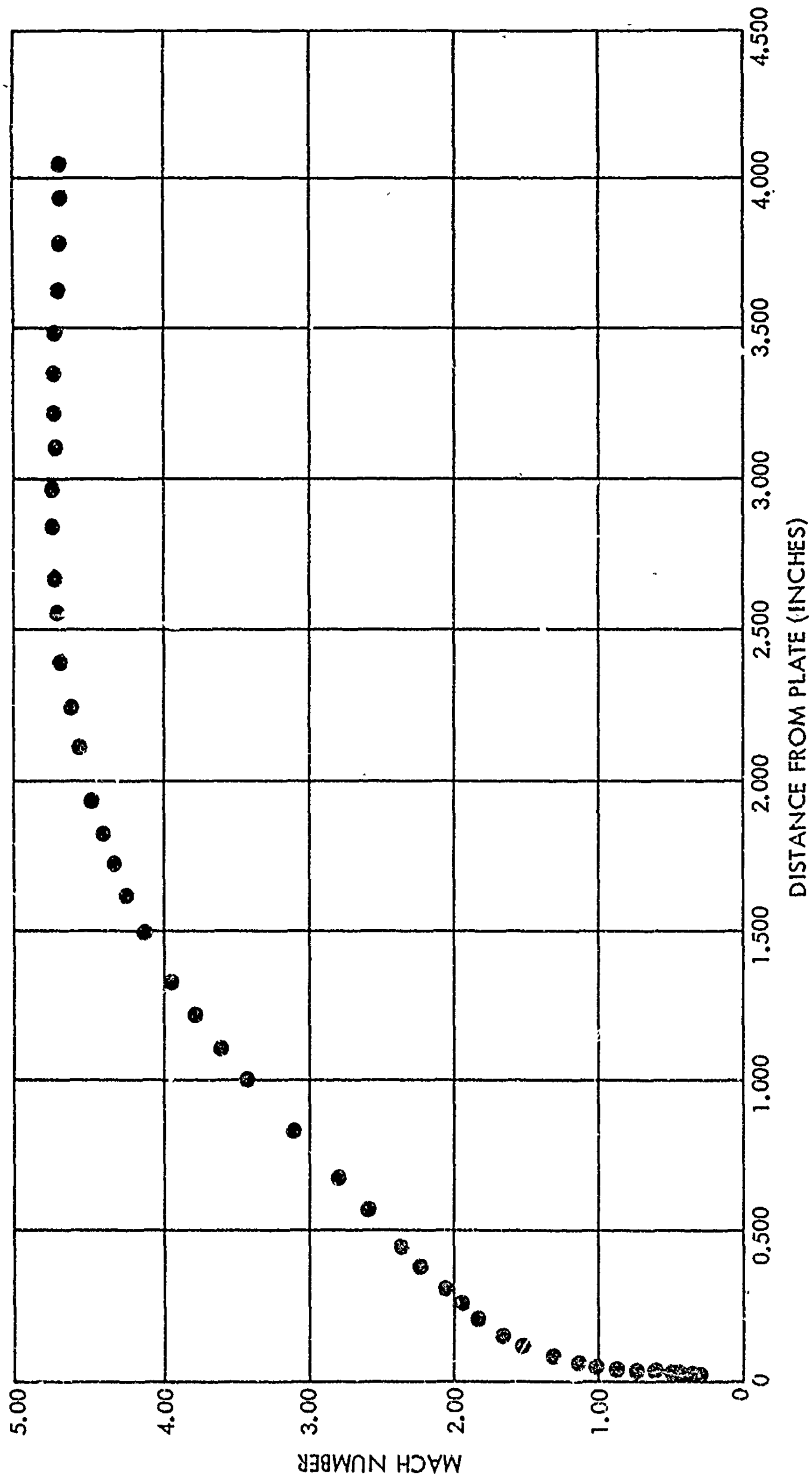

FIG. B-16 (U) MACH DISTRIBUTION: PO = 14.9 PSIA; TO = 586 °R; STATION = 60 INCHES (U)

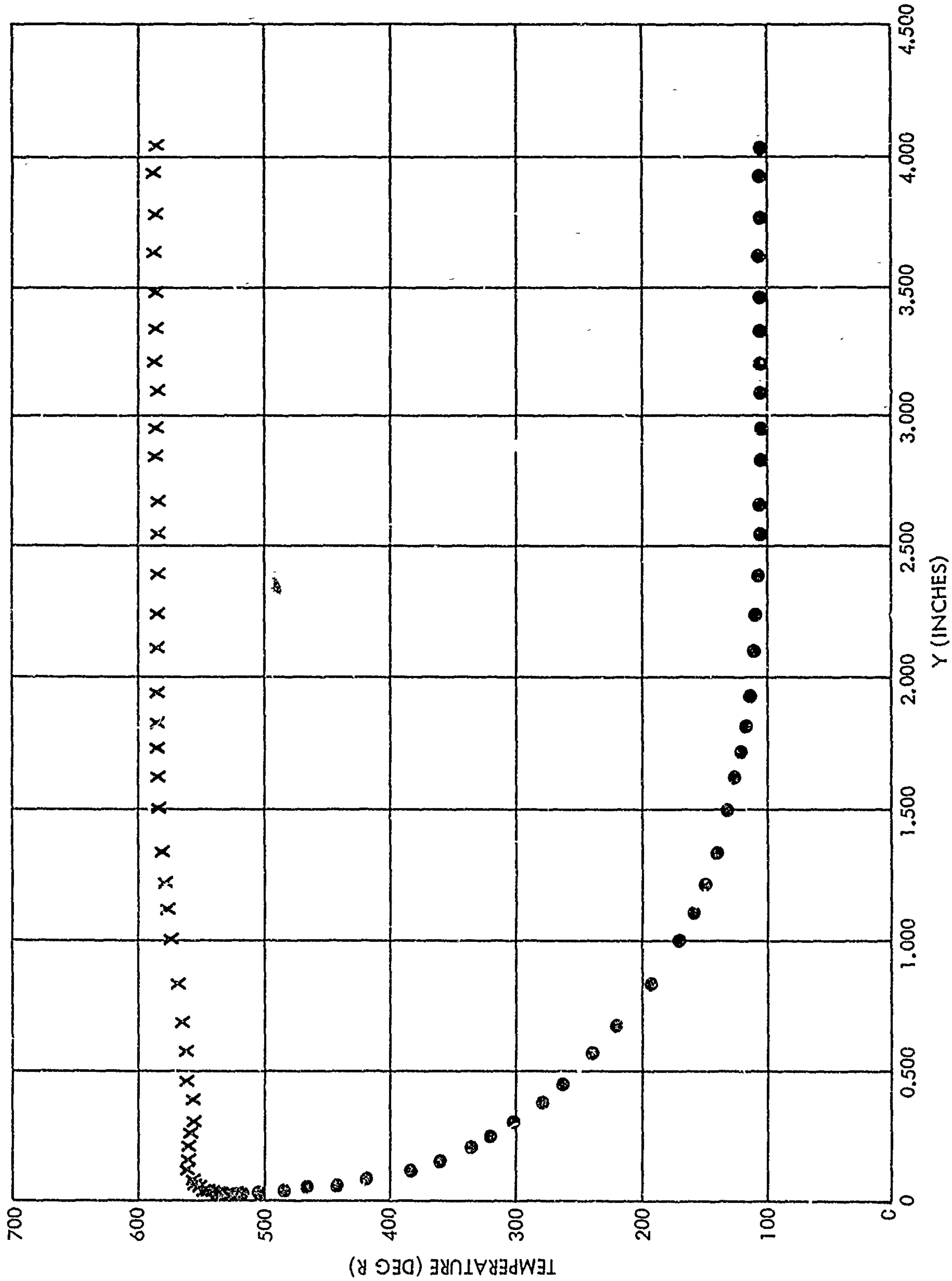

FIG. B-17 (U) TEMPERATURE DISTRIBUTION: PO = 14.9 PSIA; TO = 586 °R; STATION = 60 INCHES (U)

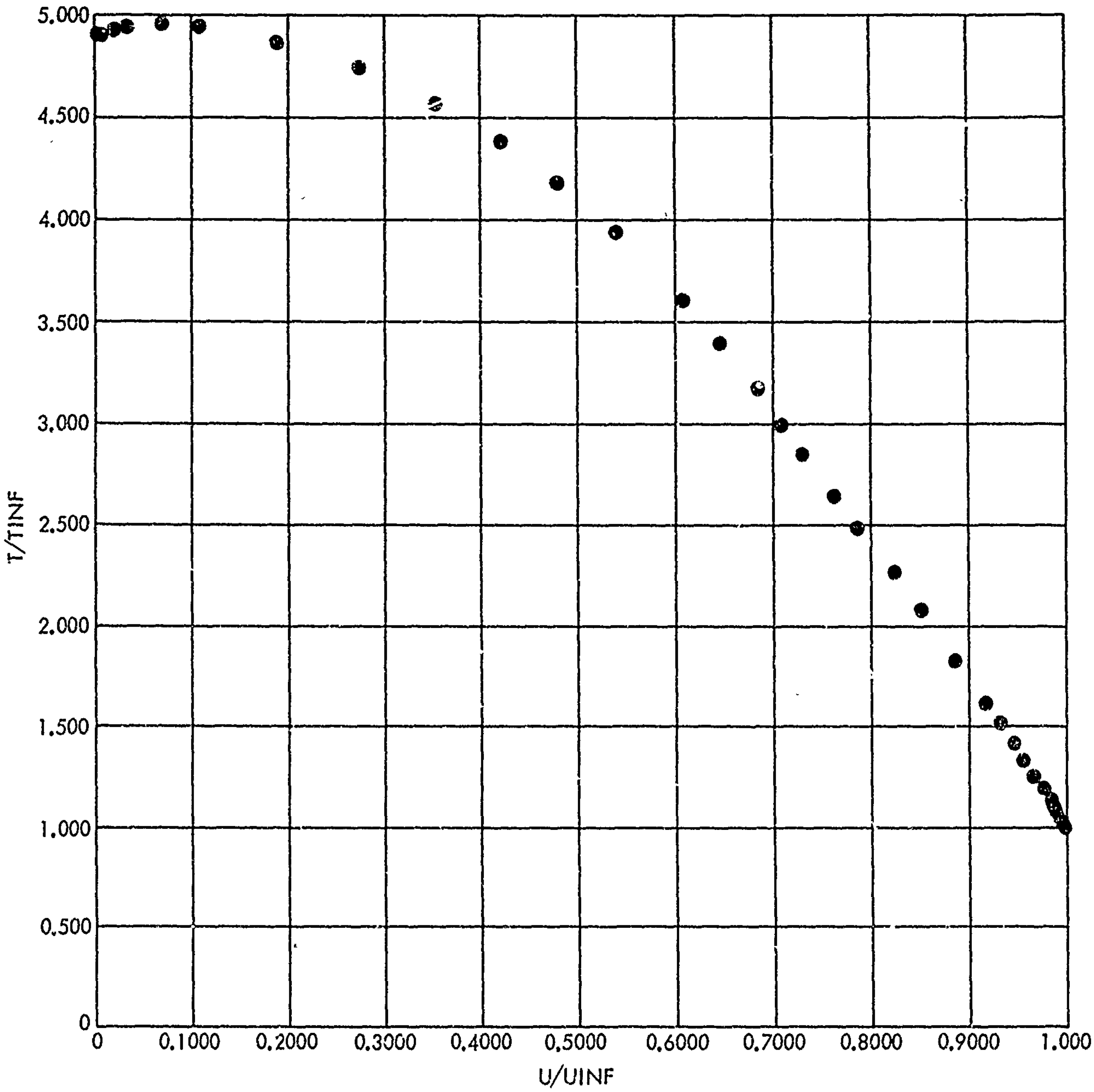

FIG. B-18 (U) DIMENSIONLESS TEMPERATURE-VELOCITY DISTRIBUTION:
PO = 14.9 PSIA; TO = 586 °R; STATION = 60 INCHES (U)

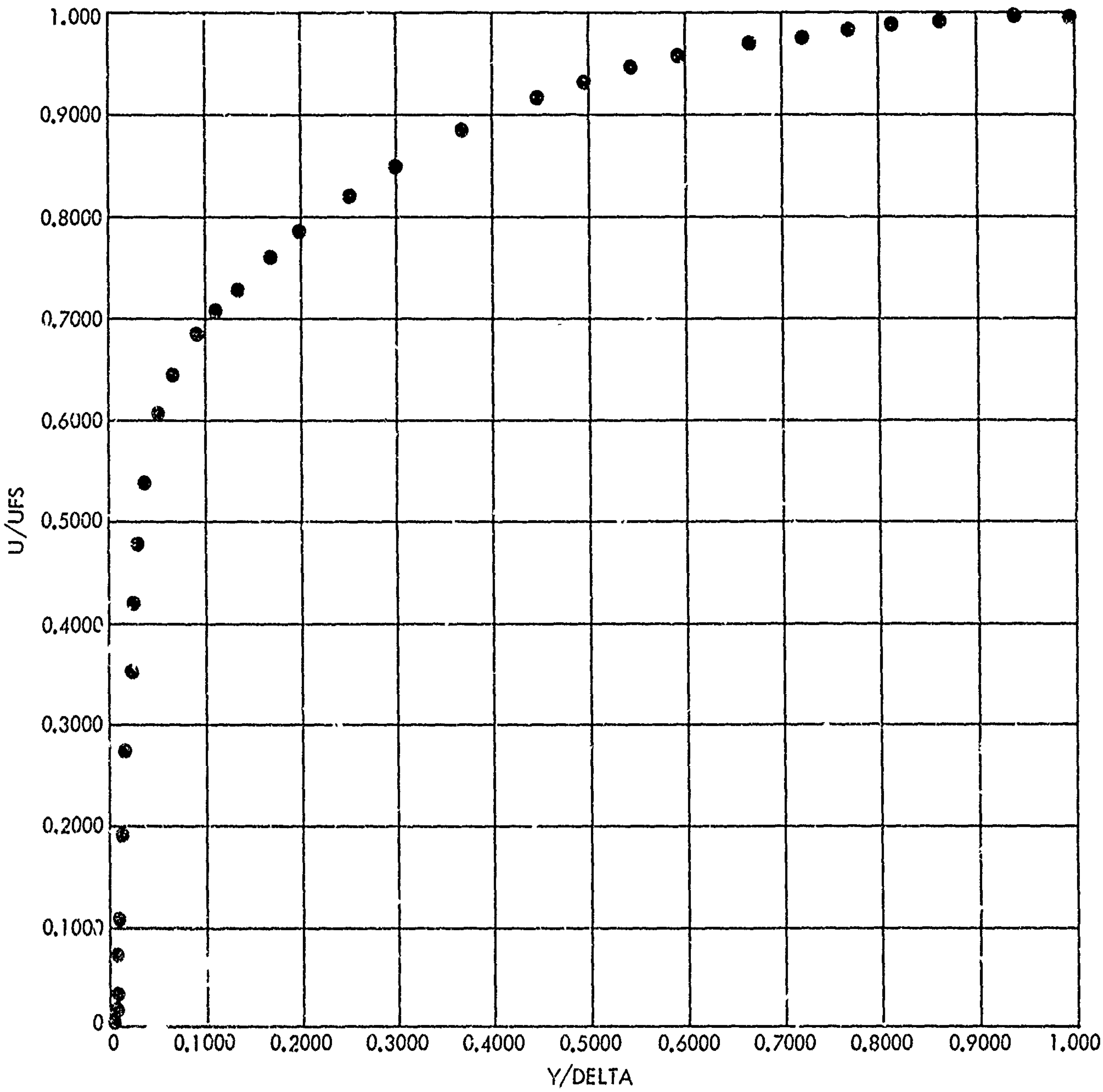

FIG. B-19 (U) DIMENSIONLESS VELOCITY-DISTANCE DISTRIBUTION:
PO = 14.9 PSIA; TO = 586 °R; STATION = 60 INCHES (U)

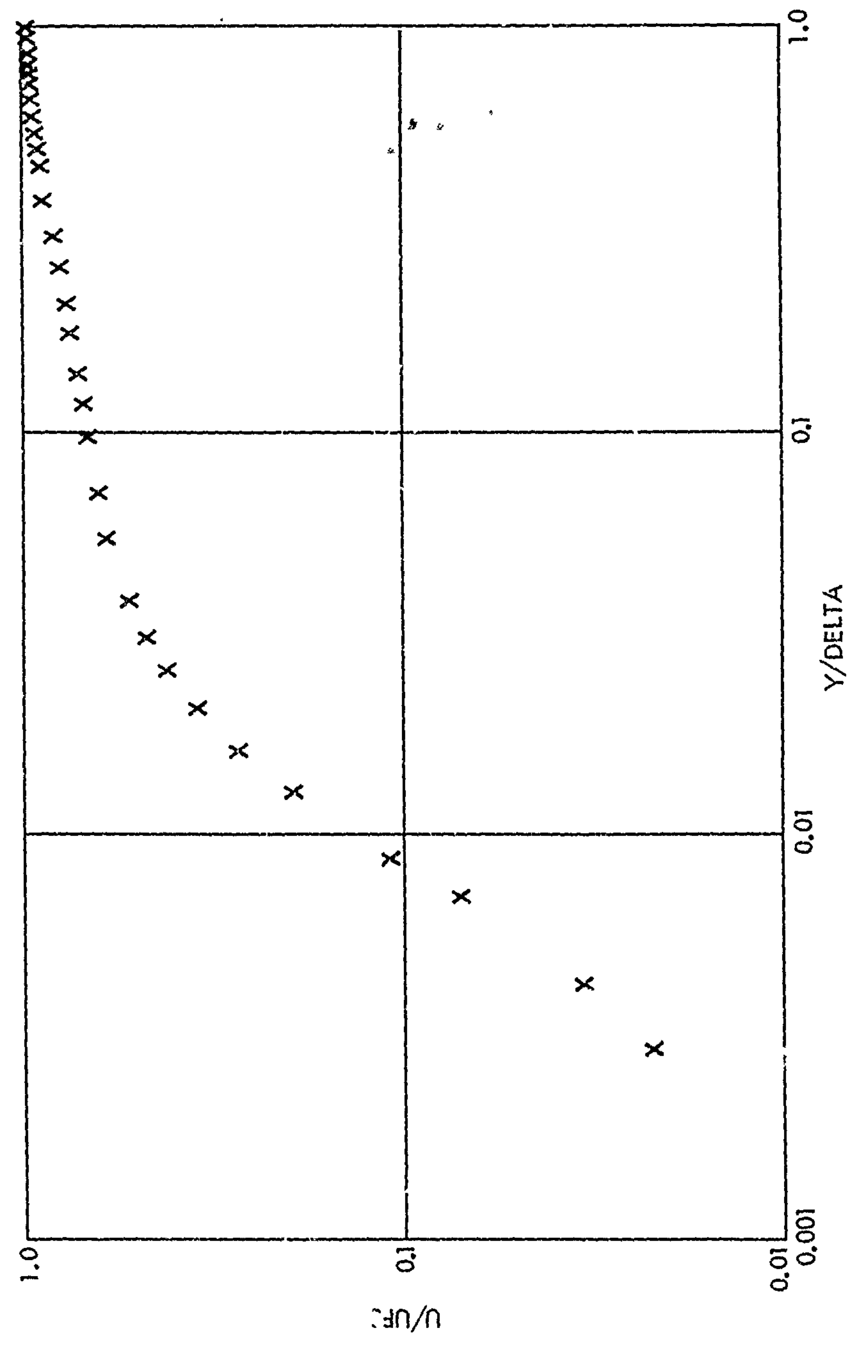

FIG. B-20 (U) LOGARITHMIC VELOCITY DISTRIBUTION: PO = 14.9 PSIA; TO = 586 °R; STATION = 60 INCHES (U)